DOCTORAL SCHOOL
BIOMEDICAL SCIENCES

Zika Virus Genetic and Physiopathological Evolution: Emergence of a Threat

Jury:

Supervisor:	Prof. Catherine Sadzot-Delvaux (Uliège)
Co-supervisor:	Prof. Johan Neyts (KU Leuven)
Chair examining committee:	Prof. Pedro E. Marques (KU Leuven)
Chair public defence:	Prof. Denis Baurain (Uliège)
Jury members:	Prof. Laurens Liesenborghs Prof. Julia Edgar Prof. Marielle Lebrun Prof. Els Henckaerts Prof. Pedro E. Marques Prof. Laurent Gillet

Dissertation presented in partial fulfilment of the requirements for the joint degree of Doctor in Sciences (Uliège) and Doctor in Biomedical sciences (KU Leuven)

Maïlis Darmuzey

2024

Acknowledgments

Acknowledgments

This section will be a bit long as I had the chance to meet a lot of amazing people, so for those that are not interested they can jump directly to the page 6

All acknowledgments written below are my personal point of view, none of them are due to social or political conventions. I sincerely hope that I will not forget a person here but if it is the case, please forgive me, it is not intentional.

The amazing promotors

I would like to thank **Prof. Catherine Sadzot** that in trouble times for me, agreed to inherit the hot potato (me) which is something that is never easy and requires a great sense of humanity and also solid nerves. Thank you, a lot, for giving me the opportunity to pursue my PhD thesis.

Prof. Johan Neyts, dear Johan. I guess that usually people write very classical acknowledgments that we can read in all or almost all PhD thesis but it is not in my personality. I would like to thank you first for the trust that you gave me by welcoming me into your laboratory while I was coming from nowhere and more importantly an uneasy situation. People might think that it is because you are a big name and in a very powerful position so that it was not a "risk" for you, but I see that more as an act of kindness from a boss who has not traded his humanity for power. I'm also really grateful that despite the fact that I was not working on the core subject of your lab (antivirals), you never made me feel that I was not an integral part of the laboratory. Thank you for the trust and the freedom that you gave me to perform my research, it has been an amazing journey!

The two most important people in my scientific adventure

Ivan Gladwyn-ng. Ivan, one day Romain told me that there is different kind of love; the love for our family, the love for our partner in life and the love for our mentor. I have no shame to say that I love you dear mentor. You were, you are and you will remain the best mentor that I could have or dream of. Working with you has been so incredible that it is difficult to describe to people that never met you. Being your student was like trying to catch a high-speed train and that was amazing, thanks to your mentoring I have been able to grew up a lot. You gave me the passion for science and the will to pursue for a PhD. So, if someone has to complain about the fact that I decided to enroll for a PhD, I must say that it is 100% your fault!

Suzanne Kaptein. So much to say with so few words, but I will try. You are the best supervisor ever, no one can compete, sincerely. Usually, even when people are very happy with their supervisors, there is always a little things/details that could be improved, in my case, there is not even an infinitesimal detail that I would like to change. I will never be grateful enough for what you did for me, you reached out and offered me so much when you owed me nothing, it's priceless. On top of being one of the best persons I have ever met, you were also the best supervisor, offering me the chance to work on the side of a brilliant scientist. If each lab had the chance to have a Dr. Suzanne Kaptein, academia would be the best place to work in the world.

The amazing Neuro colleagues-friends

Christian Alfano. My dear friend, we went through crazy times together but I will always remember that even facing the most absurd and sometimes cruel situations we never gave up on each other. We fought shoulder to shoulder and never backed down to help the other. I do not know how it is for you, but I will never forget this and you will always remain in my heart as my teammate in the face of adversity. I'm your James, dear Bond. Ah and "Forget about laboratory biosafety, I want superpowers". 😉

Carla. "Passionate about science" is the first thoughts that comes to my mind when I think about you and I realize how lucky I have been over the past years to meet brilliant, passionate and incredible human being. You were and will remain an example of dedication to perform excellent science. I learnt so much on your side, such as critical thinking, when to take my time, when to rush an experiment but above all the most important, tenacity. I know that some moments can be tough for you because you decided to choose the most difficult way in the academic world by believing first in ideas and in the beauty of research rather than in the star system. However, I have to say that I admire much more people like you that promotes science rather than their names, you are the real driving force behind academic research. BTW, I just remember that it is you who taught me that if I have a good idea that can be tested with the material that I have but that I am not sure that my boss will agree, I must do it, if it works then show the results to the boss, if does not work, don't say anything, no one will notice xD. BRAVO such a good influence <3

Fanny. Kindness, tenacity, incredible friend, incredible supportive coworker, hard worker are some of the few things that come to me when I think about you. You are an amazing personality, I have been so lucky to share that many years with you, you made the daily lab life so full of joy. I am a disaster when it comes to say my feelings about people, I would like to be much better in expressing myself but what I would like to tell you is that you are **a rare jewel**.

Romain, Silvia, Jolien (and Fanny 😉). What to say except, the DREAM TEAM? Working with you is one of the best experiences that I will have in my life for sure. You are all the best teammate that we can dream of, brilliant, funny, supportive, present in the good and bad moments. You are among my best memories about master and PhD thesis. **Romain**, a crazy and brilliant colleague with such a big heart, always willing to help and share, crazy biker. **Silvia**, the funniest, craziest colleague ever made, you have such a big heart, you were always a shiny light spreading positive energies everywhere you go. **Jolien**, my dear Cluster friend (funniest joke ever, no?), your passion for science is an example and an inspiration for me, I will never forget your energy, your willpower and your kindness even in harsh moment.

Alexandre Hego. My friend, thank you so much for all our discussions about anything and everything, it helped many times to be able to share these moments with you around extremely expensive fluorescent microscopes xD. I truly hope that we will keep in touch in the future even if I will not spend anymore that much evenings in the imaging facility.

The amazing Uliège people

Prof. Laurent Gillet. I did not forget all the effort that you made for me while not being part of your laboratory, like going to the lab during the weekend to amplify the mCMV in order to

provide it to me as soon as possible and all the suggestions and help for the first project of my PhD about mCMV. It is incredibly kind and human that despite being an extremely busy and overwhelmed person, you still find the time to try to help a student that is not part of your laboratory and to whom you have no obligation. We are lacking of people like you.

Prof. Denis Baurain. Thanks for being there, thank you for listening to me when I had the feeling to be facing all that disaster alone. Your attentiveness and support have had more weight and value that you can imagine. Thanks again for all.

The amazing Viro colleagues-friends

Prof. Leen Delang. Thanks for your support and being ready to help me in difficult circumstances. I was greatly touched by your kindness and humanity during these times. Moreover, you are such a full of positive energy person that it really illuminates around you sharing positives feelings.

Xin. Can we expect a better colleague to start in a new environment? I don't think so. I'm so grateful that you are who you are, and that your incredible positive and shiny personality was my first introduction to the lab.

Stijn. My buddy. The poor guy who agreed to work with me, such a bad idea that you get my friend. I'm happy to share this time with you, you should believe much more in yourself because you are an amazing and beautiful person, I mean you can walk along with me, you must be a warrior xD. No, seriously, you are full of qualities and I'm delighted to have meet you.

Arno. After Xin, you are the person that really helped me to feel comfortable in my new environment. Kindness, positiveness, happiness, all of these parts of your personality were a great source of peaceful feelings for me.

Sander. Your personality touched me like rarely before. I don't know what life will be made of for you in the future, but I really wish you to find your way and all the best. You deserve it.

Lorena. Incredibly beautiful personality. You are such a beautiful person, it's amazing. Thank you for all your kindness, your help and dedication.

Li-Hsin. You are a warrior young girl, never forget it!

Ana, Alina, Sam. Such a team! Beautiful, Smart, Kind, Shining women! OMG, when I think about you, I'm always smiling as you represent so much the happiness in this grey world.

Jana. OMG, thank you so much for your help and positivity at all times! I hope to continue to share good times with you in the future years!

JN group. Manon, Dirk, Niels, Caroline, Tina, Kim, Jasper, Thibault, Winston, Sofie, Katelijne, Lara, Elias, Rana, Viktor, Emma, Yana, Yuxia, Xinyu, Elke. Thanks to all of you for all your help and support!

Valentijn, Kristof, Femke, Shana, Annelies, Mathias. You are the BEST. We are so spoiled with you, I would like to really thank you for all your help and kindness at any time. You do an amazing and essential job. Thanks so much!

Dominique, Inge, Cathy, Patrick. Best administrative team ever! Thank you to always be so kind and willing to help even with the most stupid questions. You are making our life so simple that's amazing.

Dad. Ah ah ah ah et voilà, je devrais enfin l'avoir ce doctorat ! Et ne t'inquiète pas je m'arrête là, plus de stress 😉. Merci d'être là même si cela n'a pas toujours été facile, tu n'as pas hérité de la fille la plus conventionnelle du siècle mais elle a l'air de s'en sortir pas trop mal 😉 Je t'aime le vieux et puis bon les chiens ne font pas des chats, c'est aussi de ta faute, il ne fallait pas me refiler les mauvais gènes xD.

Alex. Je te dédie une grande partie de cette thèse. A nous, ceux sur qui personne n'aurait misé un centime fût un temps. Regarde où nous en sommes maintenant l'ami, 15 ans après notre première rencontre.

Michael. Le dernier mais tout bonnement le plus important de tous. Que dire, je sais que tu es comme moi, extrêmement mal à l'aise vis-à-vis de ce genre de remerciement mais je ne peux passer à côté tant tout ceci n'aurait jamais pu se réaliser sans toi. Cela fait plus de 11 ans maintenant que tu me supportes tous les jours dans les bons comme les mauvais. Je sais bien la façon dont les gens nous regardent, mais mon dieu ce que je n'en ai rien à faire, pire je leur souhaite à tous d'avoir un jour ce que j'ai trouvé avec toi ; mon alter ego. Un jour Stijn m'a demandé si je pourrais vivre dans un monde postapocalyptique et ma seule question fût de savoir si tu serais là à mes côtés car si tu es là, alors peu importe le monde dans lequel on évolue, ça vaut le coup de le partager avec toi.

Table of Contents

List of abbreviations:

C	Capsid protein
CDC	Centers for Disease Control and Prevention
CSF	Cerebral spinal fluid
CZS	Congenital Zika Syndrome
DENV	Dengue virus
DPI	Days post-infection
E	Envelope protein
epZIKV	epidemic ZIKV
FFU	Focus-forming units
GBS	Guillain-Barré Syndrome
hNPCs	Human Neural Progenitor Cells
IFN	Interferon
IL-10	Interleukin 10
IL-6	Interleukin 6
IPCs	Intermediate progenitor cells
JEV	Japanese encephalitis virus
M	Membrane protein
NEC	Neuroepithelial progenitor cells
NHP	Non-human primate
oSVZ	Outer sub-ventricular zone
PFU	Plaque-forming units
preZIKV	pre-epidemic ZIKV
prM	premembrane protein
RGC	Radial Glial Cells

List of abbreviations:

SNP	Short neural precursors
SVZ	Sub-ventricular zone
TORCH	Toxoplasmosis, Other, Rubella, Cytomegalovirus, Herpes
VZ	Ventricular zone
WHO	World Health Organization
WNV	West Nile virus
YFV	Yellow fever virus
ZIKV	Zika virus

Résumé

Le virus Zika (ZIKV) a été isolé pour la première fois en 1947 en Ouganda. Au cours de son histoire, le ZIKV a évolué pour donner naissance à deux lignées : la lignée africaine ancestrale et la lignée asiatique. Auparavant, les infections par le ZIKV n'étaient associées qu'à des cas asymptomatiques ou à de légers symptômes grippaux. Toutefois, en 2015, lors de l'épidémie brésilienne, le virus Zika a été associé pour la première fois au développement de malformations neurologiques chez les nouveau-nés. Le développement d'altérations du cerveau chez les nouveau-nés n'a été associé qu'à des infections causées par des ZIKV de la lignée asiatique.

Bien que certaines études indiquent que la transmissibilité et la pathogénicité du ZIKV africain sont plus élevées que celles du ZIKV asiatique, l'utilisation d'un ZIKV africain ancien et/ou passé à grande échelle atténue la pertinence biologique de ces études dans l'évaluation du potentiel épidémique du ZIKV africain actuellement en circulation. C'est pourquoi, dans le **chapitre III**, nous avons évalué le potentiel épidémique du ZIKV asiatique et de récents ZIKV africains. Pour ce faire, nous avons évalué le taux d'infection et de transmission de différentes souches asiatiques et africaines du ZIKV par le moustique *Aedes aegypti*. Nous avons constaté que les souches africaines du ZIKV présentaient un taux de transmission plus élevé que leurs homologues asiatiques. En outre, la modélisation *in silico* a montré que la probabilité et l'ampleur des épidémies humaines étaient remarquablement plus élevées pour les souches africaines du ZIKV. Ensuite, la pathogénicité des souches africaines du ZIKV a été étudiée chez les souris immunodéprimées AG129 ainsi que chez des embryons murins. Nous avons montré que les souches africaines de ZIKV étaient plus létales que les souches asiatiques de ZIKV pour les souris AG129 immunodéprimées. En outre, les souches africaines de ZIKV étaient plus susceptibles de provoquer une mort *in utero* que des malformations congénitales. Dans l'ensemble, nous avons démontré que les ZIKV africains actuellement en circulation ont un potentiel épidémique et une pathogénicité plus importants que les ZIKV asiatiques.

Dans le **chapitre IV**, nous avons étudié l'évolution de la pathogénicité entre les souches asiatiques pré-épidémiques et épidémiques du ZIKV chez des embryons de souris immunocompétents ainsi que les facteurs ayant pu l'influencer. En utilisant un modèle de souris qui imite une infection congénitale du cerveau par le ZIKV au cours du premier trimestre de la grossesse, nous avons observé que toutes les souches asiatiques du ZIKV présentaient des propriétés de neurotropisme et de neurovirulence. De plus, les infections par des souches pré-épidémiques de ZIKV ont conduit plus systématiquement à des anomalies cérébrales graves que les infections par des souches épidémiques de ZIKV. En outre, les embryons infectés par

l'une ou l'autre des souches pré-épidémiques du ZIKV risquent davantage de développer un phénotype d'œdème sous-cutané à un stade précoce que ceux infectés par les souches épidémiques du ZIKV. Nous avons ensuite cherché à savoir si la plus grande pathogénicité des souches pré-épidémiques de ZIKV pouvait être liée à une meilleure capacité de réplication. Cependant, les niveaux d'ARN viral mesurés dans les cerveaux à différents moments après l'infection ne différaient pas entre le ZIKV pré-épidémique et le ZIKV épidémique. En outre, les capacités de réplication des différentes souches du ZIKV *in vitro* ne reflètent pas la pathogénicité observée *in vivo*.

Nous avons ensuite étudié la réponse du système immunitaire dans des cerveaux infectés par le ZIKV pré-épidémique ou épidémique. Nous avons constaté que tous les ZIKV induisaient une réponse immunologique, mais que celle-ci différait d'une souche à l'autre, indépendamment de leur statut pré-épidémique ou épidémique.

Enfin, nous avons évalué le rôle qu'a pu avoir le changement d'acide aminé d'une sérine par une asparagine dans le génome des souches épidémiques du ZIKV et qui a été décrit précédemment comme étant potentiellement impliqué dans la neurovirulence. En remplaçant la sérine par une asparagine dans la souche pré-épidémique du ZIKV thaïlandais, nous avons observé que cela ne diminuait pas la pathogénicité du virus *in vivo* mais modifiait son profil de réplication *in vitro* dans les cellules cérébrales humaines, avec une capacité de réplication accrue par rapport à la souche WT du ZIKV thaïlandais.

Ainsi, dans le chapitre 4, nous avons démontré que les souches asiatiques de ZIKV partagent des propriétés neurotropes et neurovirulentes et que la lignée asiatique a progressivement évolué vers une pathogénicité atténuée. De plus, les différences observées entre in vitro et in vivo ont démontré la nécessité de développer des modèles holistiques *in vivo* pour étudier les propriétés pathogènes.

Summary

Zika virus (ZIKV) was first isolated in 1947 in Uganda. During its history, ZIKV has evolved to give rise to two lineages: the ancestral African lineage and the Asian lineage. Initially, ZIKV infections were only associated with asymptomatic cases or with mild flu-like symptoms. However, in 2015, during the Brazilian outbreak, ZIKV was for the first time linked to the development of neurological defects in newborns. Moreover, the development of congenital Zika Syndrome (CZS) has only been associated with infections by ZIKV from the Asian lineage.

While some studies point towards a higher transmissibility and pathogenicity of African ZIKV relative to Asian ZIKV, the use of historical and/or extensively passaged African ZIKV strains raises questions about the biological relevance of these studies to assess the epidemic potential of currently circulating African ZIKV strains. Therefore, in **chapter III**, we assessed the relative epidemic potential of contemporary African and Asian ZIKV strains. To that purpose, we evaluated the infection rate and transmissibility for different African and Asian ZIKV strains in wild-type *Aedes aegypti* mosquitoes. We also performed an *in silico* outbreak simulation on the epidemiological dynamics for each ZIKV strain. We found that African ZIKV strains displayed a higher transmission efficiency than their Asian ZIKV counterparts. In addition, the *in silico* modeling indicated a remarkably higher probability and magnitude of human outbreaks by African ZIKV strains. Subsequently, the difference in pathogenic potential between African and Asian ZIKV strains was investigated in AG129 mice, while in embryonic wild-type (WT) mice the difference in the ability to cause birth defects was assessed. We showed that African ZIKV strains were more lethal to immunocompromised AG129 mice than Asian ZIKV. Moreover, African ZIKV strains were more likely to cause fetal death rather than birth defects. Overall, we demonstrated that currently circulating African ZIKV strains have a greater epidemic potential and pathogenic profile than Asian ZIKV strains.

In **chapter IV**, we fully focused on the Asian ZIKV lineage as we also noticed differences in fetal pathogenicity of the two Asian ZIKV strains one being a pre-epidemic and the other an epidemic strain that were evaluated in the embryonic mice (**chapter III**). We thus studied the differences in the pathogenic profile between pre-epidemic and epidemic Asian ZIKV strains in WT embryonic mice. In addition, we examined a genetic factor (present in contemporary Asian ZIKV strains) on embryonic brain development. By using a mouse model that mimics congenital ZIKV infection of the brain during the first trimester of pregnancy, we demonstrated that all Asian ZIKV strains were neurotropic and neurovirulent. Infections by pre-epidemic

ZIKV strains, however, led more consistently to severe brain defects in fetal mice than infections by epidemic ZIKV strains. In addition, we showed that mouse embryos infected by any of the pre-epidemic ZIKV strains are at greater risk of developing subcutaneous oedema at an early stage than those infected by epidemic ZIKV strains. The greater pathogenicity of pre-epidemic ZIKV strains was not linked to a higher viral replication fitness (*in vitro* and *in vivo*) of these strains, as viral RNA levels at different timepoints post-infection did not differ between pre-epidemic and epidemic ZIKV. Furthermore, while all ZIKV strains induced an immunological response in the fetal brain, as evidenced by an increase in immune mediators such as IL-6, IL-10 and CXCL10, differences were observed, albeit not between the two groups (pre-epidemic versus epidemic ZIKV), but between individual strains.

Finally, we assessed the impact on embryonic brain development of the serine to asparagine amino acid change that occurred in epidemic ZIKV, which was suggested to have exacerbated the neurovirulent profile of epidemic ZIKV. Swapping the serine for an asparagine in the pre-epidemic Thailand ZIKV strain did not significantly alter the pathogenicity of the modified strain as compared to that of the parental strain. By contrast, differences were observed in the replication profile in human brain cells, with the modified Thailand ZIKV exhibiting an increased replication fitness as compared to the WT Thailand ZIKV strain. Taken together, we demonstrated in **chapter IV** that the evolution of the Asian lineage resulted in an attenuated fetal brain pathogenicity. Moreover, the differences between the outcomes of the *in vitro* and *in vivo* experiments underscore the need for holistic *in vivo* models for deciphering the pathogenic properties of ZIKV strains.

Chapter I : General Introduction

I.1 General introduction to Orthoflaviviruses

The *Orthoflavivirus* genus belongs to the *Flaviviridae* family of positive single-stranded enveloped RNA viruses and comprises over 70 members that include the dengue virus (DENV), the yellow fever virus (YFV), the West Nile virus (WNV), the Japanese encephalitis virus (JEV), and the Zika virus (ZIKV)[1]. These viruses are also categorized as arboviruses (ARthropod-BOrne VIRUSes), which refers to the blood-feeding arthropod vectors that transmit these viruses. The *Aedes* mosquito is the primary vector for transmitting ZIKV, DENV and YFV while the *Culex* mosquito for JEV and WNV[2,3]. In the past, the geographical distribution of the arthropod vectors, particularly the *Aedes* mosquitoes, has limited the spread of the orthoflaviviruses and hence the incidence of the viral disease caused by these viruses. The *Aedes* mosquitoes were historically regionalized to the Asian and African continents, but have nowadays colonized many, if not all, countries in the Pacific, Asia and Latin and South America. Within Europe, the *Aedes albopictus* mosquito has colonized more than 20 countries, including countries far to the north at 51° latitude, and was additionally introduced in at least 5 countries[4,5]. This massive habitat expansion of the *Aedes* mosquitoes has been linked to an increase in the human population as well as urbanization, an increase in international trade and travel, and global warming[5] , which all have contributed to a favorable environment for this mosquito species[6]. The expansion of the habitat of the *Aedes* mosquitoes is under close surveillance as it may lead to a major public health crisis imminently. Indeed, orthoflaviviruses are already responsible for periodic epidemics and some massive outbreaks, such as those caused by YFV in 2016 in Angola, the Democratic Republic of the Congo, and Uganda[7]. Overall, the incidence of orthoflavivirus infections has been increasing over time (WHO, World Health Organization). DENV infections have increased 8-fold over the past three decades, with DENV now responsible for 100 to 400 million infections every year. From 2015 to 2019, DENV caused multiple epidemics in the Americas (WHO)[8], Pacific-Asian region[9] and Africa[10]. The closely related ZIKV was not regarded as a health threat because of the mild clinical symptomatology caused by this virus, such as rash, fever, conjunctivitis, muscle and joint pain, malaise and headache[11]. However, in 2015-2016, ZIKV caused a massive outbreak in Brazil, leading to 1.3 million infections[12]. This unprecedented ZIKV epidemic as well as the dramatic neurological manifestations in babies born to infected mothers, led the WHO to declare Zika a Public Health Emergency of International Concern. Retrospectively, ZIKV is suspected to be responsible for the unbeknownst outbreaks in the Yap Islands and French Polynesia in 2007 and 2013, respectively[13].

Orthoflaviviruses yearly pose a huge clinical pathophysiology and socioeconomic burden in (sub-)tropical regions. Although antiviral treatment is lacking, clinically approved vaccines are available for some of the orthoflaviviruses (i.e., for YFV, JEV, tick-borne encephalitis virus [TBEV] and DENV)[14]. These vaccines generally present a good safety profile and significant efficacy, but their use can have some limitations. For instance, the dengue vaccine Dengvaxia© is recommended for use in dengue endemic areas and only in people who have experienced a previous infection with DENV in the past to prevent the development of severe disease manifestations that require hospitalization. This risk is increased in naive patients as vaccination in naive recipients can be considered a natural DENV infection. Subsequently, they may experience a secondary-like, enhanced infection when facing a true DENV infection for the first time[15]. In addition to vaccination campaigns, governments in endemic countries try to limit the incidence of orthoflavivius infections by implementing vector control strategies and preventive measures, including pesticides, repellents, traps, the deployment of sterile mosquitoes or those presenting dominant lethal mutations, and the release of male mosquitoes infected with the *Wolbachia* bacteria[16]. However, even this multidisciplinary approach of vaccine campaigns with vector control strategies has failed to prevent large orthoflavivirus outbreaks in the past decades. Given the expansion of the mosquito vectors and the increasing annual incidence of orthoflavivirus infections, more studies are required to better understand their biology and evolution in order to develop efficient therapeutics and mitigation strategies that could complement the current counteracting measures against the orthoflaviviral threat.

Zika virus evolution

ZIKV was first isolated from a febrile sentinel rhesus monkey in 1947 in Uganda, Africa. Serological data indicate that prior to the 2015 Brazilian ZIKV epidemic, Zika was endemic for decades on the African continent and subsequently in Asia without any reported cases of ZIKV-associated morbidity and mortality in humans. Prior to 2015, ZIKV was not considered an epidemiological threat as the majority of infected people were asymptomatic or developed only mild symptoms, such as rash, fever, myalgia, and headache. However, in 2015, a massive outbreak of approximately 1.3 million ZIKV infections occurred in Brazil, with devastating consequences for newborns. This outbreak highlighted that, in addition to mosquito-borne transmission, ZIKV could now be transmitted from person to person by vertical transmission (and to a lesser extent, sexual transmission)[17,18]. Moreover, additional and more severe morbidities associated with ZIKV infections were documented in adults and fetuses - such as the neuro-immunological Guillain-Barré Syndrome (GBS) as well as the neurodevelopmental

abnormalities and other birth defects (Congenital Zika Syndrome, CZS) respectively[19]. A retrospective analysis of the preceding ZIKV outbreak in French Polynesia in 2013 revealed that between October 2013 and April 2014, 66% of the total population had been infected with ZIKV. Also, 41 out of 42 patients diagnosed with Guillain-Barré syndrome had anti-ZIKV IgM or IgG antibodies, and all patients had neutralizing antibodies against ZIKV. The increased incidence of GBS immediately followed the peak of ZIKV infections[20]. Another retrospective study of the same 2013-ZIKV outbreak documented a strong correlation between an increase in the incidence of microcephaly cases and ZIKV infections in pregnant women during their first trimester of pregnancy[21]. Collectively, these retrospective studies demonstrate that ZIKV was responsible for the severe clinical outcomes reported prior to the Brazil epidemic.

The ZIKV outbreaks in the past decade at dispersed geographical locations and in distinct populations necessitated a thorough study into the determinants of ZIKV evolution that may have led to the emergence of the new pathogenic traits. During its circulation, ZIKV evolved into two distinct lineages: the ancestral African lineage and the descendant Asian lineage. Phylogenetic analyses of the circulating ZIKV strains during the outbreaks in French Polynesia and Brazil revealed that these strains belonged to the Asian lineage[22], which had undergone numerous mutations, giving rise to a large number of ZIKV variants (Figure 1.1).

Several single mutations (highlighted and written in bold in Figure 1.1) appeared within the ZIKV genome that may have affected viral replication and infectivity of the virus[23]. Furthermore, mutation V763M acquired by recent Asian ZIKV strains was shown to increase pathogenicity, neurovirulence[24] and transmissibility[25]. However, all these mutations emerged in Asian pre-epidemic ZIKV strains, which arose before the French Polynesian strain, and were not associated with the development of neurological defects. The French Polynesian strain marks the emergence of epidemic, CZS- and GBS-associated ZIKV strains[23]. The serine (S) to asparagine (N) amino acid change at position 139 in the ZIKV polyprotein that occurred in the French Polynesian strain and that is present in all subsequent epidemic ZIKV strains was proposed to be the predominant causative genotypic mutation underlying the neurovirulent phenotype[26]. When injected in embryonic mouse brain, the pre-epidemic Cambodia ZIKV strain (S139) was less neurovirulent by causing less brain damage than the epidemic Venezuela ZIKV strain (N139)[26]. Finally, the amino acid substitution M/T2634V occurred in the non-structural protein NS5 of ZIKV strains in the Latin-America which could influence the replication of these ZIKV strains. Taken together, these studies suggest that epidemic ZIKV from the Asian lineage evolved towards more pathogenic and neurovirulent capacities[27].

Akin the Asian ZIKV lineage, a similar pathogenetic trajectory can be hypothesized for the African ZIKV lineage. However, no ZIKV outbreaks linked to the African lineage have been reported since its discovery. Some studies have assessed the pathogenicity of ZIKV from the African lineage. However, most of them employed the ancestral African ZIKV strain MR766, which was isolated in 1947 but has since then been passaged numerous times within a laboratory setting (around 150 times)[28]. Experiments performed with the MR766 ZIKV strain may hence not be representative of the pathogenicity elicited by the recently and currently circulating African ZIKV strains. This led to a lack of knowledge about the evolution of the African lineage and its potential to cause future outbreaks with similar human health consequences as those elicited by epidemic ZIKV strains from the Asian lineage.

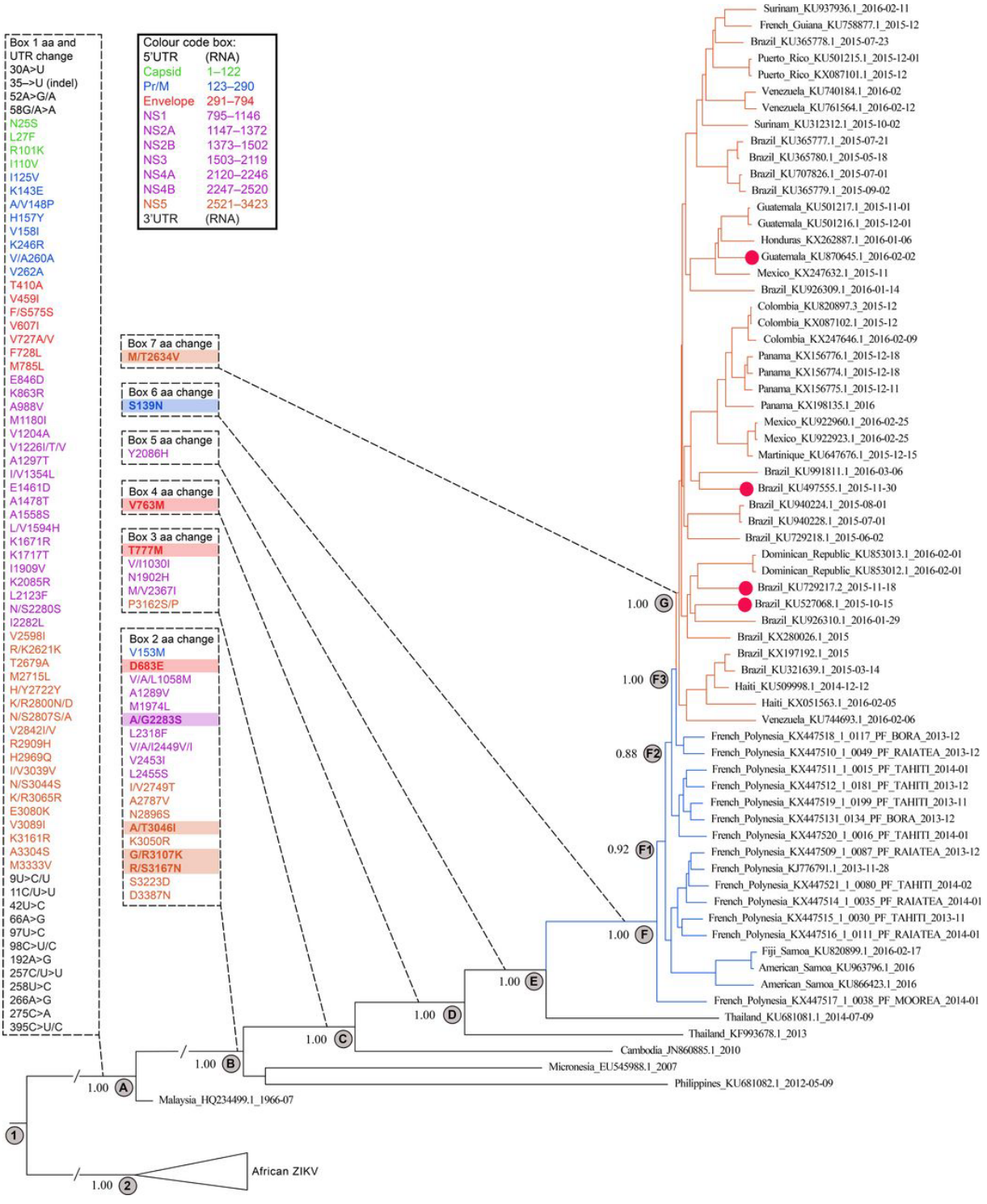

Figure 1.1: ZIKV phylogeny of African-Asian/Pacific and Latin American virus isolates, including mapping of amino acid substitutions[23]. The different amino acid substitutions that arose in the genome of the different ZIKV strains are displayed in the boxes. The red circles indicate ZIKV strains that were associated with congenital Zika syndrome.

I.2 The role of ZIKV proteins in the viral life cycle, immune systme evasion, and ZIKV pathogenicity

I.2.1 Zika virus genome and life cycle

The ZIKV genome is approximately 11 kilobases in size and encodes a single polyprotein, which is cleaved into three structural proteins and seven non-structural proteins. The structural proteins include the capsid (C), the envelope (E) and the pre-membrane (prM) protein, which are involved in the viral particle formation. The seven non-structural (NS) proteins are NS1, NS2A, NS2B, NS3, NS4A, NS4B and NS5 that not only contribute to viral replication level and viral particle assembly but also interact with the host immune system[29] (Figure 1.2).

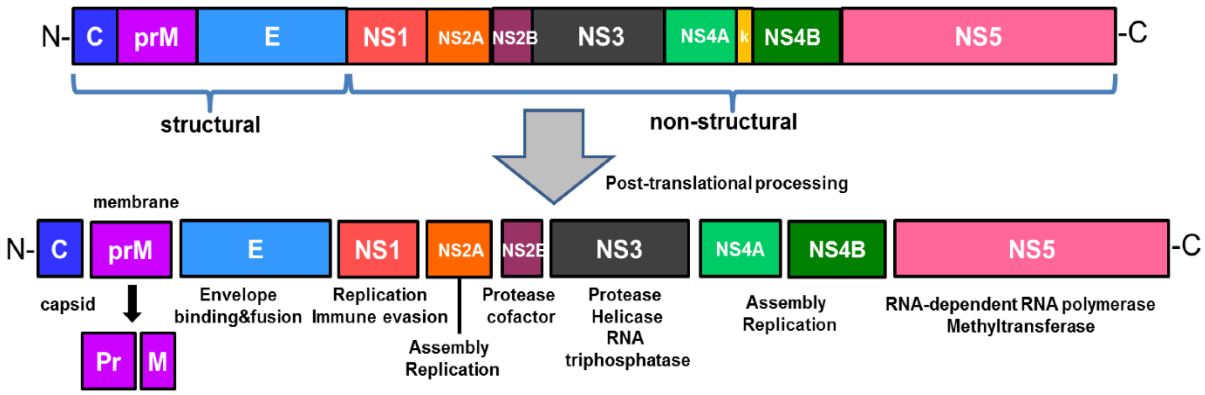

Figure 1.2: The structure of Zika virus (ZIKV) genome and its encoded proteins[282].

The single open reading frame encodes a polyprotein precursor that is post-translationally cleaved into three structural proteins (capsid, membrane and envelope) and seven non-structural proteins (NS1, NS2A, NS2B, NS3, NS4A, NS4B, and NS5).

The orthoflavivirus life cycle starts with the recognition and the specific binding between the viral envelope to human host-cell receptors. ZIKV can enter various cell types by interacting and binding to diverse host cell factors present on the cell surface such as heparan sulfates, and specific receptors (Axl, Tyro3, DC-SIGN)[30] (Figure 1.3). Notably, Tyro3 and Axl receptors are present in different cells of the central nervous system (CNS) such as neurons, astrocytes and microglia which may explain the neurotropism of ZIKV[31]. Subsequently, the virus enters the cell mainly in clathrin-dependent endocytic vesicles[32]. Under low-pH conditions the virus is uncoated and the viral genome is released into the cytoplasm[33]. At the surface of the endoplasmic reticulum (ER), the viral genome is first translated by host ribosomes into a single polyprotein which is then anchored to and inserted into the ER membrane. Next, the polyprotein is cleaved by host and viral proteases to produce the individual structural and non-structural viral proteins. Subsequently, the non-structural proteins induce ER membrane rearrangements to create vesicle pockets in which the non-structural proteins assemble to form the replication complex[34]. Following replication, the newly synthesized positive RNA strand associates with

the capsid protein to form the nucleocapsid before it is packaged into immature ZIKV particles (Figure 1.3, 1.4).

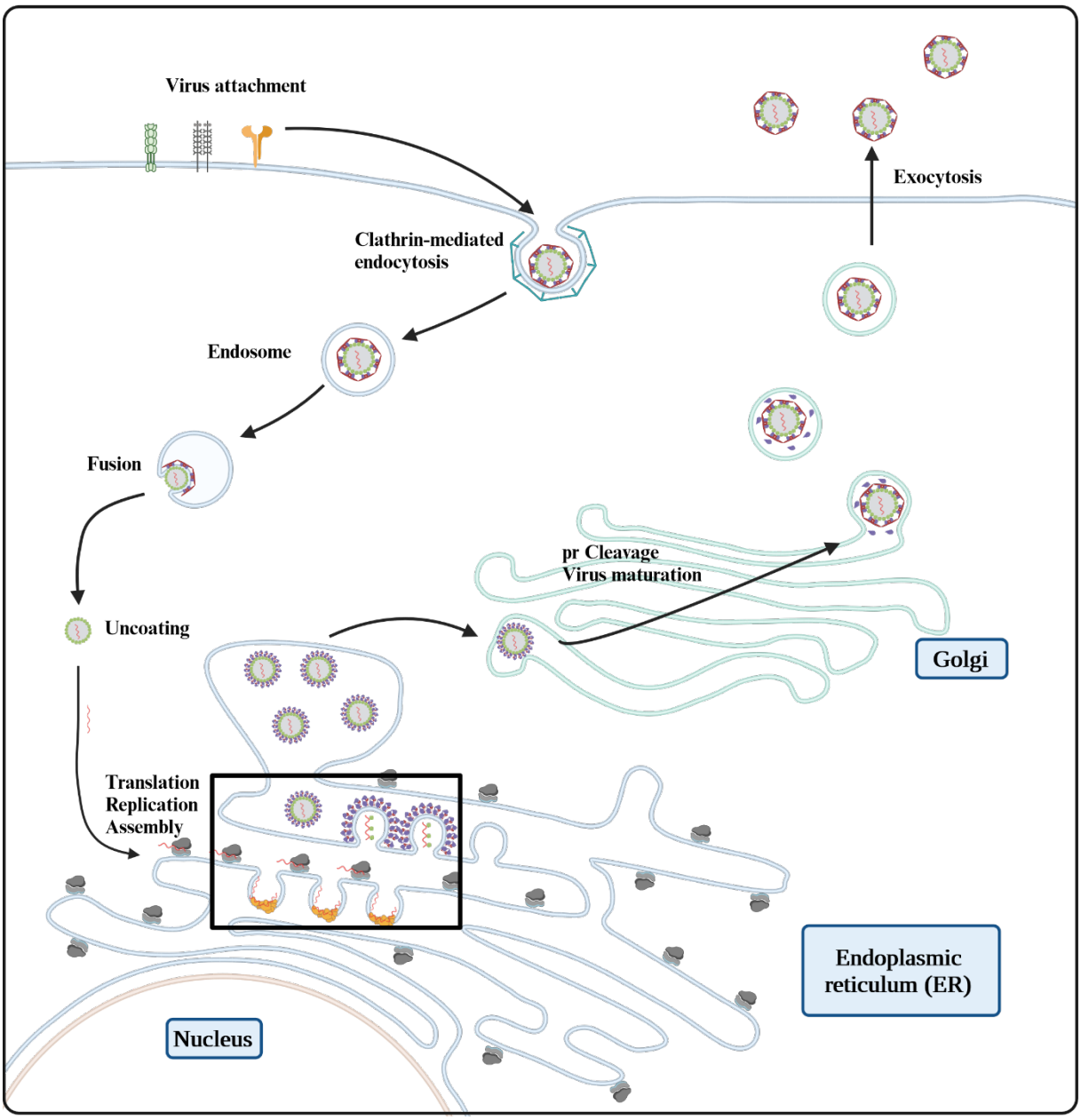

Figure 2.3: The flavivirus replication cycle.
The different steps of the flavivirus cell life cycle. Entry and internalization by endocytosis is followed by viral replication, translation and viral particle assembly at the endoplasmic reticulum. Virus maturation occurs during ER transport and transport through the Golgi apparatus. Finally, the virus is released from the cells by exocytosis. Adapted from Pierson, T. C. & Diamond, M. S [34] , created with Biorender.com.

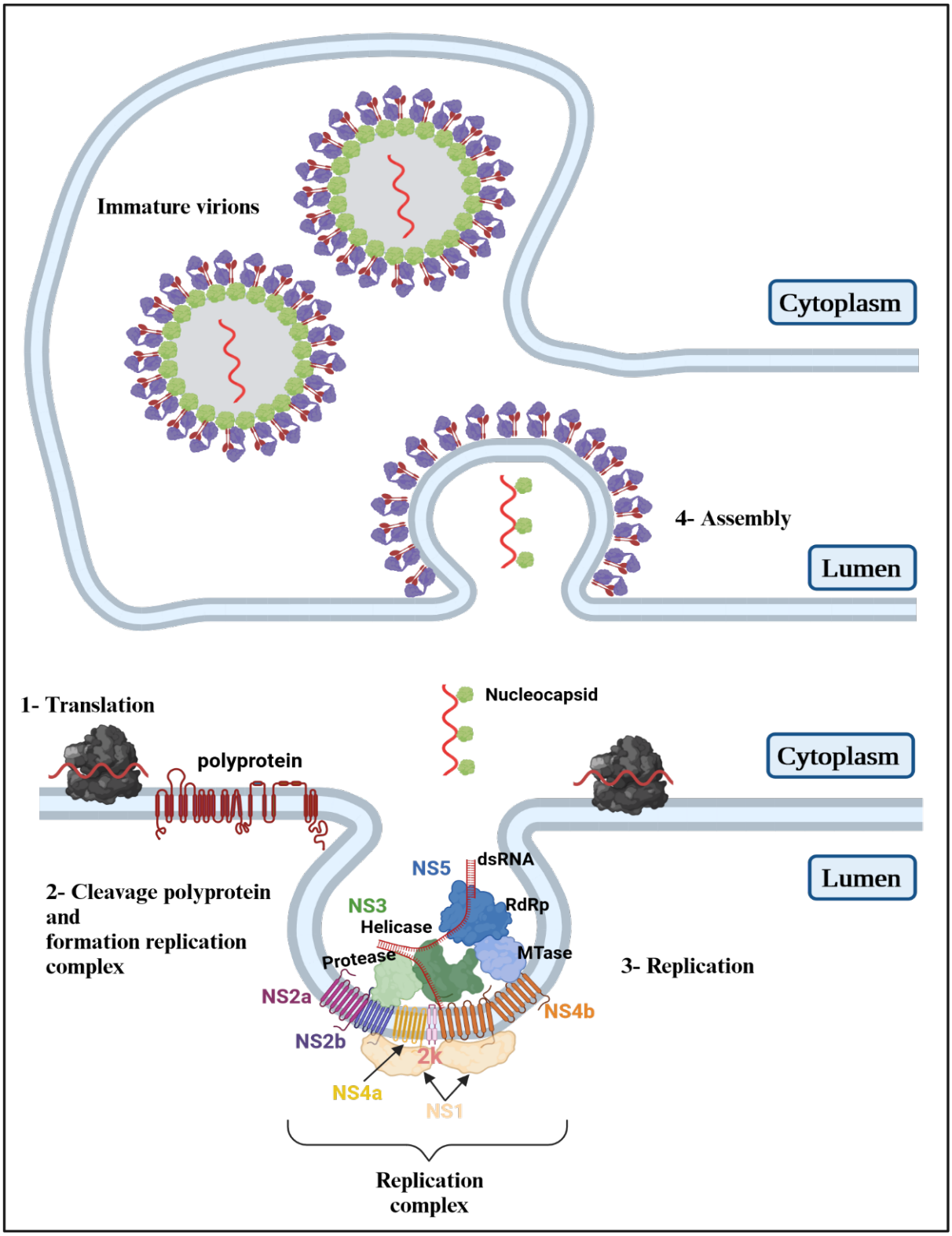

Figure 1.4: Translation, Replication and Assembly of ZIKV.
First step (1-) is the translation of the viral RNA followed by the cleavage of the polyprotein and the formation of the replication complex (2-) in which the replication occurs (3-). Finally, the newly synthesized viral genome is assembled (4-). Adapted from [283], created with Biorender.com

In more detail, the membrane (M) protein is first synthesized as a precursor protein. This prM is continuously associated with the E protein (prM-E complexes) during the transport from the ER to the Golgi apparatus to protect the E protein from a premature E protein fusion that would lead to the release of immature virions[35]. During virus particle assembly, the capsid binds to the single stranded RNA to facilitate its packaging and form the nucleocapsid. The latter interacts with the prM-E complexes and acquires a lipid membrane by budding through the ER membrane, forming an immature ZIKV particle[36]. The immature ZIKV particle surface is formed by 60 spikes made of trimers of the prM-E complexes which undergoes a final maturation process through the Golgi network by furin cleavage of the pr peptide from prM. This cleavage results in a conformational change of the E protein and the release of fully mature ZIKV particles by exocytosis[30] (Figure 1.3).

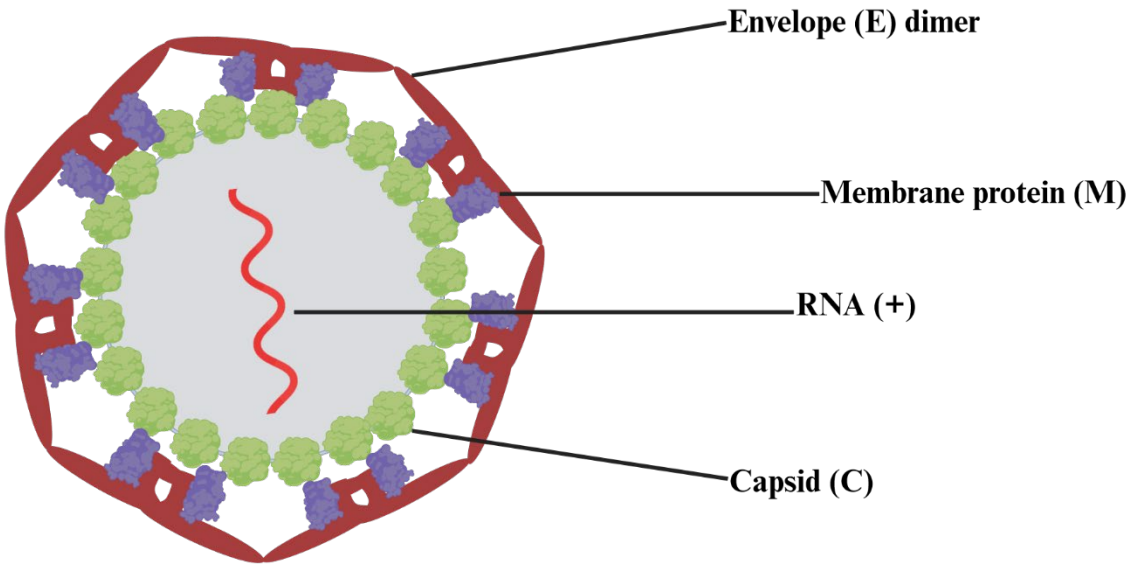

Figure 1.5: ZIKV mature virion.
ZIKV mature particle contain a single positive strand RNA, capsid proteins (C), membrane proteins (M) and dimers of envelope proteins (E). Created with Biorender.com

In addition to the structural proteins, the non-structural proteins play a major role in the life cycle of the virus. The NS1 protein is localized in the lumen of the ER and supports the viral RNA synthesis[37]. NS2A is a hydrophobic membrane protein which is involved in the assembly of the viral RNA complex and the virion particle[36]. By recruiting the NS2B-NS3 complex, NS2A will allow the cleavage of the C protein[38]. NS2B forms a complex with the protease NS3, in which it serves as a cofactor. This complex ensures the cleavage of the polyprotein at the NS1-NS2A, NS2A-NS2B, NS2B-NS3, NS3-NS4A, NS4A-2K and NS4B-NS5 junctions[39]. In addition to its protease activity, NS3 possess other enzymatic properties. NS3 also harbours a viral helicase and a 5'RNA triphosphatase to allow the capping of the viral RNA by NS5.

Besides a RTPase, NS3 also codes for a nucleoside 5′-triphosphatase (NTPase), responsible for NTP hydrolysis. This reaction provides energy for a variety of processes, including the binding of viral RNA by the replicase complex, the unwinding of the nascent RNA duplex after virus replication, and the removal of the secondary structure on the RNA template. NS4A and NS4B interact together to form a complex that will sustain the replication complex as well as organize and modify the activity of the NS3 helicase[40]. Finally, NS5 is endowed with viral RNA polymerase activity and, as previously mentioned, is responsible for the capping of the newly synthesized viral RNA thanks to its mRNA capping methyltransferase activity[37].

I.2.2 Non canonical functions of ZIKV proteins in immune system response

In addition to their role in the ZIKV life cycle and ZIKV pathogenicity, the viral proteins (both structural and non-structural) also exert important functions in mitigating the immune response following a ZIKV infection. The capsid protein of ZIKV was demonstrated to suppress DICER activity. The endoribonuclease DICER is involved in the antiviral response through the identification of dsRNA and its cleavage into virus-derived small interfering RNAs (vsiRNAs)[46]. These vsiRNAs are used by the RNA-induced silencing complex (RISC) to identify viral RNA leading to its cleavage and its degradation[47]. Thus, by suppressing DICER activity, the capsid protein counteracts the host's antiviral response.

Interferons (type I, II and III) are major components of the antiviral response of the host cell upon viral infection, by inducing a cascade of signaling pathways, resulting in up- or down-regulation of gene expression. The structural prM protein of ZIKV was demonstrated to be able to suppress interferon-1 (IFN-1) production[48]. The non-structural proteins NS2A, NS2B, NS4A, NS4B and NS5 were shown to impede interferon signaling by inhibiting IFN-β through the RIG-I pathway *in vitro*[49]. Moreover, NS1 and NS4B were reported to suppress type 1 IFN signaling, while the NS2B-NS3 complex impaired JAK-STAT signaling by preventing the induction of interferon stimulated genes *in vitro*[50]. In addition, the polymerase NS5 plays an important role in controlling the immune system by binding the human STAT2 IFN-regulated transcriptional activator, leading to its degradation by the proteasome[51]. Altogether, the non-canonical functions of the structural and non-structural proteins allow ZIKV to evade the immune system response.

Although ZIKV found various ways to evade the immune system, as described above, it is also capable of triggering a strong inflammatory response, resulting in increased levels of both pro- and anti-inflammatory cytokines/chemokines. Elevated levels of inflammation modulators were found in human fetal brains affected by CZS[52]. Several studies also reported that following

a ZIKV infection, increased expression of cytokines and chemokines was observed in human peripheral blood cells[53,54], in an *in vitro* human blood brain barrier model[55], in human iPSC-derived astrocytes[56], and in brain of adult mice[57]. Moreover, while infections with ZIKV from both lineages can elicit a strong inflammatory response, the response was reported to differ between the African and Asian lineages, as was shown in human blood monocytes. Infections with the African ZIKV strain led to the conversion of blood monocytes to a M1 pro-inflammatory profile while infections by an Asian ZIKV strain led to a M2 anti-inflammatory state[53]. Whether this results in improvement or worsening of ZIKV disease requires further investigation.

I.2.3 Non canonical functions of ZIKV proteins in pathogenicity

In addition to their canonical functions in viral particle formation, the structural proteins have also been recently shown to play a role in the pathogenicity of ZIKV. Indeed, specific mutations within prM were shown to affect its replication efficiency and thus ZIKV infectivity and cytopathogenicity[41]. Moreover, mutations in the E protein could lead to an increase in neurovirulence *in vivo*[24] but also to increased ZIKV fitness[25]. Besides hampering the antiviral response, suppression of the DICER activity by the ZIKV capsid may also disrupt neurogenesis, leading to enhanced ZIKV pathogenicity. Indeed, the regulation of the biogenesis of miRNA, small interfering RNA and small RNA from various sources by DICER enzyme is essential for a proper brain development as a DICER activity deficiency leads to microcephalic phenotypes[42].

The non-structural proteins exert several non-canonical functions that contribute to ZIKV pathogenicity, as was shown for the structural proteins. Several non-structural proteins were reported to be involved in brain alterations, amongst others. By using its protease activity, the NS2B-NS3 complex was shown to cleave the host-protein Septin-2, a cytoskeletal factor involved in cytokinesis, leading to mitotic dysfunction in neural progenitors[43]. The NS4A-NS4B complex was found to dysregulate Akt-mTOR signaling in human fetal neural stem cells, which is essential for proper neurogenesis and future migration and maturation[44]. The NS5 protein can interact and activate the p53 protein, inducing p53-mediated apoptosis in human neural precursor cells[45]. Altogether, the multiple roles of ZIKV structural and non-structural proteins demonstrate the complexity of the mechanisms underlying ZIKV pathogenicity.

I.1 Animal model: the mouse

I.1.1 The mouse as an *in vivo* model for cortical development and cortical malformations

The use of animal models has facilitated our understanding of the human brain as well as neurodevelopmental and neurobehavioral disorders. Rats and mice have been the principal choice of *in vivo* models in preclinical research, with the latter steadily accounting for more than 50% of all rodent models utilized in neuroscience research over the past ten years[58] . The mouse possesses several advantages as a model for neurodevelopmental studies, most importantly being that the mouse brain shares similarities in neuroanatomy, cytoarchitectural organization and developmental stages with the human brain[58]. Both species also undergo similar highly regulated neurodevelopmental processes that have been well described[59]. Further microscopic histological examination of cerebral neocortices of both the human and mouse species are stratified into six different cellular layers, where each layer consists of many highly specialized cells with distinct identities, morphologies, and functions such as excitatory neurons, inhibitory neurons, oligodendrocytes, astrocytes, and microglia. Furthermore, mice have an advantageous fecundity (approximately 6 to 18 pups per litter) and gestation period (approximately 19. 5 days) as compared to other *in vivo* models such as the non-human primate rhesus macaque (166.5 days), thus allowing researchers to perform many experiments[60]. Taken together, this has supported the mouse as an appropriate and increasingly accepted model for elucidating the mechanisms of human brain development.

I.2 Cerebral cortex development

I.2.1 The progenitors of the cerebral cortex

The cerebral cortex is a complex structure within the brain that forms in a highly regulated spatiotemporal developmental process. The first step of murine brain development is the formation of the neural plate originating from the ectoderm at the embryonic day 7.5 (E7.5). Around E9.5-E10, the neural tube will undergo a final closure leading to a physical separation of the neuroectoderm that will become the central nervous system (CNS) and the skin[61]. Following this separation, the neuroectoderm will differentiate to give rise to the neuroepithelial progenitors (NECs) that will give rise to all subsequent cortical progenitors and their progenies[62]. From E10, these NECs undergo neurogenesis for the generation of new neurons and give rise to the second wave of cortical progenitors, the Radial Glial Cells (RGCs)[63]. The RGCs progressively transition from symmetric to asymmetric divisions during cerebral cortical development. The former is characterized by the generation of two identical RGCs and leads to the expansion of the pool of cortical progenitors, which occurs from E10.5 to E11.5 within the

murine brain. Conversely, the latter allows the self-renewal of progenitor populations as well as the generation of one non-progenitor neuronal progeny[64]. Through a highly regulated spatiotemporal cascade of symmetric and asymmetric divisions, RGCs give rise to new neurons either via direct or indirect neurogenesis. Direct neurogenesis occurs when an RGC undergo asymmetric division for self-renewal as well as the generation of one neuronal progeny whereas indirect neurogenesis occurs when an RGC undergo asymmetric division to produce intermediate progenitor (IPCs) and outer SVZ progenitor cells (oSVZ)[65]. A third population of progenitors is present in the cortex, the short neural precursors (SNPs), but it is unclear yet if they are progenies of RGCs[66]. Following this, a small portion of IPCs may first undergo symmetric division to self-renew before transitioning towards symmetric terminal divisions to give rise to post-mitotic neurons. The oSVZ exhibits a similar developmental program with the RGCs by the first expansion period followed by the production of neurons. Finally, SNPs will mostly directly produce post-mitotic neurons by terminal symmetric divisions[66].

All these progenitors and their respective progenies are located in specific regions within the cerebral cortex, which is a highly organized structure where distinct neuronal cell populations require specific spatial orientation for appropriate network functionality. RGCs and SNPs both reside in a layer present at the apical surface of the ventricle, named the ventricular zone (VZ). When generated, IPCs and oSVZs will have to migrate along the RGCs' processes that extend toward the pia surface to leave the VZ. IPCs will accumulate and form the subventricular zone (SVZ) above the VZ. As they are named, oSVZ progenitors will migrate to settle outside the SVZ. In mice, the oSVZ number is too limited to form a specific layer in contrast to humans[66].

Like IPCs and oSVZ, newly generated neurons will migrate along the RGCs' processes to reach their final position. Neuronal positioning and identity are determined by their birth date. Indeed, neurons are produced in sequential waves of which the birth peaks are at E11.5, E12.5, E13.5, E14.5 and E15.5. These different waves will give rise to the distinct neuronal layers of the cortex[63]. The cortical layering is established following an "inside-out fashion" mode with the first waves of early-born neurons forming the deepest cortical layers while late-born neurons give rise to the superficial layers. Thus, the first-born neurons will establish the subplate that lies above the oSVZ progenitors, the second wave will form layer VI, followed by layer V, then layer IV and finally, the last neuronal wave at E15.5 will give rise to layer II/III. Before birth, the cortical layering formed by the neurons is not completely established and the different layers form a structure called the cortical plate (CP) that will progressively disappear in favor of six well-defined layers.

Around E17.5, RGCs will progressively switch from the neurogenesis phase to the gliogenesis-generating astrocytes and oligodendrocytes[67]. (Figure 1.4)

Finally, while projection neurons represent 80% of the cortical cell population, interneurons are the second major population of cells present in the cortex. In contrast to the neurons that are originating from the cortex, the vast majority of the interneurons are born outside of the cortex and will have to follow long paths of migration to reach their final position. They act as inhibitory neurons that will control the total excitability of the neuronal network[66].

The balance between symmetric and asymmetric divisions must be highly controlled to ensure the generation of the proper number of progenitors and neurons. Indeed, a drift towards increased direct neurogenesis (by RGCs and/or other progenitor cells) will reduce the eventual number of neurons produced while the converse increased indirect neurogenesis will have a more indirect but equivalent effect by decreasing the pool of IPCs which is essential to generate neurons. Consequentially, the accurate and precise balance of symmetric and asymmetric divisions within different progenitor populations is paramount for the appropriate neuronal production to avoid cortical malformations and their associated diseases.

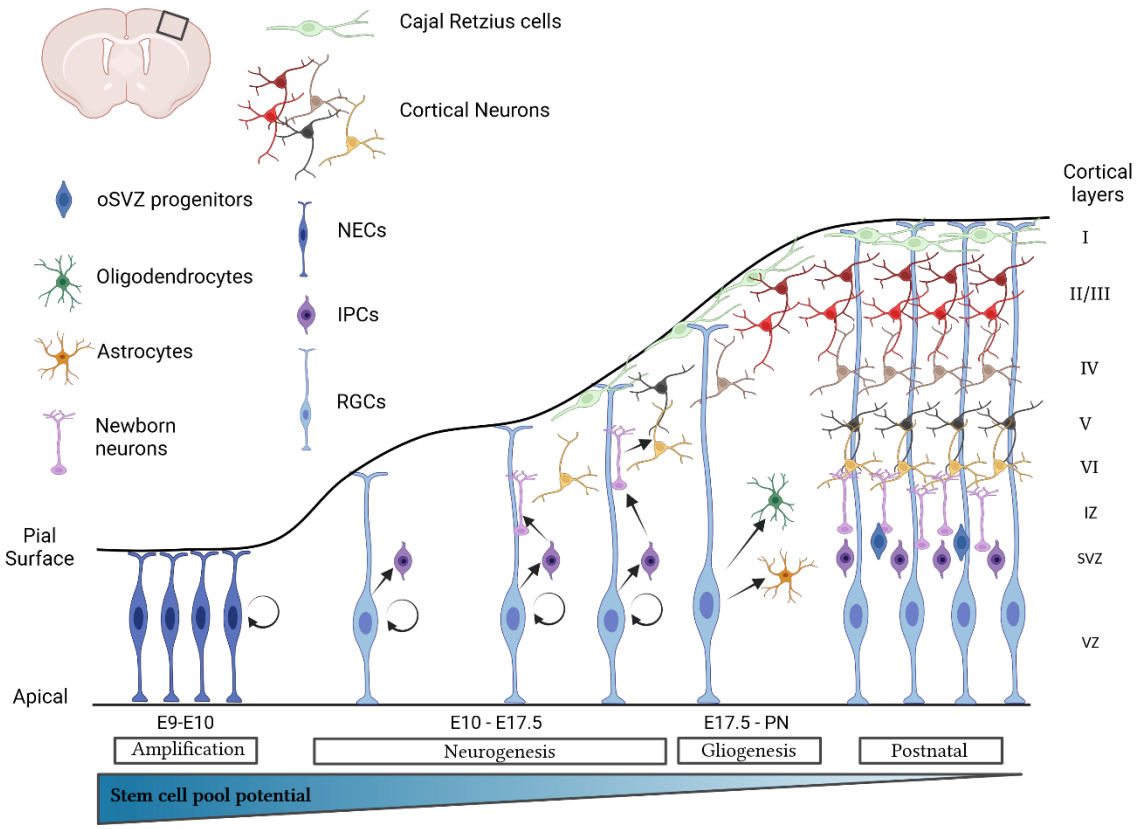

Figure 1.6: Formation and composition of the cerebral cortex layers.
Formation of the cortical layering in the brain during embryonic mouse development
Created with BioRender.com

I.3 Zika transmission and pathogenicity

I.3.1 ZIKV transmission cycles and vector competence

ZIKV is circulating via two transmission cycles: a sylvatic cycle and an urban cycle. During the sylvatic cycle, ZIKV is transmitted from its natural mosquito vector to non-human primates (NHP), which are thought to be the main animal reservoir of ZIKV. The mosquito genus *Aedes* is responsible for circulation and transmission of ZIKV in both the sylvatic and urban cycle. During the sylvatic cycle, ZIKV has been isolated from multiple *Aedes* species such as *Ae. opok*, *Ae. apicoargenteus*, *Ae. furcifer* and *Ae. aegypti formosus*[68]. In Africa, the sylvatic cycle is established and documented over time in several countries such as Senegal, Uganda, Nigeria, Central African Republic or Ivory Coast[69]. The few studies conducted in Asia, more specifically in Malaysia and Thailand, report a high ZIKV seroprevalence in NHP, suggesting established sylvatic cycles in Asia, at least in those areas[70,71]. By contrast, studies that have so far been conducted in Latin America found no or only very low seroprevalence in NHP, suggesting the absence of a sylvatic cycles of ZIKV[72]. However, most of the studies on the seroprevalence in NHP in Latin America were done in Brazil, leaving a lack of data for the other countries to confirm with certainty that a ZIKV sylvatic cycle is not present in this continent.

ZIKV transmission to the human population occurs during the urban cycle of the virus. In contrast to the sylvatic cycle where multiple *Aedes* species were identified as competent vectors, the urban cycle involves predominantly the African mosquito species *Aedes aegypti*[68]. Furthermore, a study on peridomestic ZIKV transmission in Gabon in 2007[73] along with several experimental studies revealed that the Asian *Aedes albopictus* mosquito species is also a competent vector of ZIKV[74].

I.3.2 Human to human transmission

Prior to the ZIKV epidemic in Brazil in 2015, the virus was assumed to be exclusively transmitted by mosquitoes. However, emerging clinical and preclinical findings demonstrated that ZIKV can also disseminate within the human population via either horizontal or vertical transmission, specifically between partners during sexual intercourse or from mother to fetus during pregnancy[75].

I.3.3 Horizontal transmission: Sexual intercourse

The sexual transmission of ZIKV has been documented in women with no known exposure to the mosquito vector but instead have been infected by symptomatic men who travelled to ZIKV-endemic areas[76]. Moreover, a study showed that ZIKV could persist for up to 6 months

after infection in human semen[77]. This potential chronic persistence of ZIKV in semen led the Centers for Disease Control and Prevention (CDC) to issue recommendations to men who have been travelling in endemic areas to adopt either abstinence behavior or contraceptive practices for at least three months[78]. This potential for sexual transmission is a unique characteristic of ZIKV among arboviruses[17].

I.3.4 Vertical transmission

The vertical transmission of ZIKV occurs when it is transmitted from the infected pregnant woman to her fetus through the placental barrier. While an accurate incidence of ZIKV vertical transmission is difficult to measure, however a study from a cohort of French Guinean patients estimated a transmission rate of around 18%[79]. The pathophysiological impact of ZIKV vertical transmission has been linked to several pre- and post-partum defects and abnormalities in fetuses and infants respectively, which have been collectively categorized as Congenital Zika Syndrome (CZS)[80]. The development of CZS has been correlated to the stage of pregnancy when ZIKV was contracted. Indeed, the prevalence of CZS is higher in infants that have been infected during the first trimester of pregnancy and decreases when infections occurred in the second or third trimester of pregnancy[81]. Unfortunately, no direct links could be established between the mother's viremia levels and the probability for the fetus to develop CZS and its severity[18]. This recent documentation of the vertical transmission of ZIKV as well as its associated congenital defects such as CZS has led to its inclusion as a new member of the TORCH (Toxoplasmosis, Other (Zika), Rubella, Cytomegalovirus, Herpes) panel of viruses.

I.3.5 Congenital Zika Syndrome

As described previously, ZIKV can lead to the development of a Congenital Zika Syndrome (CZS) that is characterized by severe peripartum clinical manifestations. The most common brain abnormalities (and their corresponding prevalence) observed in clinical studies are a reduction of the brain volume (92%), the presence of calcifications (92%), cortical malformations (89%) and ventriculomegaly (92%)[82], and microcephaly (varies between 33% and 64%)[18]. The following paragraphs will describe the different clinical manifestations in greater detail.

During perinatal examination, cortical malformations can be identified based on aberrant gyral patterns such as the overall reduction in gyration, polymicrogyria and/or heterotopia[82]. These aberrant gyral patterns are due to an altered neuronal migration and cortical organization which will lead to an excess (polymicrogyria) or lack of gyri (reduction in gyration) and misplaced

neurons (heterotopia). These abnormalities are detrimental causing epilepsy, developmental delay, intellectual disability or cerebral palsy[83]. Another common fetal cortical malformation is microcephaly which has been reported by multiple groups to be caused by the tropism of ZIKV for neural progenitors. ZIKV-infected neural progenitors exhibited abnormal division patterns[84], cell-cycle arrest[85], defective maturation and differentiation[86] and cell death[85]. These defects will result in abnormal neurogenesis within the cerebral cortex during fetal development and may ultimately lead to microcephalic phenotypes[18]. Another cortical malformation detected in CZS is ventriculomegaly which is a condition whereby the brain ventricles are enlarged and can occur when the cerebral spinal fluid (CSF) is trapped in the ventricle's spaces[87]. In relation, Pomar and co-workers reported that ZIKV caused peri-ventricular and germinative necrosis that led to ventriculomegaly[18].

Brain calcifications can occur in the parenchyma which results from the excess deposition of calcium in necrotic cells. The calcium deposit can also be present in proximity or within the blood vessels[88]. In the case of ZIKV infection, Chen *et al* reported that brain calcifications might also be the consequence of overexpression of osteogenic genes by fetal pericytes upon ZIKV infection[89].

As a consequence of the above-mentioned brain defects, children affected by CZS may present with a large spectrum of severe neurological sequelae such as motor disabilities that were predominantly characterized by hypotonia and/or hypertonia[90], epilepsy (which affects approximately 60% of CZS-affected infants)[91], and mental retardation[92]. Other complications associated with CZS include ocular malformations that may be vision-threatening[93] as well as arthrogryposis which consists of joint contractures[94].

While microcephaly should not be considered as the determinant marker in the development of CZS as its prevalence is lower than for ventriculomegaly and brain calcifications, the microcephaly development has shed light on the potentially severe consequences of a ZIKV fetal infection.

I.3.6 Guillain-Barré Syndrome

The recent ZIKV epidemics have uncovered a novel association between the incidence of ZIKV infections and the prevalence of Guillain-Barré Syndrome (GBS) patients. GBS is a rare but rapid-onset muscle weakness characterized by an auto-immune response that damages the peripheral nerves in humans. These patients typically present with symptoms such as muscles weakness, pain, numbness, problems with balance and coordination at the early stages of the

disease followed by progressive severity to paralysis of the limbs and face, difficulty walking, difficulties to breath and talk, persistent and/or severe pain[95]. In rare cases, GBS can lead to death, with a reported mortality rate of 2.8% in the USA[96]. However, most patients will fully recover with about 20% of affected patients retaining long-term disabilities[97]. There is no curative treatment for GBS patients but only symptomatic management strategies such as plasma exchange or intravenous immunoglobulin therapy for patients with severe symptoms to abrogate the auto-immune driven damage of the peripheral nerves[98]. The WHO reported an increase in incidence of 19% in GBS patients during the 2015 Brazilian ZIKV outbreak, although Barbi and co-authors reported a lower prevalence of ZIKV-associated GBS, namely 1.23%[97]. While the ZIKV-GBS association may appear low, the socio-economic burden upon affected countries was exorbitant reaching up to 10 billion US dollar for the entire Latin-American region during the ZIKV epidemics from 2015 to 2017(ref.[99]).

: General Introduction

Chapter II : Aim of the thesis

: Aim of the thesis

In 2015, the world experienced the emergence of ZIKV as a new public health threat. The development of neurological defects in infants infected *in utero* by ZIKV shed light on the dramatically altered pathogenic profile of a virus that was initially considered a benign virus. While ZIKV has evolved to give rise to two lineages, ZIKV outbreaks with increased cases of CZS were only linked to ZIKV strains of the Asian lineage.

Despite the efforts of a number of research groups, it remained unclear whether African ZIKV, like Asian ZIKV, poses a public health threat. Possible reasons might be the use of old or extensively passaged African ZIKV as well as the use of only a few ZIKV strains. By deploying multiple ZIKV strains that circulated more recently, in **chapter III**, we therefore wanted to define the epidemic potential of African ZIKV strains to that of their Asian counterparts. In addition, we also wanted to examine their pathogenic profile and their propensity to cause birth defects.

The Asian ZIKV lineage emerged decades ago from the African lineage and was first detected in the 1960s. However, the first Asian ZIKV outbreak associated with CZS was only reported in 2013. In **chapter IV**, we aimed to better understand whether the occurrence of the recent CZS-associated ZIKV outbreaks may be due to the acquisition of new traits and/or a change in the neuropathogenicity of epidemic Asian ZIKV compared to the pre-epidemic strains. Moreover, we sought to investigate which factors could have driven the changes in the pathogenic profile between pre-epidemic and epidemic Asian ZIKV.

The overall aim of the thesis is to determine whether African ZIKV strains pose a threat to public health and which factors during the Asian ZIKV evolution may have favored the sudden appearance of brain abnormalities in fetuses.

Chapter III : Recent African strains of Zika virus display higher transmissibility and fetal pathogenicity than Asian strains

III.1 Abstract

The global emergence of Zika virus (ZIKV) revealed the unprecedented ability for a mosquito-borne virus to cause congenital birth defects. A puzzling aspect of ZIKV emergence is that all human outbreaks and birth defects to date have been exclusively associated with the Asian ZIKV lineage, despite a growing body of laboratory evidence pointing towards higher transmissibility and pathogenicity of the African ZIKV lineage. Whether this apparent paradox reflects the use of relatively old African ZIKV strains in most laboratory studies is unclear. Here, we experimentally compare seven low-passage ZIKV strains representing the recently circulating viral genetic diversity. We find that recent African ZIKV strains display higher transmissibility in mosquitoes and higher lethality in both adult and fetal mice than their Asian counterparts. We emphasize the high epidemic potential of African ZIKV strains and suggest that they could more easily go unnoticed by public health surveillance systems than Asian strains due to their propensity to cause fetal loss rather than birth defects.

This chapter has been published in Nature Communications.

The mosquito work and the mathematical modelling were performed at Pasteur Institute Paris. The mouse work was performed at KU Leuven and Uliège.

Fabien Aubry‡, Sofie Jacobs‡, **Maïlis Darmuzey‡**, Sebastian Lequime, Leen Delang, Albin Fontaine, Natapong Jupatanakul, Elliott F. Miot, Stéphanie Dabo, Caroline Manet, Xavier Montagutelli, Artem Baidaliuk, Fabiana Gambaro, Etienne Simon-Lorière, Maxime Gilsoul, Claudia M. Romero-Vivas, Van-Mai Cao-Lormeau, Richard G. Jarman, Cheikh T. Diagne, Oumar Faye, Ousmane Faye, Amadou A. Sall, Johan Neyts, Laurent Nguyen, Suzanne J. F. Kaptein*, Louis Lambrechts*

III.2 Introduction

Zika virus (ZIKV) is a flavivirus mainly transmitted among humans through the bite of infected *Aedes aegypti* mosquitoes[100,101]. After its first isolation from a sentinel monkey in Uganda in 1947, ZIKV was shown to circulate in enzootic sylvatic cycles in Africa and continental Asia, but human infections were only sporadically reported for half a century[102–104]. The first documented human epidemic of ZIKV occurred in 2007 on the Pacific island of Yap, Micronesia[105]. Subsequent larger ZIKV outbreaks were recorded in French Polynesia and other South Pacific islands in 2013-2014 (refs.[106,107]). In May 2015, ZIKV was detected for the first time in Brazil from where it rapidly spread across the Americas and the Caribbean, causing an epidemic of unprecedented magnitude involving hundreds of thousands of human cases[108]. Whereas human ZIKV infections are usually asymptomatic or result in a self-limiting mild illness, ZIKV was associated for the first time with severe neurological complications such as Guillain-Barré syndrome (GBS) in adults, and congenital Zika syndrome (CZS), a spectrum of fetal abnormalities and developmental disorders including microcephaly, when mothers were infected during early pregnancy[21,109]. Within less than a decade, ZIKV went from a poorly known virus causing sporadic human infections in Africa and Asia to a nearly pandemic neurotropic virus with active circulation detected in more than 87 countries and territories[108]. Phylogenetic analyses of ZIKV genetic diversity identified two major ZIKV lineages referred to as the African lineage and the Asian lineage, respectively[28]. Strikingly, all ZIKV strains responsible for human outbreaks to date belong to the Asian lineage[108,110].

The explosiveness and magnitude of worldwide ZIKV emergence increased awareness and surveillance in regions with seemingly favorable conditions, such as Asia or Africa. Retrospective analyses of samples and surveillance programs in several Asian countries revealed that ZIKV had circulated at low but sustained levels for decades[111,112]. Improved case recognition shed light on small outbreaks in Singapore[113], Vietnam[114] and India[115] and led to the first reports of birth defects caused by indigenous ZIKV strains in South East Asia[116–119]. In Africa, where both ZIKV and *Ae. aegypti* mosquitoes are present, only one human outbreak was reported in the archipelago of Cape Verde between 2015 and 2017 (ref.[120]). Autochthonous ZIKV transmission was also detected in Angola during the same time period with four confirmed acute Zika cases and several suspected cases of microcephaly. Phylogenetic analyses revealed that the ZIKV strains detected in Cape Verde and Angola belonged to the Asian lineage and were probably independently imported from Brazil[121,122]. So far, the African ZIKV

lineage has never been detected outside the African continent and never been associated with epidemic transmission, birth defects or neurological disorders[108,110].

Surprisingly, a growing body of experimental evidence, both *in vitro* and *in vivo*, points towards a higher transmissibility and pathogenicity of the African ZIKV strains compared to their Asian counterparts[110]. African ZIKV strains typically cause more productive and more lethal infections than Asian strains in cell culture[86,123–128], they are more transmissible by mosquitoes[129–132] and they are associated with more severe pathology in adult mice and mouse embryos[128,133–141]. A few studies, however, reported evidence supporting the opposite conclusion in non-human primates[142–144], various cell types[145,146] and mosquitoes[140]. This discrepancy may reflect the lack of standard panels of ZIKV strains and/or the scarcity of recent African ZIKV strains available from public biobanks and laboratory collections. Indeed, most of the available African ZIKV strains were isolated several decades ago and often underwent numerous passages in cell culture and/or suckling mouse brains[147], questioning their biological relevance for comparative studies and experimental assessments of their epidemic potential.

To more rigorously assess the relative epidemic potential of the Asian and African ZIKV lineages, we compared their transmissibility by mosquitoes and pathogenicity in immunocompromised mice using a panel of seven recent, low-passage ZIKV strains representing the current viral genetic diversity. Using the newly generated empirical data and a previously described stochastic agent-based model[148], we performed outbreak simulations *in silico* to quantify the epidemiological dynamics of each ZIKV strain. Finally, we used a mouse model of ZIKV-induced microcephaly to evaluate the ability of the ZIKV strains to disrupt embryonic development *in utero*.

III.3 Materials and Methods

Ethics and regulatory information

Human samples. This study used fresh human blood to prepare mosquito artificial infectious blood meals. For that purpose, healthy blood donor recruitment was organized by the local investigator assessment using medical history, laboratory results and clinical examinations. Biological samples were supplied through the participation of healthy adult volunteers (seronegative for ZIKV) at the ICAReB biobanking platform (BB-0033-00062/ICAReB platform/Institut Pasteur, Paris/BBMRI AO203/[BIORESOURCE]) of the Institut Pasteur in the CoSImmGen and Diagmicoll protocols, which had been approved by the French Ethical Committee Ile-de-France I. The Diagmicoll protocol was declared to the French Research

Ministry under reference 343 DC 2008-68 COL 1. All human subjects provided written informed consent.

Animal experiments. The mouse experiments conducted at Institut Pasteur were approved by the Institut Pasteur Animal Ethics Committee (project number dap170045) and authorized by the French Ministry of Research (authorization number 12861). The Institut Pasteur animal facility had received accreditation from the French Ministry of Agriculture to perform experiments on live animals in compliance with the French and European regulations on the care and protection of laboratory animals (authorization number 75-15-01). Mouse experiments conducted in Belgium strictly followed the Belgian guidelines for animal experimentation and the guidelines of the Federation of European Laboratory Animal Science Associations. Mouse experiments were performed with the approval of the Ethical Committees of the Animal Research Center of KU Leuven (authorization number P019-2016) and of the University of Liège (authorization number 16-1837), in accordance with the guidelines of the Belgian Ministry of Agriculture, and in agreement with the European Community Laboratory Animal Care and Use Regulations (86/609/CEE, Journal Officiel des Communautés Européennes L358, 18 December 1986).

ZIKV strains

Seven low-passage ZIKV strains (≤5 passages in cell culture) were chosen based on their geographical origin and year of isolation to best represent the current breadth of ZIKV genetic diversity (Table S1). ZIKV strains were obtained from the World Reference Center for Emerging Viruses and Arboviruses at the University of Texas Medical Branch (PRVABC59, FSS13025), the Armed Forces Research Institute of Medical Sciences (PHL/2012/CPC-0740, THA/2014/SV0127-14), the Institut Louis Malardé in French Polynesia (PF13/251013-18) and the Institut Pasteur in Dakar (Kedougou2011, Kedougou2015). High-titered stocks were prepared and their infectious titers were measured by focus-forming assay[149,150] (FFA) or by plaque assay[151] in Vero cells. For FFA, a commercial mouse anti-flavivirus group antigen monoclonal antibody (MAB10216; Merck Millipore) diluted 1:1,000 in phosphate-buffered saline (PBS; Gibco Thermo Fisher Scientific) supplemented with 1% bovine serum albumin (BSA; Interchim) was used as the primary antibody. The secondary antibody was an Alexa Fluor 488-conjugated goat anti-mouse antibody (A-11029; Life Technologies) diluted 1:500 in PBS supplemented with 1% BSA.

Genome sequencing of ZIKV strains

The consensus genome sequences of the seven ZIKV strains of the panel were obtained by high-throughput sequencing[121,149]. Briefly, RNA was extracted from virus stock using QIAamp Viral RNA Mini Kit (Qiagen) and treated with TURBO DNase (Ambion). The Senegal_2011 and Senegal_2015 strains also underwent depletion of host ribosomal RNA following a homemade protocol. cDNA was produced with random hexameric primers (Roche) using M-MLV (Invitrogen) or Superscript IV (Thermo Fisher Scientific) reverse transcriptase. After second-strand synthesis with Second Strand Synthesis Buffer (New England BioLabs), dsDNA was used for library preparation using Nextera XT DNA Kit (Illumina) or NEBNext Ultra II RNA Library Prep kit (New England Biolabs) according to the manufacturer's instructions. The final libraries were checked on a Bioanalyzer (Agilent) and combined with other libraries from unrelated projects to be sequenced on an Illumina NextSeq 500 instrument (150 cycles, paired ends). Raw sequencing datasets were deposited to the European Nucleotide Archive database under accession number PRJEB39677. The sequencing data were processed through a custom pipeline[152]. Briefly, nucleotides with a quality score <30 were trimmed using Trimmomatic v0.36 (ref.[153]). Reads were filtered against the *Aedes albopictus* reference genome using Bowtie2 v2.3.4.3 (ref.[154]) and the remaining reads were subjected to *de novo* assembly with the Ray v2.3.1-mpi tool[155] or metaSPAdes[156]. Scaffolds were subjected to a blastn search in the nucleotide NCBI database using BLAST v2.2.40 (ref.[157]). The closest hit was used to produce a chimeric genome sequence that served as a reference to re-map the filtered reads with Bowtie2 v2.3.4.3 and generate a consensus sequence.

Phylogenetic analyses

Genome sequences of ZIKV and Spondweni virus were retrieved from GenBank. The nucleotide sequences were aligned using MAFFT[158]. The phylogenetic analyses were performed based on nucleotide (open reading frame), amino-acid, and codon alignments using the maximum-likelihood method with substitution models (GTR+F+G4, FLU+G+R3, and SCHN05+FU+R4, respectively) selected with ModelFinder[159]. Support for the tree was assessed with 1,000 ultrafast bootstrap replicates[160]. The consensus trees were reconstructed with IQ-TREE v1.6.3 (ref.[161]) and visualized in FigTree v1.4.4 (https://github.com/rambaut/figtree/releases). The phylogenetic tree root position was in agreement among the nucleotide-based tree without an outgroup (midpoint), amino-acid or codon tree with Spondweni virus as an outgroup, as well as with previously published ZIKV phylogenetic trees[162]. In addition to the seven genome sequences generated in this study, the

alignment used to construct the tree included 37 sequences from GenBank (accession numbers: MK241416; MF574587; KX198135; KU647676; KY693679; KU497555; MF794971; MK829154; MH882540; KY014295; MH063262; KY631494; KY693677; MF434522; MF801378; KU758877; KU937936; KY693680; KU509998; KX806557; LC191864; KU963796; MF036115; LC219720; MN190155; KY241695; MH013290; MK238037; KX051562; EU545988; KX377336; MN025403; MF510857; KU963574; KF268948; MK105975; KY288905).

Mosquitoes, mice and cell lines

Mosquitoes. All mosquito experiments used the 4th and 5th generations of an *Ae. aegypti* colony established from wild specimens caught in Barranquilla, Colombia, with the exception of the mouse-to-mosquito transmission experiment that used the 9th generation of an *Ae. aegypti* colony from Saint François, Guadeloupe and the 13th generation of an *Ae. aegypti* colony from La Lopé, Gabon. Mosquitoes were maintained under controlled insectary conditions (28°±1°C, 12h:12h light:dark cycle and 70% relative humidity)[149]. Larvae were reared in dechlorinated tap water supplemented with a standard diet of Tetramin (Tetra) fish food. Adults were kept in insect cages (BugDorm) with permanent access to 10% sucrose solution.

Mouse strains. In-house-bred, 6- to 12-week-old male AG129 mice (Marshall BioResources, Hull, UK), deficient in both interferon (IFN)-α/β and IFN-γ receptors, were used for experimental ZIKV infections. In-house-bred, 10-week-old male and female 129S2/SvPas mice deficient for IFN-α/β receptors (*Ifnar1*$^{-/-}$), were used for the mouse-to-mosquito ZIKV transmission assay. Time-mated, wild-type immunocompetent SWISS mice (Janvier Labs, Saint Berthevin, France) of 8-12 weeks of age were used for ZIKV vertical transmission experiments. Mice were maintained under standard housing conditions (18-23°C, 14h:10h light:dark cycle and 40-60% relative humidity).

Cell lines. The *Aedes albopictus* cell line C6/36 (ATCC CRL-1660) was used for amplification of all virus stocks and testing of mosquito saliva samples. C6/36 cells were maintained at 28°C under atmospheric CO_2 in Leibovitz's L-15 medium (Gibco Thermo Fisher Scientific) with 10% fetal bovine serum (FBS), 2% tryptose phosphate broth (Gibco ThermoFisher Scientific), 1× non-essential amino acids (Gibco ThermoFisher Scientific), 10 U/ml of penicillin (Gibco Thermo Fisher Scientific) and 10 µg/ml of streptomycin (Gibco ThermoFisher Scientific)[150,151]. The *Cercopithecus aethiops* cell line Vero (ATCC CCL-81) was used for titration of virus stocks by FFA. The *C. aethiops* cell line Vero E6 (ATCC CRL-1586) was used for titration of

virus stocks by plaque assay. Vero cells were maintained at 37°C under 5% CO_2 in Dulbecco's Modified Eagle Medium (Gibco Thermo Fisher Scientific) with 10% FBS, 10 U/ml of penicillin, and 10 µg/ml of streptomycin[150,151].

Mosquito exposure to ZIKV via artificial blood meals

Mosquitoes were orally challenged with ZIKV by membrane feeding[149]. Briefly, seven-day-old females deprived of sucrose solution for 24 hours were offered an artificial infectious blood meal for 15 min using a Hemotek membrane-feeding apparatus (Hemotek Ltd.) with porcine intestine as the membrane. Blood meals consisted of a 2:1 mix of washed human erythrocytes and ZIKV suspension. Adenosine triphosphate (Merck) was added to the blood meal as a phagostimulant at a final concentration of 10 mM. Fully engorged females were sorted on wet ice, transferred into 1-pint cardboard containers and maintained under controlled conditions (28°±1°C, 12h:12h light:dark cycle and 70% relative humidity) in a climatic chamber with permanent access to 10% sucrose solution. After 7, 10, 14, and 17 days of incubation, mosquitoes were paralyzed with triethylamine to collect their saliva *in vitro*. The proboscis of each female was inserted into a 20-µl pipet tip containing 10 µl of FBS. After 30 min of salivation, the saliva-containing FBS was mixed with 30 µl of Leibovitz's L-15 medium (Gibco Thermo Fisher Scientific), and stored at –80°C for later testing. The saliva samples were subsequently thawed and inoculated onto C6/36 cells for ZIKV detection by FFA as described above without subsequent dilution. Mosquito bodies were homogenized individually in 300 µl of squash buffer (Tris 10 mM, NaCl 50 mM, EDTA 1.27 mM with a final pH adjusted to 8.2) supplemented with 1 µl of proteinase K (Eurobio Scientific) for 55.5 µl of squash buffer. The body homogenates were clarified by centrifugation and 100 µl of each supernatant were incubated for 5 min at 56°C followed by 10 min at 98°C to extract viral RNA. Detection of ZIKV RNA was performed using a two-step RT-PCR reaction to generate a 191-bp amplicon located in a conserved region of the ZIKV genome between the 3' end of the *NS1* gene and the 5' end of the *NS2A* gene. Total RNA was reverse transcribed into cDNA using random hexameric primers and the M-MLV reverse transcriptase (Thermo Fisher Scientific) according to the following program: 10 min at 25°C, 50 min at 37°C and 15 min at 70°C. The cDNA was subsequently amplified using DreamTaq DNA polymerase (Thermo Fisher Scientific). For this step, 20-µl reaction volumes contained 1× of reaction mix and 10 µM of each primer, whose sequences are provided in Table S3. The thermocycling program consisted of 2 min at 95°C, 35 cycles of 30 sec at 95°C, 30 sec at 60°C, and 30 sec at 72°C with a final extension step of 7 min at 72°C. Amplicons were visualized by electrophoresis on a 2% agarose gel.

Mouse-to-mosquito ZIKV transmission assay

Ten-week-old 129S2/SvPas *Ifnar1*$^{-/-}$ mice (males and females) were intraperitoneally injected with a 200-µl inoculum containing 10^5 focus-forming units (FFU) of ZIKV (Cambodia_2010 strain). From day 1 to day 5 post inoculation, mice were anesthetized daily using 80 mg/kg of ketamine and 5 mg/kg of xylazine administered by the intraperitoneal route. Each anesthetized mouse was placed on the netting-covered top of two 1-pint cardboard boxes, each containing 25 two- to four-day-old *Ae. aegypti* females either from Guadeloupe or Gabon colonies, which differ significantly in their ZIKV susceptibility[163]. Mosquitoes previously deprived of sucrose solution for 24 hours were allowed to blood feed on the mouse for 15 min. Fully engorged females were sorted on wet ice, transferred into fresh 1-pint cardboard containers and maintained under controlled conditions (28°±1°C, 12h:12h light:dark light cycle and 70% relative humidity) in a climatic chamber with permanent access to 10% sucrose solution. After 14 days of incubation, saliva and bodies were collected and analyzed by FFA and RT-PCR as described above.

ZIKV experimental infections of immunocompromised mice

Survival. AG129 mice (6- to 12-week-old males) were intraperitoneally injected with 10^3 PFU of ZIKV (2 × 5 mice per ZIKV strain). Upon infection, mice were observed daily for changes in body weight and clinical symptoms of virus-induced disease including dehydration, hunched back, and paralysis. Mice were euthanized when body weight loss was >20% or when other humane endpoints were met according to the ethical guidelines. During days 1–8 of infection, mice were bled by submandibular puncture to monitor viremia kinetics. Plasma viremia was measured every other day from two alternating sub-groups of 5 mice each. Upon euthanasia, the brain, spinal cord, testis, and epididymis were collected and blood was collected by intracardiac puncture. After collection, tissues were immediately placed on dry ice and stored at –80°C until further processing.

Tissue tropism. AG129 mice (6- to 12-week-old males) were intraperitoneally injected with 1 PFU (8 mice per ZIKV strain). Upon infection, mice were observed daily for changes in body weight and clinical symptoms of virus-induced disease in case euthanasia would be required based on humane endpoints. Mice were bled by submandibular puncture on days 3, 4, and 5 post infection. On day 7 post infection, all animals were sacrificed and blood was collected by intracardiac puncture. All animals were euthanized by intraperitoneal injection of Dolethal (Vétoquinol). The brain, spinal cord, testis, epididymis, heart, liver and kidney were collected

after transcardial perfusion with PBS. After collection, tissues were immediately placed on dry ice and stored at –80°C until further processing.

ZIKV vertical transmission in immunocompetent mice

Intraplacental injections. Timed-mated, wild-type pregnant SWISS dams (8- to 12-week-old) were housed under standard conditions and allowed to acclimate for at least 24 hours upon receipt with access to food and water *ad libitum*. The surgeries were performed at the same time of day, with noon of the day after mating set as embryonic (E) 0.5. Preoperative analgesia was administered subcutaneously with 0.1 mg/kg of buprenorphine (Temgesic) before induction of anesthesia with isoflurane (Abbot Laboratories Ltd.) in an oxygen carrier. A 1.0- to 1.5-cm incision was performed through the lower ventral peritoneum and the uterine horns were careful extracted onto warm humidified gauze pads. The intraplacental injections of embryos were performed at E10.5 (ref.[84]). The fast green dye concentration was 0.05% and placenta was injected with either ZIKV or mock medium. The animals were randomly assigned to receive a 1.0- to 2.0-µl injection of mock medium or ZIKV stock containing 5×10^5 PFU/ml.

Immunohistochemistry. After dissection, E18.5 mouse heads and E14.5 embryos were fixed in 4% paraformaldehyde in PBS for 24h at 4°C. Brains were dissected in 0.1 M PBS (pH 7.4). E18.5 brains and E14.5 embryos were cryoprotected (20% sucrose in PBS) before being embedded in OCT (Richard-Allan Scientific Neg-50 Frozen Section Medium, Thermo Scientific) for cryosectioning 14-µm sections for brains and 20-µm sections for embryos (Leica) onto slides (SuperFrost Plus, VWR International). For fluorescence immunohistochemistry[84], a solution of antigen retrieval (Dako Target Retrieval Solution) was pre-heated at 95°C for 40 min and antigen retrieval of mouse brains and whole embryos were performed at 95°C for 5 min before incubation with primary antibodies. The primary antibodies were rabbit anti-cleaved caspase 3 (1:300, #9661, Cell Signaling Technologies), mouse anti-flavivirus group antigen (1:800, MAB10216, Merck Millipore) and goat anti-Iba1 (1:300, ab5076, Abcam). The respective secondary antibodies were donkey anti-rabbit, anti-mouse and anti-goat antibodies conjugated with Alexa Fluor-488, Alexa Fluor-555, and Alexa Fluor-647 (A-21206, A-31570, A-21447, Life Technologies) and diluted 1:1,000. Nuclei were counterstained with DAPI (1:1,000, Sigma) and mounted in Dako Fluorescence Mounting Medium (Agilent).

Image acquisition and processing. Immunofluorescence images of embryonic brains (E18.5) and internal organs (E14.5) were acquired in magnified fields (20× and 25×) with either Nikon

A1 or Zeiss LSM 880 AiryScan Elyra S.1 confocal microscopes and further processed with ImageJ 1.42q 276 (Wayne Rasband, National Institutes of Health), Fiji (v2.0.0-rc-54/1.51 h, https://imagej.net/Fiji) and Zen (Blue edition, Carl Zeiss Microscopy GmbH) software.

ZIKV detection and quantification in mouse samples

Quantification of ZIKV RNA by qRT-PCR. Total RNA was isolated from microdissected embryonic mouse (E14.5) tissues using Trizol (Ambion, Life Technologies) according to the manufacturer's protocol. For adult mouse samples, sections of whole tissue were weighed and transferred to 2-ml Precellys tubes containing 2.8-mm zirconium oxide beads (Bertin Instruments). RLT lysis buffer (RNeasy Mini Kit, Qiagen) was added at a ratio of 19 times the weight of the tissue section. Tissue sections were homogenized in three cycles at 6,800 Hz with 30-sec intervals using the Precellys24 homogenizer (Bertin Instruments). Homogenates were cleared by centrifugation (10 min, 14,000 rcf, 4°C) and total RNA was extracted from the supernatant using the RNeasy Mini Kit (Qiagen) according to the manufacturer's protocol. For plasma samples, viral RNA was extracted using the NucleoSpin RNA kit (Macherey-Nagel) following the manufacturer's instructions. Viral RNA was eluted in 50 µl of RNase-free water. Quantification of ZIKV genome copy numbers was performed by quantitative reverse transcription PCR (qRT-PCR) using the Applied Biosystems 7500 Fast Real-Time PCR System (Thermo Fisher Scientific). The Asian ZIKV strains were detected and quantified using a specific primer pair and a double-quenched probe (Integrated DNA Technologies). The African ZIKV strains were detected and quantified using the same probe as for the Asian ZIKV strains but a different primer pair to accommodate several mismatches. Standard curves were generated based on 10-fold serial dilutions of gBlock synthetic oligonucleotides (Integrated DNA Technologies) whose sequences were specific to the Asian and African ZIKV lineages. Ct values were converted into a relative number of ZIKV RNA copies/mg of tissue or ml of plasma using the formula $y=a*\ln(x)+b$, where a is the slope of the standard curve, b is the y-intercept of the standard curve and y is the Ct value for a specific sample.

Endpoint titration of infectious ZIKV. The amount of infectious virus present in brain and testis samples was estimated by 50% tissue-culture infectious dose ($TCID_{50}$) endpoint titration. Tissue sections were weighed and homogenized in 500 µl of Vero E6 cell culture medium (with 2% FBS) as described above. The homogenates were cleared by centrifugation (10 min, 14,000 rcf, 4°C). Vero E6 cells were seeded at a density of 1×10^4 cells/well in 96-well microtiter plates and incubated overnight. The next day, they were inoculated with triplicate 10-fold serial dilutions of the supernatant samples. After 7 days of incubation, the cells were examined

microscopically for virus-induced cytopathic effects. A well was scored positive if any signs of virus-induced cytopathic effects were observed compared to the uninfected control cells. The $TCID_{50}$/mg tissue was calculated using the method of Reed and Muench[164].

Statistics

Statistical analyses were performed using JMP v10.0.2 (www.jmpdiscovery.com), GraphPad Prism v8.02 (www.graphpad.com) and the packages *car*, *userfriendlyscience* and *DescTools* of R v3.6.0 (www.r-project.org). Binary variables were analyzed by logistic regression followed likelihood-ratio χ^2 tests. Body weight and $\log_{10}$-transformed viremia levels were compared by repeated measures analysis (restricted maximum likelihood method) using a mixed model in which ZIKV strain was nested within lineage, and mouse (random effect) was nested within ZIKV strain. Other continuous variables were analyzed by analysis of variance (ANOVA) when the underlying assumptions were satisfied. They were analyzed by Brown-Forsythe and Welch ANOVA when the homoscedasticity assumption was unmet and by Kruskal-Wallis rank-sum test when both the normality and the homoscedasticity assumptions were unmet. Survival curves were compared by log-rank test. Differences were considered statistically significant when $p<0.05$.

Epidemiological modeling

Model overview. To assess the epidemiological potential of ZIKV strains from empirically observed variation in mosquito infection dynamics, stochastic agent-based simulations were performed using the R package *nosoi*[148] (available from https://github.com/slequime/nosoi). This modeling framework accounts for the influence of within-host infection dynamics on transmission probability during mosquito-human infectious contacts in a full epidemiological context[165]. Virus transmission was assumed to only occur either between an infected human and an uninfected mosquito, or between an infected mosquito and an uninfected human. Sexual and vertical transmission modes were considered epidemiologically insignificant[166,167] and ignored in the model, and so were superinfections. The human and mosquito populations were considered homogeneous. Mosquito daily survival probability was set to 0.85 (ref.[168]). The daily number of mosquitoes biting a human was drawn from a Poisson distribution ($\lambda=2.1$) assuming a daily biting probability of 0.7 (ref.[169]) and a relative mosquito density of 3 (ref.[168]).

Human-to-mosquito transmission. Probabilities of human-to-mosquito ZIKV transmission were inferred from empirical data obtained with the mouse-to-mosquito transmission assay described above (Fig. S1). Mean transmission probabilities (μ) and their standard deviations

(sd) were estimated from the infection rates of mosquitoes tested by RT-PCR 14 days post infectious blood meal as described above. Transmission probabilities were used to derive a beta distribution of parameters $\alpha=((1-\mu)/sd^2-1/\mu)*\mu^2$ and $\beta=\alpha*(1/\mu-1)$ from which daily transmission probability for each simulated human was drawn until 6 days post infection. The parameters governing human-to-mosquito transmission were shared among all ZIKV strains.

Mosquito-to-human transmission. The cumulative proportion of infectious mosquitoes over time for each ZIKV strain was described by a two-parameter log-logistic model using the *drm* function in the R package *drc*[170]. This model (LL.2 equation in the *drm* function) has a lower limit fixed at 0 and an upper limit fixed at 1 and is given by the formula: $f(x,(b,e))=1/(1+\exp(b*\log(x)-e))$. The probability of mosquito-to-human transmission for each contact between a human and an infected mosquito was determined by the predicted transmission probability inferred for each ZIKV strain. For each mosquito, an individual extrinsic incubation period (EIP) was drawn from the empirically determined log-logistic distribution of EIP values (location = $\log(e)$, scale = $1/b$). The EIP value was used as a threshold for the individual probability of virus transmission over time. Transmission probability was 0% before the EIP and 100% after the EIP.

Implementation. Epidemiological simulations were run in R v3.6.0 using the packages *foreach* (https://cran.r-project.org/web/packages/foreach/foreach.pdf), *doParallel* (https://cran.r-project.org/web/packages/doParallel/doParallel.pdf), and *nosoi*[148]. The custom code is provided in Supplementary Software 1. Briefly, simulations were initiated with one infected human and zero infected mosquitoes and run for 400 days or until 100,000 humans or 1,000,000 mosquitoes were reached, whichever occurred first. A total of 100 independent replicate simulations were run for each ZIKV strain.

III.4 Results

To perform a comprehensive phenotypic characterization in both mosquito and mouse models, we assembled a set of seven recently isolated ZIKV strains based on their broad phylogenetic coverage, worldwide geographical distribution and minimal passage history. Our ZIKV panel included two recent strains from the African lineage (Senegal_2011; Senegal_2015), three non-epidemic strains from the Asian lineage (Philippines_2012, Cambodia_2010, Thailand_2014) and two epidemic strains from the Asian lineage (F_Polynesia_2013, Puerto_Rico_2015) (Table S3.1; Fig. 3.1).

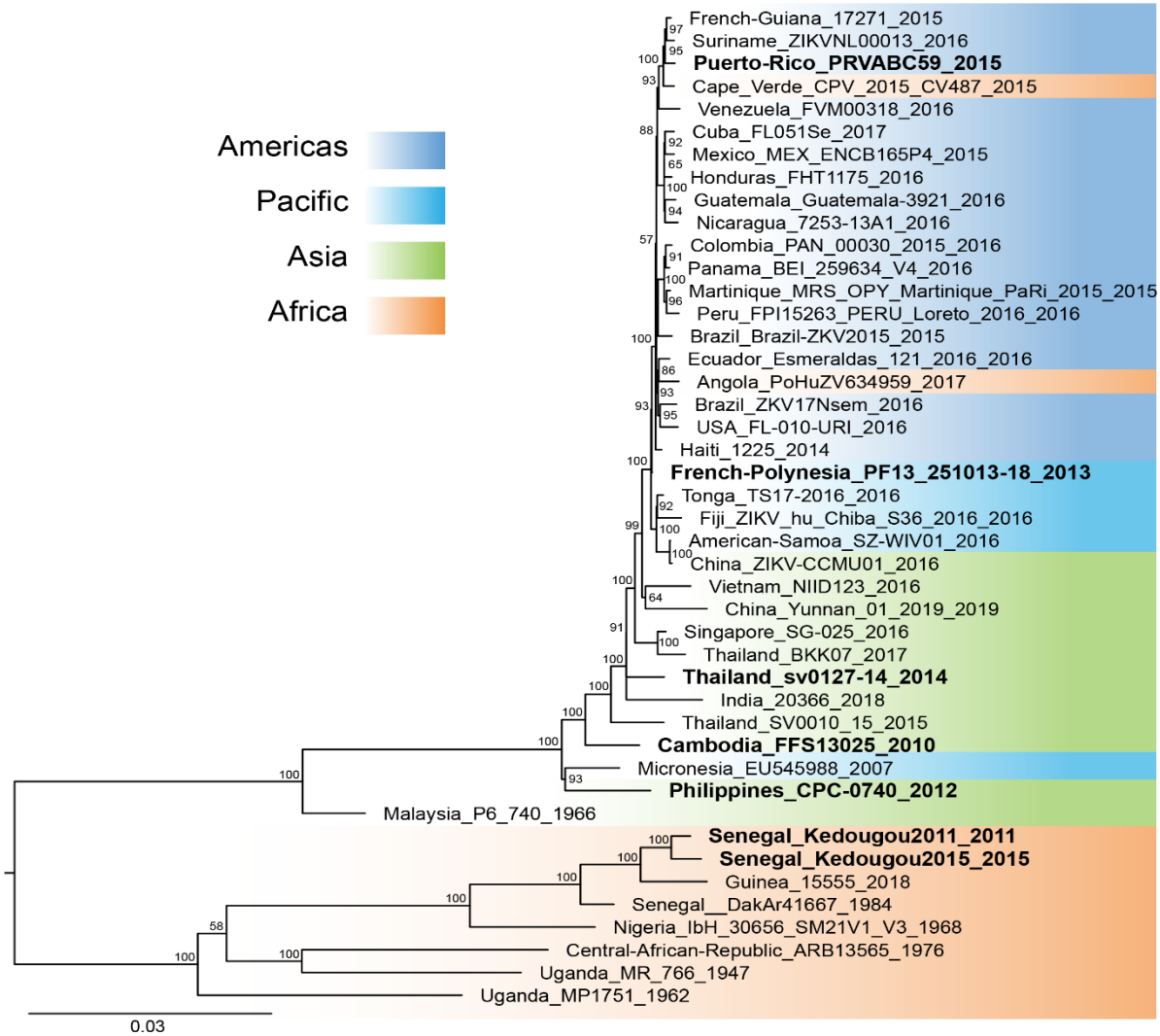

Figure 3.1: Phylogenetic position of ZIKV strains used in this study.

The phylogenetic tree shows the seven ZIKV strains of the panel (in bold) among a backdrop of ZIKV strains spanning the current viral genetic diversity. The colored background represents the geographic origin of ZIKV strains. The consensus tree was generated from 1,000 ultrafast bootstrap replicate maximum likelihood trees, using a GTR+F+G4 nucleotide substitution model of the full ZIKV open reading frame. The tree is midpoint rooted and the root position is verified by the Spondweni virus outgroup on amino-acid and codon-based trees. Support values next to the nodes indicate ultrafast bootstrap proportions (%) and the scale bar represents the number of nucleotide substitutions/site.

III.4.1 African ZIKV strains are more transmissible by mosquitoes than Asian strains

To evaluate variation in transmissibility by wild-type *Ae. aegypti* between the ZIKV strains, we examined the mosquito infection rate (proportion of blood-fed mosquitoes with body infection, determined by RT-PCR) and transmission efficiency [proportion of blood-fed mosquitoes with infectious saliva, determined by focus-forming assay FFA)] following exposure to an artificial infectious blood meal. We monitored infection rate and transmission efficiency from day 7 to day 17 post oral exposure because transmission rarely occurs and infection rates can be underestimated at earlier time points[171]. In a first experiment, mosquitoes were orally exposed to a relatively high dose of the five Asian ZIKV strains and of the Senegal_2015 strain. Experimental variation in infectious dose was minimal between the ZIKV strains, ranging from 5.6 to 5.8 $\log_{10}$ focus-forming units (FFU) per ml of artificial blood meal. Based on a typical blood meal size of 2.5 µl[172], this corresponded to an ingested dose ranging from 995 to 1,577 FFU per *Ae. aegypti* female. The mosquito infection rates were consistently high, ranging from 82% to 100% across ZIKV strains and time points (Fig. 3.2a). They did not differ statistically at any of the time points with the exception of day 7 (logistic regression: p=0.0155). In contrast, the transmission efficiency of the Senegal_2015 strain was significantly higher at all time points (logistic regression: p=0.0224 on day 7 and p<0.0001 at later time points), reaching 83% of infectious mosquitoes at the end of the time course (Fig. 3.2b). Infectious viral particles were detected in mosquito saliva as early as 7 days post blood meal for the Senegal_2015 strain and only after 10 days for the Cambodia_2010 strain, 14 days for the Philippines_2012, F_Polynesia_2013 and Puerto_Rico_2015 strains, and 17 days for the Thailand_2014 strain. Final transmission efficiency also differed between Asian strains, ranging from 10% for the Thailand_2014 strain to 50% for the F_Polynesia_2013 strain on day 17 post blood meal.

Next, we tested whether the superior transmissibility of the Senegal_2015 strain was representative of the African ZIKV lineage or specific to this strain. We conducted a second experiment that included the two African ZIKV strains of the panel and the F_Polynesia_2013 strain, which was the best-transmitted Asian strain in the first experiment. To avoid saturation and increase our ability to detect differences in infection rate, we used a lower infectious dose (4.7–4.8 $\log_{10}$ FFU/ml) than in the first experiment. Based on a typical blood meal size of 2.5 µl[172], this corresponded to an ingested dose ranging from 125 to 158 FFU per mosquito. The infection rates remained relatively high (68%–93%) for the two African strains, whereas it was significantly lower at all time points for the F_Polynesia_2013 strain (logistic regression: p=0.0384 on day 17 and p<0.0001 at earlier time points), increasing from 24% on day 7 to 59%

on day 17 (Fig. 3.2c). The difference was more striking (logistic regression: p=0.1086 on day 7 and p<0.0003 at later time points) for the transmission efficiency (Fig. 3.2d). Between day 7 and day 17, transmission efficiency of the Senegal_2015 and Senegal_2011 strains increased from 0% to 52% and from 7% to 70%, respectively, whereas no infectious particles were detected in any of the saliva samples collected from mosquitoes infected with the F_Polynesia_2013 strain throughout the time course. These results indicate that ZIKV strains of the African lineage, in general, display a significantly higher transmission potential than ZIKV strains of the Asian lineage.

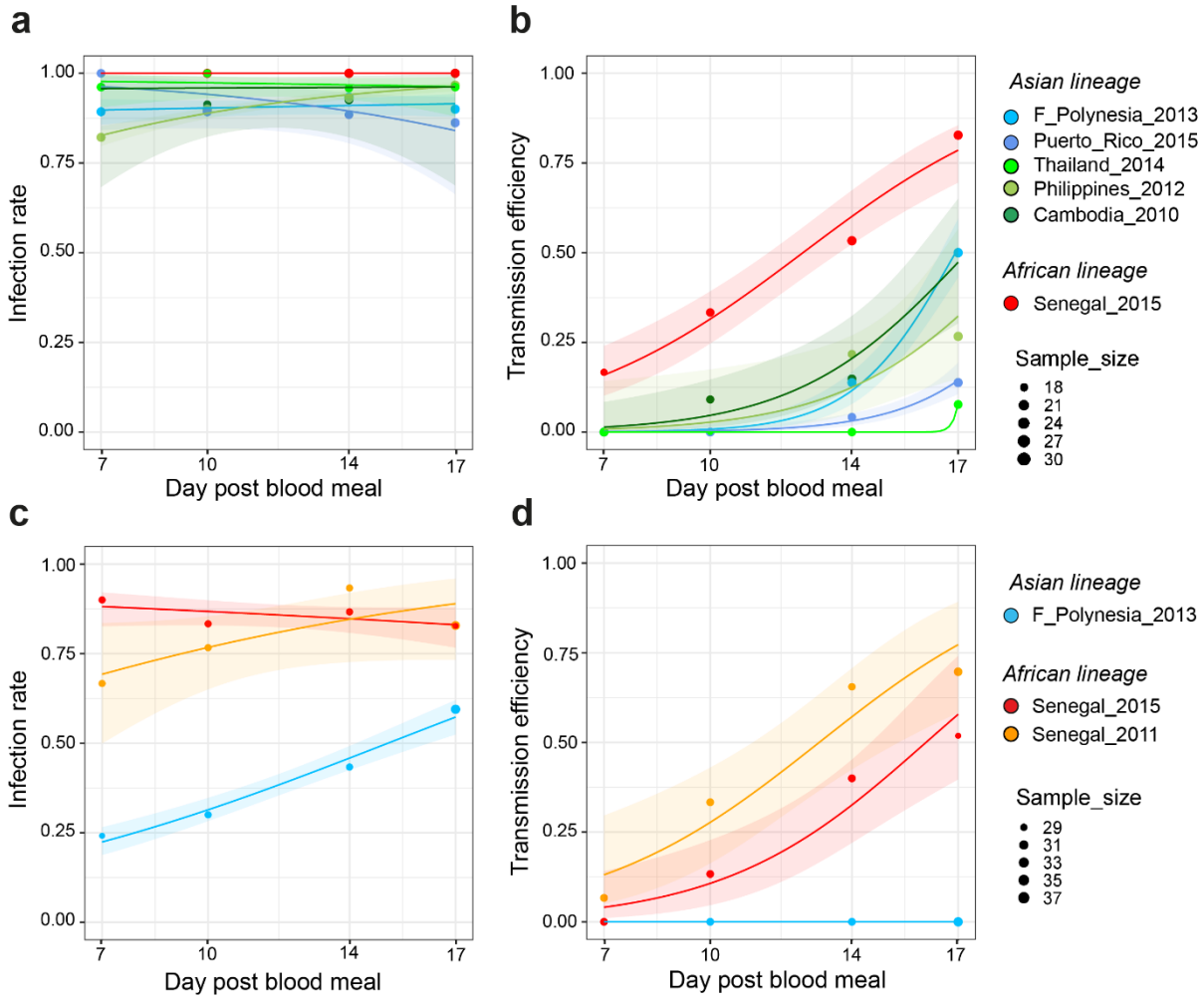

Figure 3.2: Mosquito infection rate and transmission efficiency of African and Asian ZIKV strains.

Wild-type *Ae. aegypti* mosquitoes from Colombia were orally exposed to ZIKV and collected on day 7, 10, 14 and 17 post infectious blood meal to analyze their carcasses and saliva samples collected *in vitro*. Infection rates and transmission efficiencies over time are shown for each ZIKV strain tested after oral exposure to a high dose (5.6–5.8 $\log_{10}$ FFU/ml) (**a**, **b**) or a low dose (4.7–4.8 $\log_{10}$ FFU/ml) (**c, d**) of virus. Infection rate is the proportion of ZIKV-positive carcasses among all blood-fed mosquitoes (determined by RT-PCR). Transmission efficiency is the proportion of blood-fed mosquitoes with infectious saliva (determined by FFA). The data points represent the empirically measured proportions, and their size is proportional to the sample size (high dose: n=18-30 mosquitoes per group; low dose: n=29-37 mosquitoes per group). The lines represent the logistic regression results and the shaded areas are the 95% confidence intervals of the logistic fits. Source data are provided as a Source Data file.

To translate the observed variation in transmissibility between ZIKV strains into differences in epidemic risk, we incorporated our empirical data into a stochastic agent-based model to perform outbreak simulations *in silico*. Mosquito-to-human ZIKV transmission events in the simulations were governed by log-logistic regression parameters (Table S2) estimated from the ZIKV strain-specific data obtained in the high-dose experiment described above (Fig. 3.2a and 2b). Human-to-mosquito transmission events depended on shared parameters among the ZIKV strains, which were derived from an independent experiment in which batches of naïve mosquitoes from Guadeloupe were allowed to feed daily on ZIKV-infected mice (Cambodia_2010 strain) during the course of their viremic period (Fig. S1). The magnitude of the outbreak was defined according to the number of secondary infections in a simulated population of 100,000 humans, ranging from a lack of outbreak (no secondary infection), to small-scale outbreaks (<100 secondary infections) and to large-scale outbreaks (>100 secondary infections). All ZIKV strains were able to cause secondary human infections, however the risk and magnitude of the outbreak greatly varied among the strains (Fig. 3.3). The proportion of simulations resulting in at least one secondary human infection ranged from 21% (Puerto_Rico_2015) to 63% (Senegal _2015). The proportion of small-scale outbreaks ranged from 2% (Senegal_2015) to 23% (Thailand_2014) and the proportion of large-scale outbreak ranged from 9% (Thailand_2014) to 61% (Senegal_2015). We did not observe a clear association between the epidemic or non-epidemic status of the ZIKV strains and the probability and magnitude of outbreaks. Using a less susceptible mosquito population from Gabon to model human-to-mosquito transmission events (Fig. S3.1) resulted in reduced epidemic potential for all ZIKV strains (Fig. S3.2). Together, the simulation results indicate that the higher transmissibility of the African ZIKV strains in our laboratory experiments translates into a markedly higher probability and size of human outbreaks predicted by our epidemiological model.

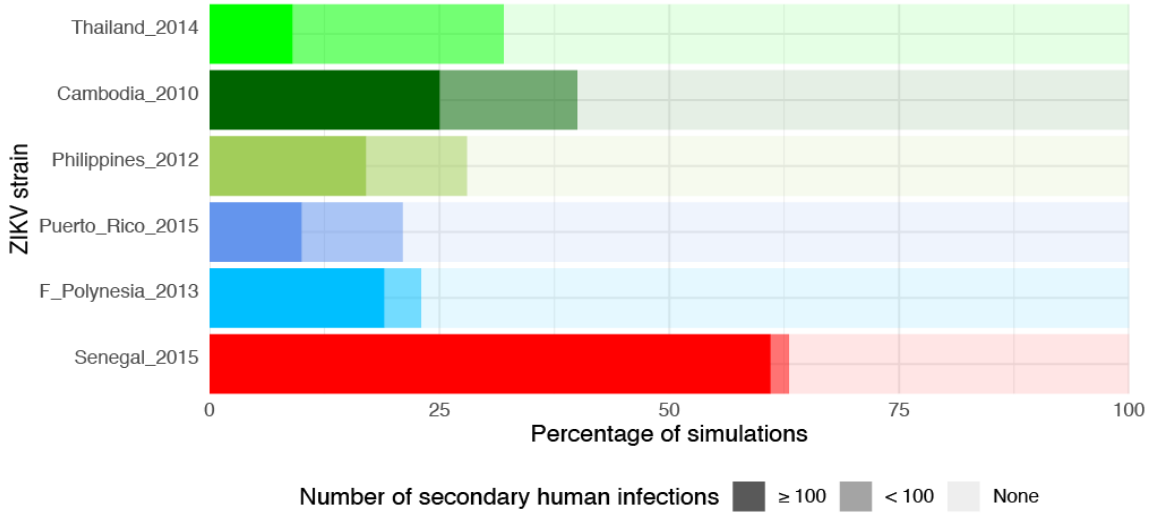

Figure 3.3: Simulated effect of empirical variation in ZIKV transmissibility on the risk and magnitude of human outbreaks.
A stochastic agent-based model was run 100 times based on the experimentally determined kinetics of mosquito transmission of six ZIKV strains. Other parameters of the model, such as the mosquito biting rate and infection dynamics within the human host, were shared between viruses. The figure shows the proportion of simulated outbreaks that resulted in ≥100, <100 and no secondary human infections.

III.4.2 African ZIKV strains are more lethal than Asian strains in immunocompromised adult mice

To assess the ability of ZIKV strains to cause more or less severe disease in a mammalian model, we inoculated AG129 mice with 10^3 plaque-forming units (PFU) of ZIKV and monitored their viremia, body weight and clinical signs of disease. Viremia levels ranged from 4.71 to 9.15 $\log_{10}$ viral RNA copies/ml of plasma and peaked on day 3 post infection except for the Philippines_2012 strain, for which viremia peaked on day 2 (Fig. S3.3). Across the viremic period, the average viremia level was 7.04 $\log_{10}$ viral RNA copies/ml for the African ZIKV lineage and 6.60 $\log_{10}$ viral RNA copies/ml for the Asian ZIKV lineage. Accounting for differences between strains within each ZIKV lineage and the random effect of individual mice, we found that the kinetics of viremia differed significantly between the Asian and the African ZIKV lineages (repeated measures analysis: $p<0.0001$). The viremia levels of African ZIKV strains increased with a lag but to higher levels during days 1-3 post infection, decreased faster during days 4-5 post infection, and increased again during days 5-6 post infection, relative to the Asian strains (Fig. S3.3). During the first 6 days of infection, the average body weight of mice infected with Asian ZIKV strains was 100.2% (range: 85.8%–109.0%) of their initial weight, however it was 92.8% (range: 74.4%–104.7%) for mice infected with African ZIKV strains (Fig. 3.4a). Accounting for differences between strains within each ZIKV lineage and the random effect of individual mice, the kinetics of body weight differed significantly between the Asian and the African ZIKV lineages (repeated measures analysis: $p<0.0001$). Mice infected with African ZIKV strains lost significantly more weight than mice infected with the

Asian strains during days 3-6 post infection (Fig. 3.4a). Following infection, mouse survival differed significantly between ZIKV strains (log-rank test: $p<0.0001$). All mice infected with the African ZIKV strains became morbid and reached humane endpoints on day 6 post infection (Fig. 3.4b). In contrast, mice infected with the Asian strains developed disease symptoms significantly later and only started to reach humane endpoints from day 9 post infection onwards. Their median time to death ranged from 10 to 10.5 days, with the exception of the Thailand_2014 strain for which 50% of the mice were still alive at the end of the follow-up period (Fig. 3.4b). These results show that both of our African ZIKV strains are more pathogenic overall than their Asian counterparts in immunocompromised adult mice.

AG129 mice are highly permissive to ZIKV[151] and viremia levels may thus easily saturate when they are inoculated with a high dose of virus. To avoid saturation and enhance our ability to detect differences in viral RNA levels in plasma and tissues, and to delay the onset of disease in mice infected with the African ZIKV strains, we performed another experiment with a 1,000-fold lower inoculum (1 PFU). This experiment included both African ZIKV strains and two Asian ZIKV strains recapitulating the variation seen in the previous experiment. The Thailand_2014 strain was chosen as a pre-epidemic strain displaying the most attenuated phenotype and the epidemic F_Polynesia_2013 strain represented the other Asian ZIKV strains. Surprisingly, using a 1,000-fold lower inoculum delayed the onset of disease by only one day for the African ZIKV strains, for which all mice had to be euthanized on day 7 post infection. This result clearly highlighted the higher pathogenicity of the African ZIKV lineage. To enable a proper comparison of viral RNA levels in mouse tissues between ZIKV strains, all the other mice were also euthanized on day 7 post infection to collect their organs. Lowering the inoculum delayed the peak of viremia in all ZIKV-infected mice, which occurred on day 5 post infection for the F_Polynesia_2013 strain and on day 4 for the other ZIKV strains (Fig. 3.4c). The level of plasma viremia was overall significantly higher (repeated measures analysis: $p<0.0001$) and decreased more sharply during days 4-5 post infection ($p<0.0001$) for the African ZIKV strains than for the Asian ZIKV strains (Fig. 3.4c). Likewise, viral RNA levels measured in organs collected on day 7 post infection were consistently higher for the mice infected with the African ZIKV strains (Fig. 3.4d). African ZIKV strains resulted in significantly higher viral loads than Asian strains in the brain ($p<0.0001$), spinal cord ($p<0.0001$), testis ($p<0.0001$), kidney ($p<0.0001$), and heart ($p<0.0001$). We confirmed that differences in viral RNA levels translated into differences in infectious titers in brain and testis samples, for which sufficient material was available to also perform endpoint titrations. Indeed,

we found that African ZIKV strains were associated with significantly higher levels of infectious virus in the brain (p<0.0001) and testis (p<0.0001) of infected mice than Asian strains (Fig. 3.4e). These results indicate that whereas ZIKV strains from both lineages can cause systemic infections with similar organ tropism in this mouse model, the African strains are more pathogenic and result in significantly higher morbidity and mortality.

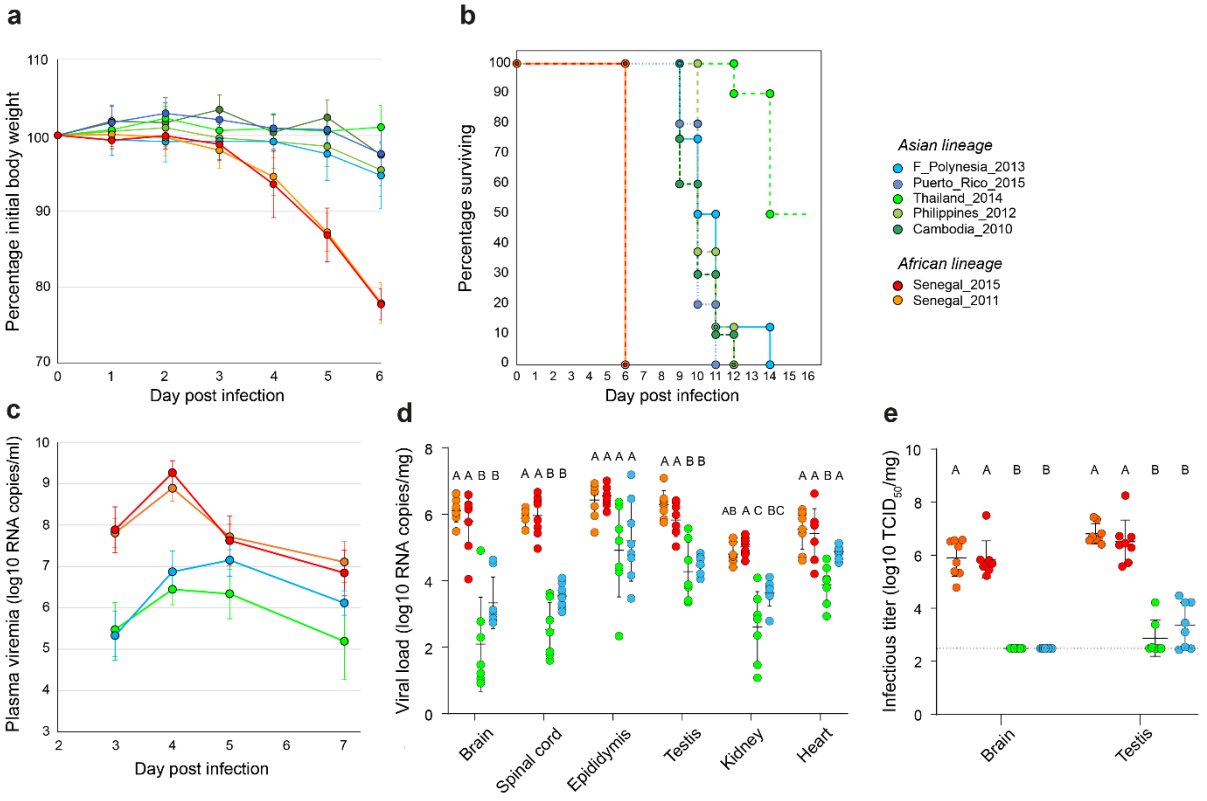

Figure 3.4: Pathogenicity of African and Asian ZIKV strains in immunocompromised adult mice.

In a first experiment (**a-b**), male AG129 mice were inoculated with 10^3 PFU of ZIKV. Each virus strain was represented by n=10 mice, with the exception of the F_Polynesia_2013 and Philippines_2012 strains that were represented by n=8 mice. (**a**) Mouse weight over time is shown as the percentage of body weight prior to infection (mean ± standard error). (**b**) Mouse survival over time is shown as the percentage of mice alive. Mice were euthanized when reaching humane endpoints (weight loss >20% or/and severe symptom onset). In a second experiment (**c-e**), male AG129 mice were inoculated with 1 PFU of ZIKV (n=8 mice per strain). (**c**) Time course of mouse viremia is shown in $\log_{10}$-transformed viral genome copies per ml of plasma (mean ± standard error). Three extreme outliers were excluded for the Senegal_2015 strain. (**d**) Viral loads in organs collected on day 7 post infection are shown in $\log_{10}$-transformed viral genome copies per mg of tissue. Statistical significance of differences was determined by one-way ANOVA followed by Tukey's post-hoc test for brain, heart and testis, by Brown-Forsythe and Welch ANOVA followed by Games-Howell's post-hoc test (two-sided) for epididymis and spinal cord, and by Kruskal-Wallis rank sum test followed by Dunn's post-hoc test (two-sided) for kidney. Viral loads were significantly higher for African than for Asian ZIKV strains in the brain (p<0.0001), spinal cord (p<0.0001), testis (p<0.0001), kidney (p<0.0001), and heart (p<0.0001). (**e**) Infectious virus in brain and testis collected on day 7 post infection are shown in $\log_{10}$-transformed 50% tissue-culture infectious dose ($TCID_{50}$) per mg of tissue. The horizontal dotted line indicates the lower limit of detection of the assay (310 $TCID_{50}$ units per mg of tissue). Statistical significance of differences was determined by Kruskal-Wallis rank-sum test followed by Steel-Dwass's post-hoc test for brain and by one-way ANOVA followed by Tukey's post-hoc test for testis. Infectious titers were significantly higher for African than for Asian ZIKV strains in the brain (p<0.0001) and testis (p<0.0001). In (**d-e**), data are presented as mean ± standard deviation and ZIKV strains not sharing a letter above the graph are statistically significantly different (p<0.05). Source data are provided as a Source Data file.

III.4.3 African ZIKV strain causes fetal death in immunocompetent mice

To investigate differences in vertical transmission phenotypes between ZIKV strains, we used a recent model of ZIKV-induced microcephaly by intraplacental injection in mouse embryos[84,173]. We first performed intraplacental injections of the Senegal_2015, Thailand_2014 and F_Polynesia_2013 ZIKV strains into the labyrinth of SWISS mouse embryos at E10.5 and compared the infection outcomes at E14.5. We observed subcutaneous edema in E14.5 embryos 4 days after intraplacental ZIKV injection for all strains (Fig. S3.4). Subcutaneous edema was significantly more frequent (p<0.0012) in embryos infected with the Senegal_2015 strain (91%; n=11) than in embryos infected with the Thailand_2014 strain (30%; n=16), the F_Polynesia_2013 strain (6%; n=16), or mock-injected embryos (0%; n=10). We next compared the extent of ZIKV systemic infection in E14.5 embryos following intraplacental injection at E10.5. ZIKV immunolabeling showed a comparable distribution of all ZIKV strains in brain, lung, heart, liver, intestine, eye, spinal cord and atriums of infected embryos (Fig. 3.5a; Fig. S3.5). The overall immunofluorescence staining was stronger for the Senegal_2015 and Thailand_2014 strains relative to the F_Polynesia_2013 strain. We confirmed these observations quantitatively by measuring viral RNA levels in the brain, lung, heart, liver and intestine. In all organs, viral loads differed significantly between ZIKV strains (p<0.0277), with the F_Polynesia_2013 strain consistently resulting in significantly lower viral loads than the Senegal_2015 strain, as well as the Thailand_2014 strain in most organs (Fig. 3.5b).

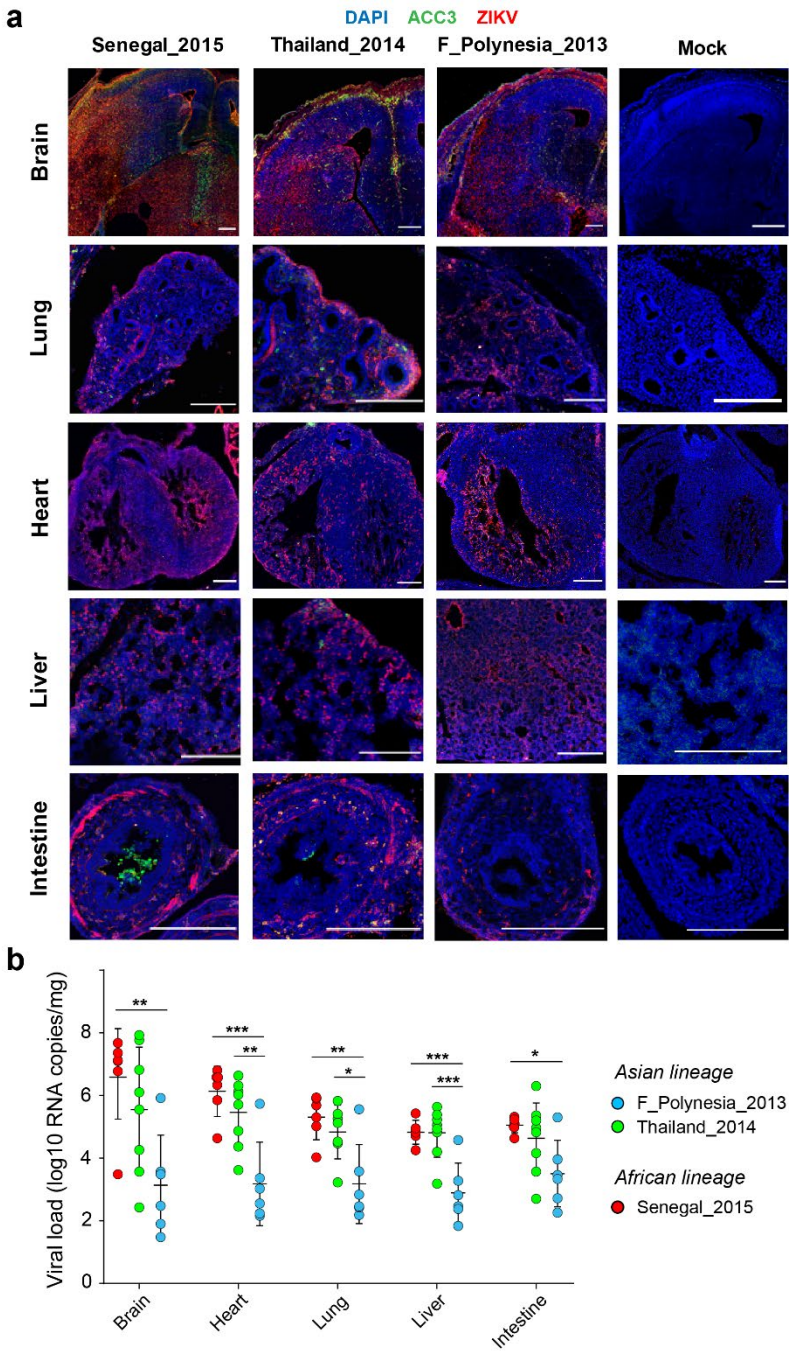

Figure 3.5: Organ tropism and viral load of African and Asian strains of ZIKV in vertically infected mouse embryos. Immunocompetent mouse embryos were infected at E10.5 by intraplacental injection of 500-1,000 PFU of ZIKV and analyzed at E14.5 by microdissection. (**a**) Immunolabeling of embryonic brain, lung, heart, liver and intestine sections representative of each ZIKV strain tested (n=3 embryos per strain). Blue, green and red colors indicate DAPI, anti-cleaved caspase 3 (ACC3) and ZIKV stainings, respectively. The scale bars represent 200 µm. (**b**) Viral load of embryonic brain, lung, heart, liver and intestine are shown for each ZIKV strain in viral genome copies per organ. Data are presented as mean ± standard deviation and represent n=6 mice for the Senegal_2015 and F_Polynesia_2013 strains and n=8 mice for the Thailand_2014 strain. Statistical significance of the differences was determined by one-way ANOVA followed by Tukey's post-hoc test and is only shown when significant (***p<0.001; **p<0.01; *p<0.05). Viral loads differed significantly between ZIKV strains (p<0.0277) in all organs. Source data are provided as a Source Data file.

To measure the impact of different ZIKV strains on embryonic brain development, we performed intraplacental injections at E10.5 and examined embryos at E18.5. Injection of the Senegal_2015 strain caused massive resorption resulting in the death of all infected embryos harvested at E18.5 (Fig. 3.6a). In contrast, infection with the Asian ZIKV strains (F_Polynesia_2013 and Thailand_2014) was not lethal to E18.5 embryos but resulted in a significant reduction ($p<0.05$) in head weight (Fig. 3.6c), cortical thickness (Fig. 3.6b and 6e) and number of cortical cells (Fig. 3.6f) compared to the mock-injected embryos. In addition, we detected a significant reduction in brain weight (Fig. 3.6d) and ventriculomegaly (Fig. 3.6b and 6g) with the Thailand_2014 strain but not the F_Polynesia_2013 strain. Together, these results show that ZIKV strains with higher levels of infection at E14.5 are also associated with more severe phenotypes at E18.5. The Senegal_2015 strain caused embryonic death before E18.5 and the Thailand_2014 strain resulted in more pronounced microcephaly and ventriculomegaly than the F_Polynesia_2013 strain.

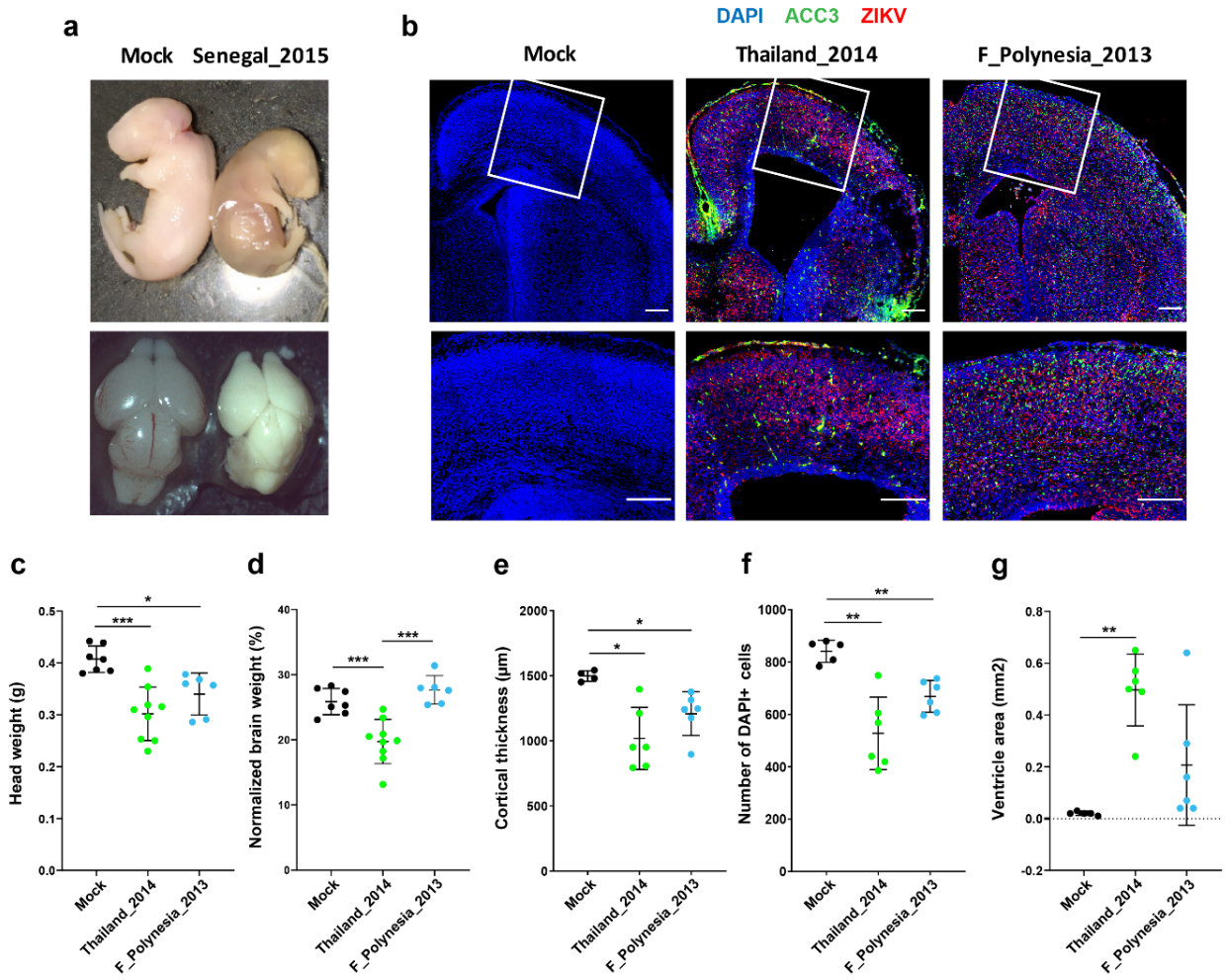

Figure 3.6: Brain phenotypes of mouse embryos vertically infected with African and Asian strains of ZIKV. Immunocompetent mouse embryos were infected at E10.5 by intraplacental injection of 500-1,000 PFU of ZIKV and analyzed at E18.5 by microdissection. (**a**) Representative view of E18.5 embryos (top) and dorsal view of E18.5 embryonic brains (bottom) after mock injection (left; n=10) or infection by the Senegal_2015 ZIKV strain (right; n=7). (**b-g**) Analyses of in utero brain development of E18.5 mouse embryos after mock injection (n=7 for head and brain measurements and n=5 otherwise) or infection by the Thailand_2014 (n=9 for head and brain measurements and n=6 otherwise) or the F_Polynesia_2013 (n=6) ZIKV strains. (**b**) Immunolabeling of embryonic brain sections representative of each ZIKV strain tested (top: full view; bottom: enlarged area within white frame). Blue, green and red colors indicate DAPI, anti-cleaved caspase 3 (ACC3) and ZIKV stainings, respectively. The scale bars represent 200 µm. (**c**, **d**) Embryonic heads and brains were examined morphologically by measuring (**c**) head weight and (**d**) brain weight normalized to head weight. (**e, f**) Microcephalic phenotypes were assessed by measuring (**e**) cortical thickness and (**f**) number of DAPI-positive cells. (**g**) Ventriculomegaly was estimated by measuring the ventricle area. In (**c-g**) data are presented as mean ± standard deviation. Statistical significance of differences was determined by Brown-Forsythe and Welch ANOVA followed by Tamhane's T2 multiple comparison test (two-sided). Only statistically significant differences are shown (***p<0.001; **p<0.01; *p<0.05). Embryos infected with the F_Polynesia_2013 and Thailand_2014 ZIKV strains had a significantly smaller head weight, cortical thickness and number of cortical cells than the mock-injected embryos (p<0.05).

III.5 Discussion

By comparing seven ZIKV strains representing the current breadth of viral genetic diversity worldwide, this study provides clear experimental evidence that recent African strains are more transmissible and potentially more pathogenic than Asian strains. In our experiments, ZIKV strains of the African lineage were more infectious to and were transmitted faster by wild-type *Ae. aegypti* mosquitoes from Colombia, translating into a higher epidemic potential in outbreak simulations. In addition, ZIKV strains of the African lineage were more pathogenic to immunocompromised adult mice and caused massive resorption and embryonic death in immunocompetent mouse embryos infected *in utero* by intraplacental injection.

Assessing ZIKV pathogenicity in the vertebrate host is complicated by the limited number of animal models that are available. Non-human primate infections closely emulate human infections but they raise ethical issues and are generally restricted to vaccine and drug development[174]. Several models of ZIKV pathogenesis in adult mice have been developed that recapitulate various features of human disease[133,175,176] In general, wild-type mice can be infected with ZIKV but they do not develop overt clinical illness and little or no viremia[133]. In contrast, mice lacking the ability to produce or respond to type I interferon typically develop severe neurological disease associated with high viral loads in key organs and substantial lethality. We used immunocompromised AG129 mice (deficient in interferon α/β and γ receptors) as a convenient proxy to assess pathogenesis in our panel of ZIKV strains. These mice are very susceptible to ZIKV infection[151], making them highly suitable to monitor viral kinetics and disease manifestations. ZIKV strains of the African lineage caused significantly more morbidity and mortality than did their Asian counterparts, despite a similar tissue tropism. Of note, the level of pathogenicity observed in the immunocompromised adult mice model was not associated with the epidemic or non-epidemic status of the Asian ZIKV strains. ZIKV also has the potential to antagonize innate immune responses of the host, which may involve various ZIKV proteins[49–51,124,177]. The mechanism by which the antagonistic effect is brought about may be shared by ZIKV strains from both lineages[49,178], may be strain- or lineage-dependent[134,179], or has only been described for specific ZIKV strains[49]. However, immunocompromised mouse models are not suitable for comparing the ability of ZIKV strains to suppress or evade the host's immune system, which may additionally contribute to their epidemic potential.

Our findings from the mosquito infection experiments and the immunocompromised mouse model support the hypothesis that worldwide ZIKV emergence in the last 15 years was not driven by adaptive virus evolution[101]. We found no evidence for enhanced transmission by the

primary epidemic vector, *Ae. aegypti*, or increased level and/or duration of viremia in the vertebrate host between epidemic Asian ZIKV strains (F_Polynesia_2013 and Puerto_Rico_2015) and non-epidemic Asian ZIKV strains (Cambodia_2010, Philippines_2012 and Thailand_2014). The Asian ZIKV strain that gave rise to the widespread epidemics in the Pacific and the Americas was probably not selected for its superior ability to infect mosquitoes and/or humans. Instead, it seems more likely that it was stochastically introduced through increased air travel and human mobility in regions with favorable epidemic conditions such as high densities of competent vectors and immunologically naïve human populations[180].

The lack of human outbreaks associated with the African lineage of ZIKV until now[108] is paradoxical because a large majority of experimental studies have found a higher transmissibility and pathogenicity of the African ZIKV strains relative to their Asian counterparts[86,123–128]. We hypothesized that this discrepancy could have reflected the lack of recent, low-passage African strains available for experimental studies. Our panel included two ZIKV strains isolated in Senegal in 2011 and 2015, which are several decades more recent than most of the African ZIKV strains used in earlier studies. Note that our two African ZIKV strains were isolated from mosquito pools whereas the Asian strains that were isolated from human serum samples, however all virus stocks were produced in mosquito cells prior to the experiments. Our study unequivocally confirms that the African lineage of ZIKV is associated with higher transmissibility and pathogenicity. The reasons why African ZIKV strains have so far not been responsible for human outbreaks (or remained unnoticed) are unknown, but may include the lack of awareness prior to the worldwide emergence, the paucity of surveillance programs in resource-poor countries, protective effects of herd immunity or cross-reactive antibodies, and/or the lower vectorial capacity of African mosquito populations.

Most ZIKV infections in humans are asymptomatic and the majority of symptomatic infections cause a non-specific acute febrile illness that can easily be mistaken for other common viral infections[181]. In the absence of severe infection outcomes such as GBS or CZS, low-level ZIKV circulation or even small-scale outbreaks could have gone unnoticed, especially before the emergence in the Pacific and Americas when ZIKV was still largely unknown. The worldwide emergence of ZIKV raised international awareness, resulting in improved surveillance including the implementation of epidemiological studies in regions where the virus was known to be present prior to the pandemic. Seroprevalence studies recently conducted across Africa generally found a low level (<6.2%) of specific anti-ZIKV antibodies[182–186]. These studies are consistent with low-level ZIKV circulation in human populations of Africa and rule out the

hypothesis that a high level of herd immunity is the main factor preventing ZIKV outbreaks in Africa. The alternative hypothesis that sustained circulation of closely related flaviviruses such as dengue virus (DENV) confers cross protection against ZIKV is also unlikely because high DENV seroprevalence has not prevented the emergence of ZIKV in South America, the Caribbean and the Pacific[187].

A possible explanation for the lack of ZIKV outbreaks in Africa despite the high epidemic potential of African ZIKV strains is a reduced vectorial capacity of African *Ae. aegypti* populations. ZIKV has been isolated from multiple mosquito species, but *Ae. aegypti* is considered the main vector of transmission between humans in the urban cycle[100,101]. In the absence of an efficient urban vector, human ZIKV infections in Africa would be limited to spillover transmission events from the sylvatic cycle via bridge vectors, which could explain the low level of ZIKV circulation[186,188]. Large-scale human outbreaks of dengue, yellow fever and chikungunya presumably mediated by *Ae. aegypti* in Africa[189,190] provide evidence that the density and human biting rate of African *Ae. aegypti* populations are sufficient to sustain urban transmission cycles. However, we recently discovered that African *Ae. aegypti* populations are significantly less susceptible to ZIKV infection than non-African populations using essentially the same panel of ZIKV strains as in the present study[163]. Although the Senegal_2015 strain was more infectious to mosquitoes relative to the other ZIKV strains, African *Ae. aegypti* populations were overall less susceptible than non-African *Ae. aegypti* populations regardless of the ZIKV strain[163]. This difference mirrors the existence of the two subspecies, *Ae. aegypti aegypti* and *Ae. aegypti formosus*, which were recognized by early taxonomists and later confirmed by modern population genetics[191]. Lower ZIKV susceptibility of the African subspecies *Ae. aegypti formosus* could have limited human ZIKV outbreaks in Africa in spite of the higher transmissibility of African ZIKV strains. This hypothesis is consistent with earlier reports of epidemic ZIKV transmission in Angola where the mosquito population consists of a genetic mixture of *Ae. aegypti aegypti* and *Ae. aegypti formosus*[192].

An important implication of our study is that the African lineage of ZIKV should be considered a major threat to public health. Although African ZIKV strains have so far never been associated with human ZIKV outbreaks, our results with wild-type *Ae. aegypti* from Colombia indicate that they may have greater epidemic potential than Asian strains if exported to regions where epidemic ZIKV transmission is realistic. We also point out that the African ZIKV strains may be associated with distinct clinical features allowing them to more easily escape surveillance systems. Our observations in an immunocompetent mouse model indicate that infection *in utero*

by African ZIKV led to fetal death, rather than birth defects. Although this finding remains to be confirmed in humans, it is consistent with the lack of reported CZS in Africa. The only confirmed cases of birth defects in Africa were caused by ZIKV strains from the Asian lineage[193]. A few suspected cases were reported in Guinea-Bissau in 2016 where the African ZIKV lineage had been detected but these have never been confirmed[194]. On the other hand, CZS is a rare symptom and its absence may also simply reflect the lack of large-scale epidemics that would allow its detection.

Bayesian reconstruction of a dated phylogenetic tree for ZIKV[23] estimated that African and Asian lineages diverged from their common ancestor between 1814 and 1852 (95% highest posterior density interval). Although viral genetic changes are generally considered the most likely explanation for the dramatic emergence and neuroinvasiveness of ZIKV within the Asian lineage[23,103], whether divergent evolution of the African and Asian lineages was driven by differential selective pressures is still an open question[110]. The lack of a sylvatic transmission cycle of ZIKV outside Africa[101] could have played an important role in the evolutionary divergence of the two lineages. However, enzootic transmission of African ZIKV strains between sylvatic mosquito species and non-human primates is at odds with their higher potential for epidemic transmission by *Ae. aegypti*, relative to Asian ZIKV strains, which are thought to primarily alternate between *Ae. aegypti* and humans[101]. Possibly, introduction of ZIKV into Asia after the mid-19th century could have been accompanied by a fitness drop due to a founder effect. Identifying the nucleotide variants underlying the phenotypic differences between the African and Asian ZIKV lineages will likely prove challenging because the nucleotide divergence between the two lineages is ~12%, which translates into more than 100 different amino-acid residues across the open reading frame[128]. In contrast, for instance, the American ZIKV strains typically differ from the rest of the Asian strains by less than ~30 amino-acid residues. Moreover, the phenotypic differences between the two lineages likely result from complex combinations of genetic variants[23181], making them less tractable by conventional methods of reverse genetics.

It also remains to be elucidated whether fetal harm has always been a possible consequence of ZIKV infection during pregnancy or whether ZIKV has recently acquired mutations conferring the ability to cause fetal harm. The recent detection of three CZS cases in Thailand and Vietnam suggest that both non-epidemic and epidemic Asian ZIKV strains are neurotropic and able to be vertically transmitted during pregnancy[117–119]. Our results, supported by recent studies performed in mouse models of vertical ZIKV transmission[138,197], indicate that African ZIKV

strains also possess the ability to cross the placenta and cause adverse perinatal outcomes. This is consistent with *in vitro* studies showing that ZIKV strains from both the African and the Asian lineages are capable of infecting different cell types of the placental barrier such as midgestation amniotic epithelial cells, cytotrophoblasts, placental villous macrophages of fetal origin (Hofbauer cells), and endothelial cells[127,198–200]. Collectively, these results reinforce the hypothesis that neurotropism and vertical transmission are not novel features of a recently emerged ZIKV variant, but rather an ancestral feature of ZIKV. In our intraplacental ZIKV challenge model, the non-epidemic Thailand_2014 strain was associated with more adverse outcomes than the epidemic F_Polynesia_2013 strain, whereas the Senegal_2015 strain led to fetal loss. Thus, ZIKV could have evolved towards attenuation by causing birth defects rather than fetal loss, supporting the counter-intuitive idea that attenuation was key to the recognition of ZIKV pathogenicity.

III.6 Supplementary Data

Supplementary Table 3.1: ZIKV strains included in this study. The name of the ZIKV strains used in the study with their country of origin, original strain name, source of isolation, year of collection and the passage history prior to use in this study are indicated. TS: *Toxorhynchites splendens* mosquitoes; C6/36: *Aedes albopictus* cells; Vero: green monkey kidney cells; SM: suckling mouse brains.

Name in this study	Country	Strain ID	Source	Year	Passage history
F_Polynesia_2013	French Polynesia	PF13/251013-18	Human serum	2013	C6/36-4
Puerto_Rico_2015	Puerto Rico	PRVABC59	Human serum	2015	Vero-2; C6/36-3
Philippines_2012	Philippines	CPC-0740	Human serum	2012	TS-1; C6/36-2; Vero-1; C6/36-1
Thailand_2014	Thailand	SV0127-14	Human serum	2014	TS-1; C6/36-2; Vero-1; C6/36-1
Cambodia_2010	Cambodia	FSS13025	Human serum	2010	Vero 2; SM-1; C6/36-1
Senegal_2011	Senegal	Kedougou2011	Pool of *Aedes* spp. and *Mansonia* spp.	2011	C6/36-2
Senegal_2015	Senegal	Kedougou2015	Pool of *Aedes* spp. and *Mansonia* spp.	2015	C6/36-2

Supplementary Table 3.2: Parameter estimates of mosquito-to-human transmission events. The transmission kinetics of each ZIKV strain were modeled with a two-parameter log-logistic function to estimate their extrinsic incubation period (EIP) distribution. In the epidemiological simulations, the probability of mosquito-to- human transmission for each contact between a human and an infected mosquito was determined by the transmission probability inferred for each ZIKV strain from the EIP log-logistic distributions of location = log(e), and scale = 1/b.

	Log-logistic parameter estimates	
ZIKV strain	*e*	*b*
F_Polynesia_2013	16.60	–10.83
Puerto_Rico_2015	20.74	–8.17
Thailand_2014	18.76	–24.86
Philippines_2012	19.01	–5.72
Cambodia_2010	17.66	–4.99
Senegal_2015	12.05	–3.24

Supplementary Table 3.3: Oligonucleotides used in this study.

Application	Oligo	Sequence (5'-3')
ZIKV RNA quantification in mosquito experiments	Forward Primer	GTATGGAATGGAGATAAGGCCCA
	Reverse primer	ACCAGCACTGCCATTGATGTGC
ZIKV RNA quantification in mouse experiments (Asian strains)	Forward primer	CCGCTGCCCAACACAAG
	Reverse primer	CCACTAACGTTCTTTTGCAGACAT
	Probe	6FAM/AGCCTACCT/ZEN/TGACAAGCAATCAGACACTCAA/ 3'IABkFQ
ZIKV RNA quantification in mouse experiments (African strains)	Forward primer	GTCGCTGTCCAACACAAG
	Reverse primer	CACCAGTGTTCTCTTGCAGACAT
	Probe	6FAM/AGCCTACCT/ZEN/TGACAAGCAATCAGACACTCAA/ 3'IABkFQ
ZIKV RNA standards in mouse experiments (Asian strains)	gBlock	GAGGCATCAATATCAGACATGGCTTCTGACAGCCGCTGC CCAACACAAGGTGAAGCCTACCTTGACAAGCAATCAGAC ACTCAATATGTCTGCAAAAGAACGTTAGTGGACAGAGGCT GGGGAAATGGATGTGGACT
ZIKV RNA standards in mouse experiments (African strains)	gBlock	GAGGCATCAATATCGGACATGGCTTCGGACAGTCGCTGT CCAACACAAGGTGAAGCCTACCTTGACAAGCAATCAGAC ACTCAATATGTCTGCAAGAGAACACTGGTGGATAGAGGTT GGGGAAATGGGTGTGGACT

Supplementary Figure 3. 1: Mouse-to-mosquito ZIKV transmission probability over time. The lines represent the proportion of *Ae. aegypti* mosquitoes from Gabon (left) or Guadeloupe (right) that tested ZIKV-positive 14 days after taking a blood meal on the same triplet of *Ifnar1*$^{-/-}$ mice inoculated with 10^5 FFU of the Cambodia_2010 ZIKV strain on day 0. A median of 11 females per time point and per mouse (range 2-17) were tested for the Gabon population. A median of 13 females per time point and per mouse (range 0-19) were tested for the Guadeloupe population. The gold dashed lines represent the transmission probabilities for the 3 individual mice during their viremic period and the black line represent their mean. Horizontal ticks indicate the 95% confidence intervals of the probabilities. Source data are provided as a Source Data file.

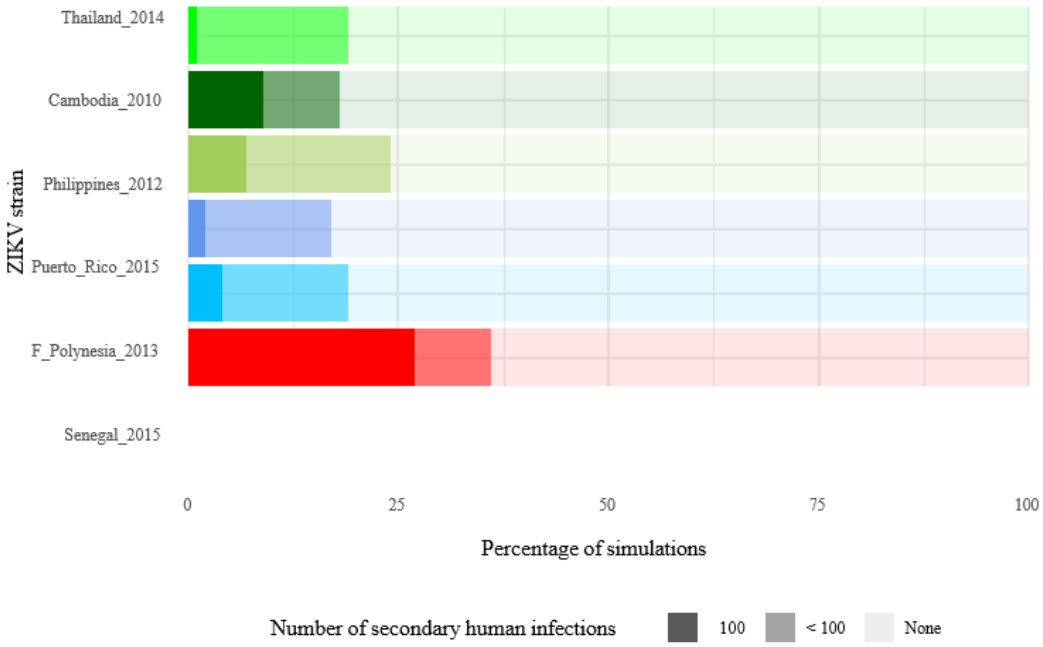

Supplementary Figure 3.2: Simulated effect of empirical variation in ZIKV transmissibility on the risk and magnitude of human outbreaks with reduced mosquito susceptibility. The figure shows the simulations results of Fig. 3 when the highly ZIKV susceptible mosquito population from Guadeloupe is replaced with a less susceptible mosquito population from Gabon (Fig. S1) to parameterize human-to- mosquito transmission events.

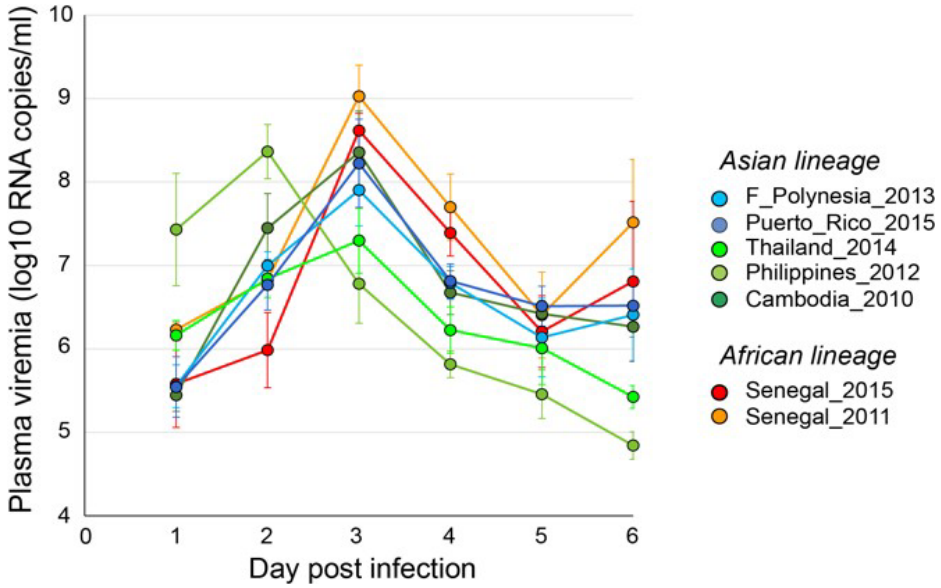

Supplementary Figure 3.3: Variation in viremia kinetics between ZIKV strains after inoculation of a high virus dose. Time course of ZIKV viremia in AG129 mice inoculated on day 0 with 10^3 PFU of ZIKV. Viremia is expressed in $\log_{10}$-transformed viral genome copies per ml of plasma (mean ± standard error). Each virus strain is represented by n=5 mice on each day, with the exception of day 6 for the Senegal_2011 and Senegal_2015 strains that are represented by n=10 mice. Source data are provided as a Source Data file.

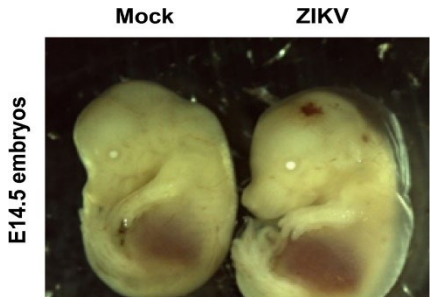

Supplementary Figure 3.4: Intraplacental injections of ZIKV induce subcutaneous edema. Photos show representative E14.5 embryos after intraplacental injection of mock inoculum (left; *n*=10 embryos) or Senegal_2015 ZIKV strain (right; *n*=9 embryos) at E10.5.

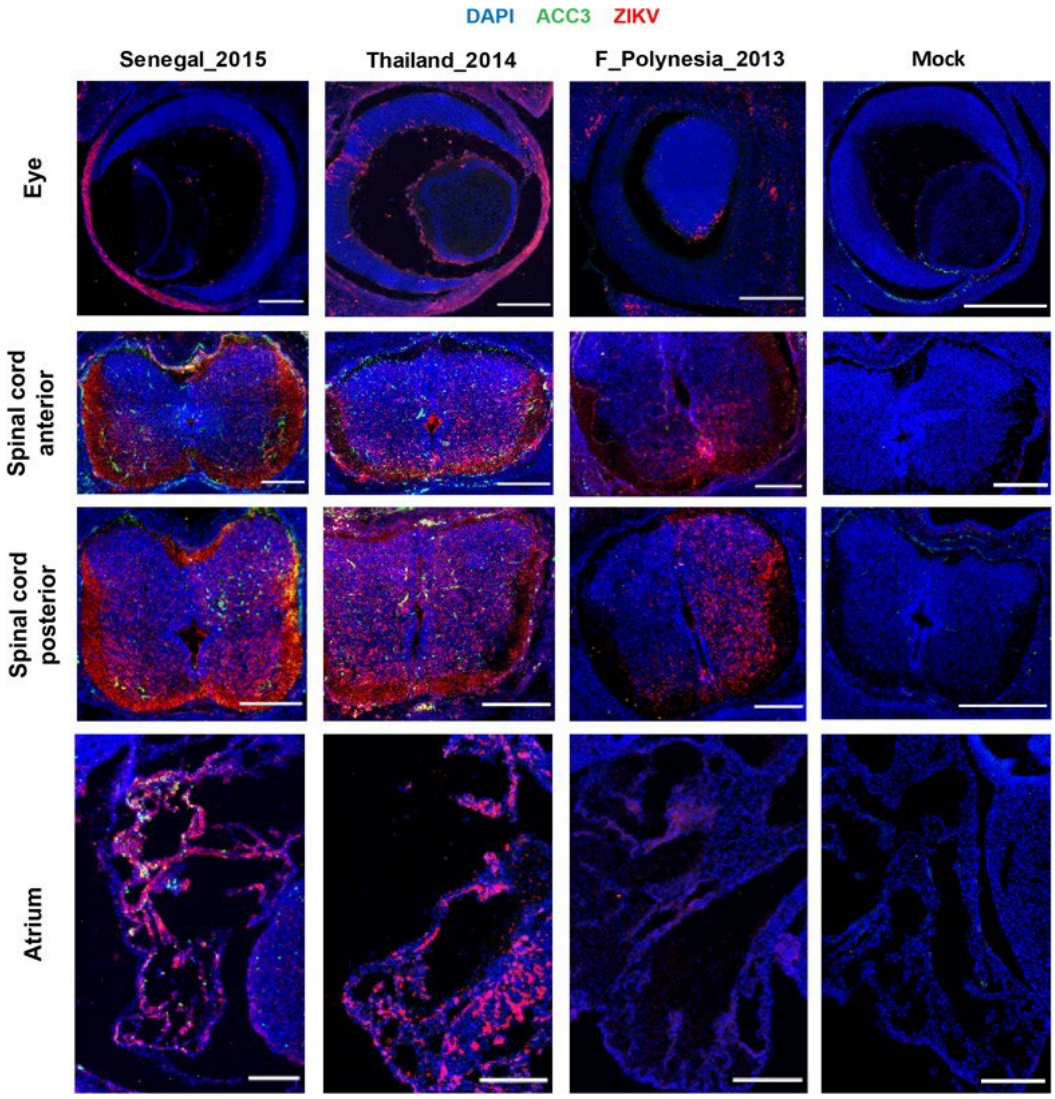

Supplementary Figure 3.5: African and Asian ZIKV strains show comparable organs tropism. Immunocompetent mouse embryos were infected at E10.5 by intraplacental injection of 500-1,000 PFU of ZIKV and examined at E14.5 by microdissection. Immunolabeling of embryonic eye, anterior and posterior spinal cord and atrium sections representative of each ZIKV strain tested (*n*=3 embryos per virus strain). Blue, green and red colors indicate DAPI, anti-cleaved caspase 3 (ACC3) and ZIKV stainings, respectively. The scale bars represent 200 µm.

Chapter IV : Evolution of Asian Zika virus strains resulted in attenuated fetal brain pathogenicity

IV.1 Abstract:

The Zika virus (ZIKV) outbreak of 2015-2016 in the Americas revealed the ability of ZIKV from the Asian lineage to cause birth defects, generically called congenital Zika syndrome (CZS). Notwithstanding the long circulation history of Asian ZIKV, no ZIKV-associated CZS cases were reported prior to the ZIKV outbreak in French Polynesia (2013) and Brazil (2015). It has remained unclear whether the sudden emergence of CZS resulted from an evolutionary event of the Asian ZIKV. We performed a comparative analysis of the pathogenicity of pre-epidemic and epidemic Asian ZIKV strains in the mouse embryonic brain. All studied (n=8) ZIKV strains of the Asian lineage were neurovirulent, but pre-epidemic ZIKV strains of this lineage were consistently more pathogenic in the embryos than epidemic ZIKV strains. The pathogenicity was, however, not directly linked to viral replication. In addition, all tested ZIKV strains triggered an immunological response, whereby the intensity of the response differed between strains but not between the groups. Our study reveals that the ZIKV strains from the Asian lineage evolved towards a pathogenic attenuation which may have resulted in the emergence of CZS in neonates instead of premature death in utero.

This chapter will be submitted to Nature Communications.

Maïlis Darmuzey[1,2], Franck Touret[3], Emily Slowikowski[4], Ivan Gladwyn-Ng[5], Karan Ahuja[6], Lorena Sanchez-Felipe[1], Xavier de Lamballerie[3], Catherine Verfaillie[6], Pedro E. Marques[4], Johan Neyts[1*], Suzanne J. F. Kaptein[1*]

: Evolution of Asian Zika virus strains resulted in attenuated fetal brain pathogenicity

IV.2 Introduction

Since its isolation from a monkey in Uganda in 1947, Zika virus (ZIKV) has circulated in human populations in Africa and the Asian-Pacific regions, causing only sporadic outbreaks associated with no or only mild symptomatic cases[19]. As a result, ZIKV was not considered a major health threat. However, between 2015-2016, ZIKV caused a massive outbreak in the Americas that was associated with an increased number of newborns with congenital Zika syndrome (CZS)[201], which encompasses a wide spectrum of birth defects, including microcephaly (smaller skull size), ventriculomegaly (enlarged ventricles), calcification of subcortical regions, neurologic impairment, ocular anomalies, and joint contractures[202,203]. The emergence of these unprecedented ZIKV-associated devastating neonatal abnormalities led the WHO to declare the 2015-ZIKV outbreak a public health emergency of international concern. Since then, various research groups have explored the underlying pathophysiological mechanisms that may explain the high neurovirulence of contemporary ZIKV strains. ZIKV has been reported to be able to infect various cell types in the brain (*in vitro* and *in vivo*), such as neural progenitors[85,145,204–206], mature neurons[204,207], astrocytes[56,208–211], oligodendrocytes[212–214], and microglia[215–218]. ZIKV infection of brain cells can induce various deleterious effects, including cell death[205,206,219,220], premature differentiation of neural progenitors[221–223], and secretion of inflammatory factors[57,215,224], which could ultimately lead to the development of a microcephalic phenotype. Although these studies provided very important insights into the pathophysiological mechanisms underlying ZIKV-associated brain defects, the question on this precipitous emergence remained unanswered. The sudden increase in cases of CZS were linked to ZIKV from the Asian lineage[22], which had evolved from the ancestral African lineage[23]. Several research groups demonstrated that ZIKV from both the African and Asian lineage is equally capable of infecting the placenta[126,225] and brain cells[134,226,227]. Intriguingly, ZIKV from the African lineage was reported to display a more pathogenic profile than ZIKV from the Asian lineage, making it more likely to be associated with miscarriages and spontaneous abortion than with birth defects[128,134,226,228,229]. Several studies aimed to identify potential genetic determinants of the sudden emergence of ZIKV-associated brain defects caused by the Asian lineage ZIKV[25,26,41,49,230], but these yielded conflicting results[25,26,134,226]. Moreover, some point mutations that were reported to affect the virulence of a particular ZIKV strain did not result in the same effect in the background of other ZIKV strains[231]. The explanation for the discrepancies in the reported findings is likely multifactorial, such as the use of different mouse models, inoculums, routes of infection, and the ZIKV strains used, amongst others. Indeed, the

diversity in the (*in vivo/in vitro*) models increases the variability in the neurovirulence results, complicating direct comparisons across studies.

To more comprehensively decipher the relationship between the evolution of Asian lineage ZIKV and the incidence of CZS, we performed a comparative study employing multiple pre-epidemic ZIKV strains (which arose before the 2013-epidemic French-Polynesia strain [PF_2013]), and epidemic ZIKV strains (evolving from PF_2013)[23]. To best recapitulate first trimester ZIKV infections in humans, which is associated with more severe cerebral pathology in newborns[31], we deployed the physiologically more relevant intraplacental challenge model to infect mouse embryos *in utero* at a very early stage of embryonic brain development. This infection route allows dissemination of ZIKV in the fetus in a more natural way, giving the virus access to the developing brain of the embryonic mice. Using this model, we additionally investigated the impact of an amino acid change that was reported to impact fetal microcephaly[40].

IV.3 Materials and Methods

Cells

Vero E6 cells (African green monkey kidney cells; Vero 76, clone E6; ATCC: CRL-1586) and HEK293T (ATCC, Cat# CRL-3216) were cultured in DMEM supplemented with 10% FBS (HyClone), 2 mM L glutamine (Thermo Fisher Scientific). In the end-point titration experiments with Vero E6 cells, 2% FBS was used. BHK-21J (baby hamster kidney fibroblasts; provided by P. Bredenbeek at the Leiden University Medical Center (LUMC), the Netherlands) and SH-SY5Y (ATCC, Cat# CRL-2266) were cultured in DMEM supplemented with 10% FBS (HyClone). Vero E6, BHK-21J, HEK293T and SH-SY5Y cells were incubated at 37 °C in presence of 5% CO_2. All cell lines (Vero E6, BHK-21J, HEK293T and SH-SY5Y) were regularly tested for mycoplasma contamination.

Differentiation of hiPSCs to cortical NPCs

Cortical neural precursor cells (NPC) were generated from Sigma-iPSC0028 hPSC line by using the protocol described by Shi et al[232]. The Sigma-iPSC0028 were plated on human Matrigel-coated 6-well plates (Corning) in mTESR (StemCell) with Revitacell (Life Technologies). These iPSCs were maintained in E8 flex medium (E8 basal medium (Gibco) complimented with E8 supplement Flex and 5 U/ml Penicillin-Streptomycin) and split twice a week with 0.5mM EDTA (Gibco). When the iPSC colonies reached 90% confluency, NPC induction was done by dissociating the iPSC colonies by accutase (Sigma) and seeding 2.5 million single cell suspension per well in a 6-well plate in neural induction media (NIM) comprising of neural maintenance medium (NMM) complemented with the dual-SMAD inhibitors SB431542 (10 µM, Tocris) and LDN193189 (1 µM, Miltenyi). The NMM comprises of a 1:1 mixture of Neurobasal medium (Gibco) and DMEM/F-12 Glutamax™ augmented with 0.5X Glutamax™ (Gibco), 50 U/ml Penicillin-Streptomycin, 0.5X B27 (Gibco), 0.5X N2 (Gibco), 0.5X MEM-NEAA (Gibco), 0.5X sodium pyruvate, 0.025 % human insulin (Sigma) and 50 µM 2-mercaptoethonal (Gibco). Media changes with NIM were performed every day for 11 days. At day 12, the neuroepithelial cells were collected using Dispase II (Sigma) and cultured for an additional 4 days with NMM spiked with 20 ng/mL bFGF. Rosette-forming neuroepithelial cells were passaged twice (after 5-7 days) using Dispase II to enrich the NPC population. The cultured NPCs were dissociated as single cells on DIV33 (33 days in vitro) and cryopreserved for further experimental use. For ZIKV infection, 1 million DIV33 NPCs per well were thawed on human Matrigel-coated 6 well plates in NMM supplemented with

RevitaCell and cultured in NMM for next 4 days. On day 38, these NPCs were dissociated as single cells using accutase and replated.

ZIKV strains

Eight ZIKV strains were selected of which three carry a serine (S) at position 139 in the polyprotein protein and five contain an asparagine (N) at position 139 (Table 1). ZIKV strains CAM_2010 (Zika virus/H.sapiens-tc/KHM/2010/FSS13025; GenBank KU955593), PR_2015 (ZIKV/Homo sapiens/PRI/PRVABC59/2015; GenBank KU501215), and MEX_2016 (ZIKV/Aedes.sp/MEX/MEX_2-81/2016; GenBank KX446950) were obtained from the World Reference Center for Emerging Viruses and Arboviruses (WRCEVA) at the University of Texas Medical Branch. ZIKV strains PHL_2012 (Zika virus/H.sapiens-tc/PHL/2012/CPC-0740; GenBank KU681082) and THA_2014 (Zika virus/H.sapiens-tc/THA/2014/SV0127-14; GenBank KU681081) were obtained from the Walter Reed Army Institute of Research (WRAIR). ZIKV PF_13 (ZIKV Pf13/251013-18; GenBank KY766069) was obtained from the Institut Louis Malardé in French Polynesia. ZIKV SUR_2016 (ZIKV SL1602[233]; GenBank KY348640) was received from LUMC in the Netherlands. ZIKV BRA_2015 (ZIKV/H.sapiens/Brazil/PE243/2015[234]; GenBank KX197192) was provided by the MRC-University of Glasgow Centre for Virus Research in the UK. High-titer virus stocks were grown on C6/36 mosquito cells and infectious titers (plaque forming units per ml; PFU/ml) were quantified by plaque assay on BHK cells, as described earlier [235].

Viral replication experiments in cells

SH-SY5Y cells were seeded at 5×10^5 cells/ml in T25-flasks and were incubated overnight at 37 °C in the presence of 5% CO_2. The following day, medium was removed, and cells were infected with one of the ZIKV strains at an MOI = 0.0001. After 3 hours, the inoculum was removed, and cells were washed 3 times with PBS. Finally, 5 ml of DMEM supplemented with 2% FBS was added to the cells. In experiments using hNPCs, cells were seeded at 1.5×10^5 or 3×10^4 per well in human Matrigel-coated 24-well or 96-well plates, respectively, and incubated overnight at 37 °C in the presence of 5% CO_2. Next day, medium was removed, and cells were infected with the one of the ZIKV strains at an MOI = 0.1 for 12 hours after which the inoculum was removed and 2.5 ml of NMM medium was added to the cells.

Mouse experiments

Breeding couples of immunocompetent SWISS/CD1 mice were purchased from Janvier Labs, Envigo or Charles River and bred at the KU Leuven Laboratory Animal Center. The SPF status of the mice was regularly checked at the KU Leuven animal facility. Mice were housed in individually ventilated cages (Sealsafe Plus, Tecniplast) at 21 °C, 55% humidity and 12:12 light/dark cycles. Animals were provided with food and water ad libitum as well as with cardboard play tunnels and cotton/tissues as extra bedding material. Allocation to experimental groups was performed randomly. Housing conditions and experimental procedures were approved by the ethical committee of KU Leuven (license P029/2021), following institutional guidelines approved by the Federation of European Laboratory Animal Science Associations (FELASA).

Intraplacental infection

Time-mated, SWISS mice, 8–12 weeks of age, were used for ZIKV vertical transmission experiments. All surgeries on SWISS wild-type female mice were performed at the same time, with embryonic day (E) 0.5 corresponding to the afternoon following the day of mating. At E10.5, mice were shaved, after which the developing embryos were challenged intraplacentally with 10^5 PFU/ml ZIKV or 2%FCS/PBS ('mock') as follows: Preoperative analgesia (0.1 mg/kg of buprenorphine; Temgesic) was administered subcutaneously before induction of anesthesia. Next, the pregnant females were anesthetized using isoflurane (Abbot Laboratories Ltd.), and a small incision (1.0-1.5 cm) was made through the lower ventral peritoneum. The uterine horns were carefully extracted and placed on warm humidified gauze pads. Following intraplacental infection, incisions were sutured and disinfected. Mice were maintained on a heat pad during the whole procedure. Eight hours post-surgery, mice received a second dose of analgesia (0.1 mg/kg of buprenorphine; Temgesic).

Quantification of cytokines and chemokines

Dissected brain tissues were weighed and homogenized in protein extraction buffer, consisting of 15 mM NaCl (VWR Chemicals, Radnor), 0.05% Tween 20 (Sigma), 5% Bovine Serum Albumin (BSA, Sigma), 10 mM EDTA (Sigma) and 1% protease inhibitor cocktail (Sigma) in PBS. Homogenates were centrifuged for 20 minutes (1000×*g*, 4 °C), supernatants were collected and concentrations of IL-6, IL-10 and CXCL10 were quantified by sandwich ELISA (DuoSet R&D Systems) according to the manufacturer's protocol. The absorbance was

determined using a spectrophotometer (BioTek) at 450 nm. Results are expressed as pg per 100 mg of brain tissue.

RNA isolation and RT–qPCR

Total RNA was isolated from embryonic tissue using Trizol (Ambion, Life Technologies) according to the manufacturer's protocol. Total RNA was isolated from cells supernatants using NucleoSpin RNA Virus, Mini kit for viral RNA from cell-free fluids (Macherey-Nagel) according to the manufacturer's protocol. Quantification of ZIKV genome copy numbers was performed by quantitative reverse transcription PCR (qRT-PCR) using one step qRT-PCR MasterMix Low ROX (Eurogentec). Ct values were converted into a relative number of ZIKV RNA copies/µl using the formula $y = a*\ln(x) + b$, where a is the slope of the standard curve, b is the y-intercept of the standard curve and y is the Ct value for a specific sample.

End-point titration

E18.5 brains were dissected, and half of the brain was used to determine End-point titration. Brain tissues were weighed and immerged in 350 µl of Vero E6 2% medium (described above) in a tube for homogenization. Tissues were homogenized and subsequently centrifuged for 10 minutes (14,000 rpm, 4 °C). Vero E6 cells (pre-seeded in 96-wells plates at 1×10^4 cells/well, 1 day earlier) were infected with supernatant from either infected homogenized brains or infected cells using ten-fold dilutions series, in triplicate. After 7 days of incubation, virus-induced cytopathic effect (CPE) was microscopically quantified and the virus titer (expressed as $TCID_{50}$ per ml) was determined using the method of Reed and Muench [164].

Generation of ZIKV_139N

The THA_139N variant was generated following the Infectious Subgenomic Amplicons (ISA) method[236]. RNA isolation was performed on virus stock using NucleoSpin RNA Virus, Mini kit for viral RNA from cell-free fluids (Macherey-Nagel) according to the manufacturer's protocol. A first fragment (pCMV-5'- 608bp) which contains the pCMV promotor and the mutation was synthesized by GenScript company.From the RNA isolation we performed RT-PCR using SuperScript™ IV One-Step RT-PCR System (ThermoFisher, 12594025) to generate two overlapping fragments of approximately 5-kb covering the full genomic sequence. After RT-PCR, the proper size of the fragments was confirmed by electrophoresis on agarose-gel. The RT-PCR products were purified using the Monarch® PCR & DNA Cleanup Kit (New England Biolabs, T1030L) according to the manufacturer's protocol.

On day 0, a mixture of 80% of HEK293T cells and 20% of BHK cells were seeded in a 96-well amine-coated plate (VWR, 734-1475). On day 1, transfection of the purified fragment was performed using Lipofectamine 3000 reagent (ThermoFisher Scientific, L3000008) according to the manufacturer protocol and 12 hours post-transfection the cells were washed three times with PBS and fresh medium was added. Six days post-transfection, the supernatant was passaged on pre-seeded VeroE6 cells in a 96-well plate (10 000 cells/well) and the transfected cells were pooled and reseeded in a 6-well plate. Seven days post-passaging and re-seeding the presence of the virus was confirmed by qRT-PCR and plaque assay. The newly generated virus was grown on VeroE6 cells and infectious titers (plaque forming units per ml; PFU/ml) were quantified by plaque assay on BHK cells. Finally, the genome integrity and the presence of the mutation was assessed by Next-generation sequencing (NGS).

Cryo-sectioning

E18.5 embryonic mouse heads were harvested and fixed overnight at 4 °C in 4% paraformaldehyde (PFA). Brains were dissected in 0.1 M PBS (pH 7.4) and cryoprotected by overnight immersion in 20% Sucrose in PBS before embedding in Polyfreeze (Sigma-Aldrich). Brain sections of 14 µm were obtained by cryosectioning (Leica) onto slides (Epredia™ SuperFrost Plus™ Adhesion slides, Fisher Scientific).

Immunohistochemistry

For immunofluorescence of brain sections, the slides were immerged in an antigen retrieval solution (Dako Target Retrieval Solution) and heated at 95 °C for 5 minutes. Next, slides were incubated in blocking solution (Normal Donkey Serum 10%, Bioconnect Life Sciences) for 1 hour at room temperature. The rabbit anti-cleaved caspase 3 (1:300, #9661, Cell Signaling Technologies), mouse anti-flavivirus group antigen (1:1000, MAB10216, Merck Millipore) and goat anti-Iba1 (1:300, ab5076, Abcam) were used as primary antibody, and slides were incubated overnight at 4 °C. The following day, slides were stained using the secondary antibodies (Life Technologies) donkey anti-rabbit Alexa Fluor-488 (A-21206), donkey anti-mouse Alexa Fluor-555 (A- 31570), all diluted 1:1000, or donkey anti-goat Alexa Fluor-647 (A-21447), and nuclei were counterstained with DAPI (1:1000) for 2 hours at room temperature. Slides were mounted in Dako Fluorescence Mounting Medium (Agilent).

For immunofluorescence of hNPCs, supernatant was removed from the cells at the indicated timepoints, and cells were washed three times with PBS. Next, cells were fixed using 4% PFA

for 30 minutes, followed by three PBS washes. Nuclei were counterstained with DAPI (1:1000) for 1 hour at room temperature. Finally, cells were washed three times with PBS.

Imaging and analysis

Confocal images of sections of E18.5 mouse brains were acquired using a NIKON A1R confocal microscope at a 20X magnification, or using a Leica DMi8 confocal spinning disc microscope at a 25X magnification. Quantification of cortical length and the number of DAPI-positive cells was performed in a region of interest (ROI). The ROI is a region of 100 µm wide in the cortex, stretching from the top of the ventricle to the outer border of the cortex. For each sample, the same region was selected as ROI. Image analysis and processing were performed with ImageJ 1.42q 276 (Wayne Rasband, National Institutes of Health), or Fiji (v2.0.0-rc-54/1.51 h, https://imagej.net/Fiji) software.

Statistics

Statistical analyses were performed using GraphPad Prism v9.3.1. Results (from brain analyses, viremia and subcutaneous edema) were first tested for normality using Shapiro-Wilk test. The Brown-Forsythe and Welch ANOVA test followed by Games-Howell's multiple comparisons post-hoc test was performed when the assumption of equal variance was not met. Alternatively, the two-sided Kruskal-Wallis test followed by Dunn's multiple comparisons test when both normality and the assumption of equal variance were not met. Differences were considered statistically significant when $p < 0.05$.

IV.4 Results

IV.4.1 Pre-epidemic ZIKV strains cause severe brain defects more consistently than epidemic ZIKV strains

Based on a comparative phylogenetic study by Pettersson and colleagues[23], we selected a panel of three pre-epidemic ZIKV (preZIKV) strains (CAM_2010, PHL_2012 and THA_2014) and five epidemic ZIKV (epZIKV) strains (PF_2013, PR_2015, BRA_2015, MEX_2016, and SUR_2016); see Supplementary Table 4.1 for details. To compare the neurovirulent potential of preZIKV and epZIKV strains, intraplacental (IPL, 5×10^5 PFU/ml) injections were performed at embryonic day 10.5 (E10.5) in immunocompetent SWISS dams (Supplementary Fig. 4.1), which is a time window corresponding to the first trimester of pregnancy in humans[237]. As the preZIKV strain CAM_2010 elicited massive fetal death before E18.5 with only 3 harvestable embryos (data not shown), results obtained with this strain were excluded from all analyses due to the small sample size. Eight days post-infection (pi) at E18.5, we assessed the severity of the brain defects as well as the presence of microcephaly and ventriculomegaly by measuring the brain weight, the thickness of the cortex, the number of cells present in the cortex, and the enlargement of the ventricle area. Both preZIKV and epZIKV were capable of inducing brain defects in embryonic mice (Fig. 4.1). However, brains infected by preZIKV were on average lower in weight than those infected by epZIKV (Fig. 4.1a), suggesting that preZIKV triggered more severe brain defects. Indeed, although both preZIKV and epZIKV caused a microcephalic phenotype, illustrated by a reduction in the cortical length and fewer cells in the cortex compared to mock-infected brains (Fig. 4.1b, c), preZIKV-infected embryonic brains consistently presented a more severe microcephalic phenotype with smaller cortices and fewer cells than epZIKV-infected embryonic brains (Fig. 4.1a-d). Similarly, ventriculomegaly was observed both in the preZIKV- and epZIKV-infected brains, but with a more significant enlargement of the ventricle area in brains infected by preZIKV (Fig. 4.1d). Even more striking was that all embryonic brains infected with preZIKV displayed an enlargement of the ventricular region. In contrast, a significant number of brains (35%, $n = 65$; $p < 0{,}0001$) infected by epZIKV did not present with ventriculomegaly because the size of the ventricular area was comparable or smaller than the maximum ventricular opening observed in mock-infected brains (represented by the dashed line in Fig. 4.1d). This is for example clearly demonstrated for BRA_2015 (Fig. 4.1e). This ZIKV strain induced a wide range of ventriculomegaly in the embryonic brain, ranging from almost non-detectable (middle panel Fig. 4.1e) to severe ventriculomegaly (right panel Fig. 4.1e), as did all the other epZIKV strains (Supplementary Fig. 4.2d). A similar trend in variation was observed in brain weight, the thickness of the cortex

and the number of cells present in the cortex of brains infected by epZIKV (Supplementary Fig. 4.2a-c). Thus, embryonic brains infected by epZIKV displayed a broader spectrum of severities, varying from unnoticeable brain defects to an extremely deleterious phenotype, while brains infected by preZIKV exhibited more uniformly severe brain abnormalities.

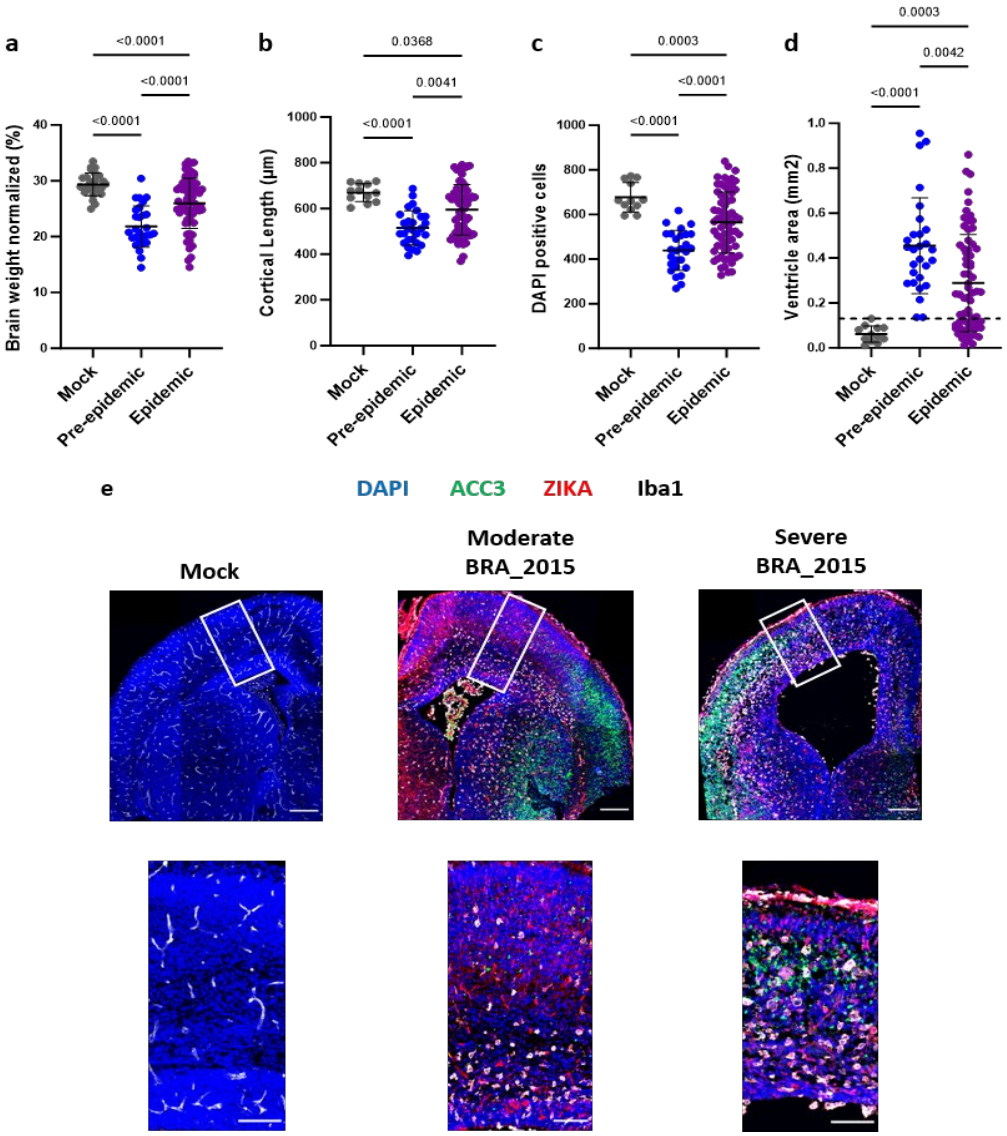

Figure 4.1: Brain abnormalities in embryonic mice caused by pre-epidemic and epidemic ZIKV strains

a-d, Analyses of E18.5 embryonic mouse brain development after mock injection (n = 26 for brain weight and n = 12 otherwise) or after infection by either pre-epidemic ZIKV strains (n = 28) or epidemic ZIKV strains (n = 68). Embryonic brains were examined morphologically by measuring the brain weight normalized to head weight (**a**). Microcephalic phenotypes were assessed by measuring (**b**) cortical length and (**c**) number of DAPI-positive cells. Ventriculomegaly was estimated by measuring the ventricle area (**d**). **e**, Representative images of E18.5 embryonic mouse brains after mock-injection (left, n = 12) or infection with the ZIKV BRA_2015 (middle, right, n = 12). Blue, green, red and white indicate DAPI, anti-cleaved caspase3 (ACC3), Zika virus and Iba1 staining, respectively. The scale bars represent 500µm. In (**a-d**) data are presented as mean ± standard deviation. Statistical significance of differences was determined by Brown-Forsythe and Welch Anova, followed by Dunnett's T3 multiple comparisons test for (**a**) and (**c**), and by one-way Anova, followed by Kruskal-Wallis' multiple comparisons test for (**b**) and (**d**). Only statistically significant differences are shown.

IV.4.2 Pre-epidemic ZIKV strains cause more readily subcutaneous edema in embryonic mice

During necropsy of the embryos infected by either preZIKV or epZIKV, subcutaneous edema was observed (Fig. 4.2a). This is consistent with our previous report, showing subcutaneous edema at E14.5 in 6% and 30% of the embryos infected with PF_2013 or THA_2014, respectively[229]. Differences in the percentage of embryos displaying subcutaneous edema may reflect differences in pathogenic profile between preZIKV and epZIKV. To assess whether the percentage of infected embryos presenting subcutaneous edema depends on the ZIKV strain used to infect them, we quantified the number of affected embryos for preZIKV and epZIKV at E13.5, E14.5 and E15.5 (Fig. 4.2b-d). At E13.5, preZIKV tended to cause subcutaneous edema in a higher proportion (18%) of the infected embryos than epZIKV (3%) (Fig. 4.2b). More specifically, 20% and 17% of the embryos infected with respectively PHL_2012 or THA_2014 displayed subcutaneous edema while it was absent in the embryos infected with any of the epZIKV strains, excepted for some of the embryos (8%) infected with BRA_2015 (Supplementary Fig. 4.3b). The trend became even more pronounced at E14.5 with a significantly higher number (48%) of the preZIKV-infected embryos presenting subcutaneous edema compared to the epZIKV-infected embryos (21%) (Fig. 4.2c). By contrast, a similar proportion of the infected embryos from both groups showed subcutaneous edema at E15.5 (61% versus 43%). (Fig. 4.2d). Of note, while the proportion of the embryos presenting edema increased from E13.5 to E15.5 for most ZIKV strains, the number remained low for PF_2013 (Supplementary Fig. 4.3, panel a versus panels b-d). Therefore, results with this strain were omitted from the analysis.

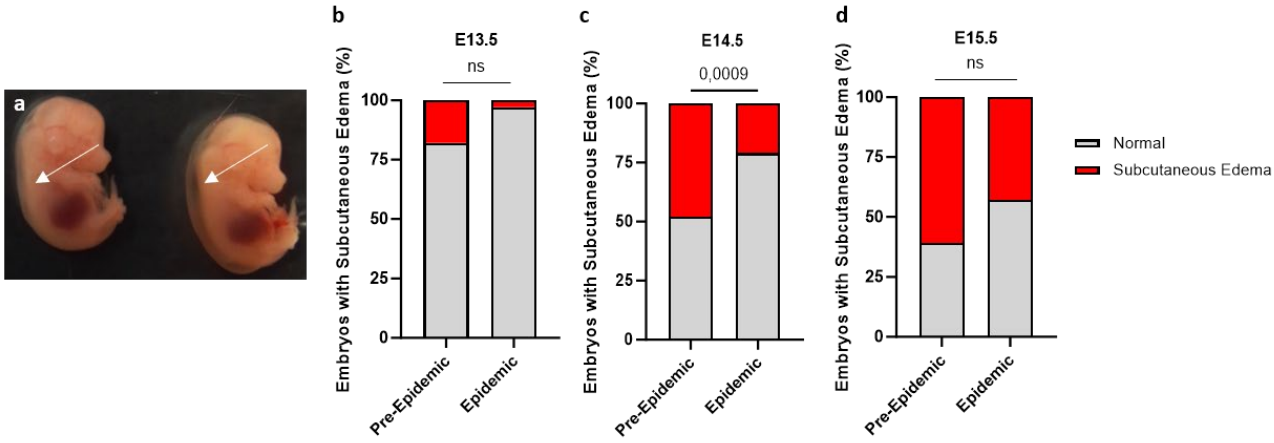

Figure 4.2: Embryos infected by ZIKV develop subcutaneous edema. (**A**), Picture showing representative E14.5 mouse embryos with mild (left arrow) and severe (right arrow) subcutaneous edema. **b**, Percentage of mouse embryos presenting subcutaneous edema at E13.5 after infection by either pre-epidemic (n = 24) or epidemic (n = 25) ZIKV strains. **c**, **d**, Percentage of mouse embryos presenting subcutaneous oedema at E14.5 (**c**) or E15.5 (**d**) after infection by either pre-epidemic (n = 31 and n = 31, respectively) or epidemic (n = 55 and n = 52, respectively) ZIKV strains. Statistical significance of differences was determined by Fisher's exact test (**b, d**).

IV.4.3 Viral replication kinetics in embryonic mouse brains

To assess whether the observed differences between preZIKV and epZIKV are associated with differences in viral replication and viral fitness within the embryonic mouse brain, viral RNA levels (by RT-qPCR) and infectious particles (by end-point titrations) were quantified at different timepoints pi. However, due to the small size of the embryonic brain on E13.5-E15.5, infectious virus levels were only determined in E18.5 brains.

At E18.5, no significant differences in viral RNA load or infectious virus in the brain were observed between both groups (Fig. 4.3a-b). One exception is the difference in infectious virus in brains infected with SUR_2016 (epidemic) as compared to those infected with THA_2014 (pre-epidemic). Infectious virus titers in brains infected with SUR_2016 were significantly higher than in brains infected with THA_2014 (Supplementary Fig. 4.4f). Similarly, no significant differences in viral RNA levels were observed between the preZIKV- and epZIKV-infected brains at E13.5 (Fig. 4.3c, Supplementary Fig. 4.4a), E14.5 (Fig. 4.3d) and E15.5 (Fig. 4.3e), again with one exception: brains infected by PH_2012 (pre-epidemic) had a higher viral RNA load than those infected by MEX_2016 (epidemic) at E14.5 (Supplementary Fig. 4.4b). The only significant difference in replication potential at E15.5 was observed between two epZIKV strains, with a significantly higher viral RNA load in brains infected by PR_2015 than in those infected by PF_2013 (Supplementary Fig. 4.4c). Overall, the preZIKV and epZIKV strains displayed similar replication profiles in embryonic mouse brains with a peak at E15.5 (Fig. 4.3f), except for PHL_2012 and BRA_2015 which both peaked one day earlier (Supplementary Fig. 4.4e).

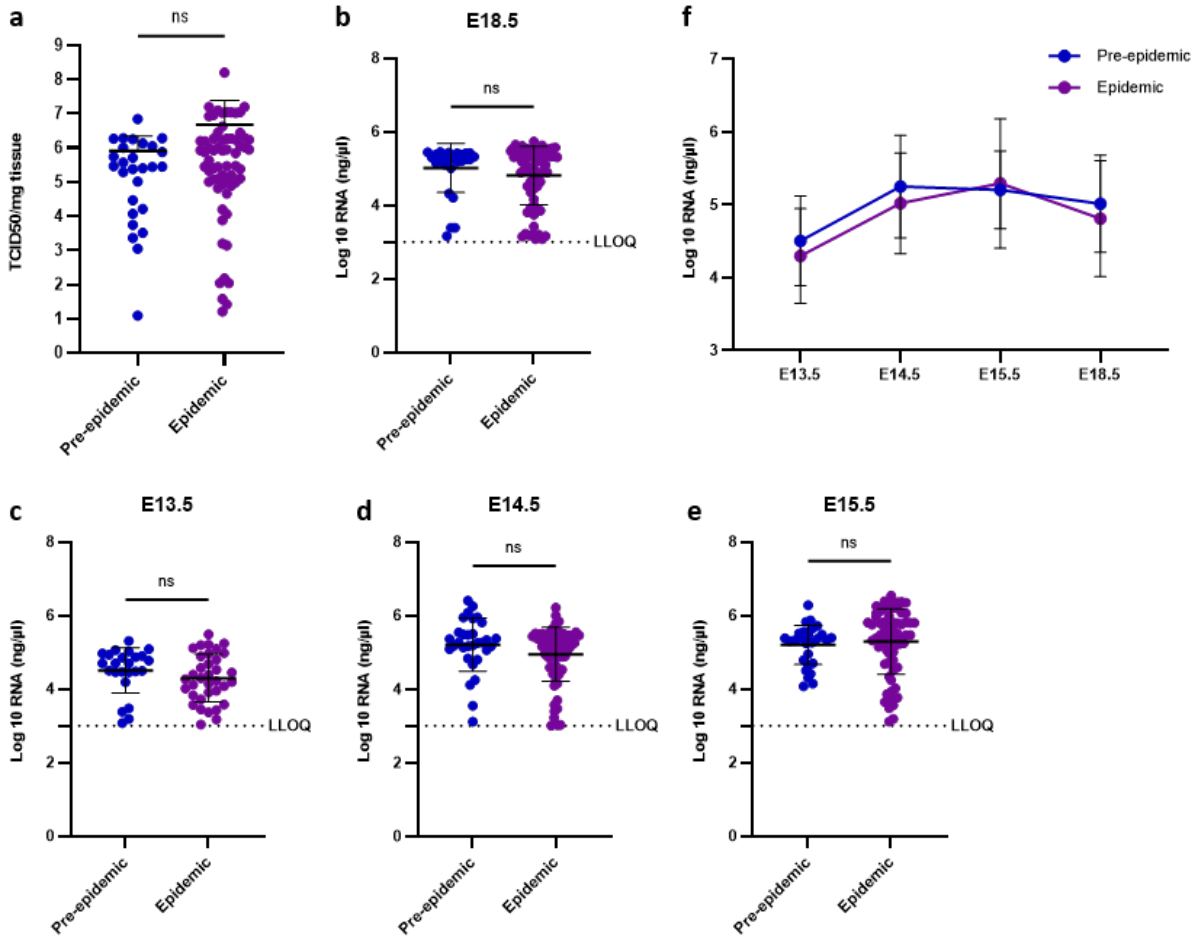

Figure 4.3: Replication kinetics of the pre-epidemic and epidemic ZIKV strains in the embryonic brain. **a**, Infectious virus in brain at E18.5, depicted as log_{10}-transformed 50% tissue culture infectious dose ($TCID_{50}$) per mg of tissue. **b-e**, Brain viral loads are shown in log_{10}-transformed viral genome copies at various timepoints: E18.5 (**b**), E13.5 (**c**), E14.5 (**d**), E15.5 (**e**). f, Replication kinetics for pre-epidemic and epidemic ZIKV strains in embryonic brains at E13.5 to E18.5. Data are summarized data from **b-e**. N numbers are present in supplementary table 2. Data are represented as mean ± standard deviation. Statistical significance of differences was determined by one-way Anova, followed by Kruskal-Wallis' multiple comparisons test. ns = not significant.

IV.4.4 ZIKV strains display different replication kinetics in human brain cells

We next defined the in vitro neurovirulent profile for each ZIKV strain in the 2 groups using two relevant brain cell types: neuroblastoma cells (SH-SY5Y) and human progenitor cells (hNPCs). In neuroblastoma cells, the course of replication was virtually the same for all ZIKV strains, i.e., increasing from d1 to d7 pi (Fig. 4.4 a). However, obvious differences were noted for some ZIKV strains. Among all ZIKV strains, viral RNA levels at endpoint were significantly the highest for BRA_2015. From 3 days post-infection (3 dpi) onwards, PR_2015 replicated to significantly higher viral RNA levels than the other ZIKV strains except BRA_2015 (Fig. 4.4a). By contrast, PF_2013 replicated less efficiently, resulting in the lowest viral load at 5 and 7 dpi. For all ZIKV strains, the production of viral particles correlated roughly with the viral RNA load, with PR_2015 and BRA_2015 yielding significantly higher virus titers from 5 to 7 dpi than did the other ZIKV strains (Fig. 4.4b). At earlier timepoints,

virus titers were lower for PR_2015 than for BRA_2015, although levels increased more rapidly from d2-d5 pi for PR_2015, indicative of a higher fitness (also considering the relatively lower viral RNA levels for PR_2015) (Fig. 4.4b).

When assessing the viral replication kinetics in hNPCs, PR_2015, BRA_2015 and SUR_2016 reached significantly and similarly higher viral RNA levels on 5 to 10 dpi than did the other ZIKV strains. At these time points, viral RNA levels were the highest for SUR_2016 than for the other two ZIKV strains. Similar to the neuroblastoma cells, the lowest viral load in hNPCs was found for PF_2013. In general, all ZIKV strains replicated to peak levels at d9 pi, after which levels slightly decreased at 10 dpi (Fig. 4.4c). As observed in neuroblastoma cells, infectious virus levels correlated with the viral RNA load in hNPCs with PR_2015, BRA_2015 and SUR_2016 yielding significantly higher virus titers than did the other ZIKV strains (Fig. 4.4d). Overall, the epidemic ZIKV strains PR_2015 and BRA_2015 exhibited on average slightly superior replication kinetics in the studied human brain cells (illustrated by higher levels of viral RNA and virus titers) than the other ZIKV strains, except for SUR_2016 in hNPCs.

IV.4.5 ZIKV strains induce different levels of immune mediators in embryonic brains

In order to determine whether the ZIKV strains induced different immune responses in the embryonic brain, we evaluated the production of IL-6, IL-10 and CXCL10 in mouse brain lysates at E14.5, which had been infected with either a preZIKV strain (PHL_2012 or THA_2014) or an epZIKV strain (BRA_2015 or SUR_2016). IL-6, a potent proinflammatory and immunostimulatory cytokine[238], was undetectable in healthy mock-infected embryonic brains, but it was significantly induced in response to infection with the BRA_2015 and SUR_2016 ZIKV strains, suggesting that they are more capable to drive immune responses than the other virus strains. Of note, IL-6 induction was significantly higher in response to SUR_2016 than that to all the other strains, including BRA_2015 (Fig. 4.5a).

Similarly, CXCL10, a chemokine induced by interferon-γ and a potent chemoattractant to monocytes, natural killer cells and T cells[239], was significantly elevated in response to infection by all 4 ZIKV strains tested. Interestingly, CXCL10 is already produced in embryonic brains in steady-state conditions, but it is substantially increased in response to ZIKV infection. This suggests that CXCL10 may serve as a marker of ZIKV infection in embryonic stages. In addition, the SUR_2016 strain was the most powerful stimulus for CXCL10 production, which

was significantly elevated when compared to both PHL_2012 and BRA_2015 ZIKV strains (Fig. 4.5b).

Lastly, we measured the levels of IL-10 in embryonic brain lysates, a cytokine known for its immunoregulatory and anti-inflammatory properties[240]. IL-10 was absent in mock-infected brains, but it was significantly upregulated upon infection with all 4 ZIKV strains. Moreover, IL-10 production was highest in brains infected with SUR_2016 and THA_2014 strains (Fig. 4.5c).

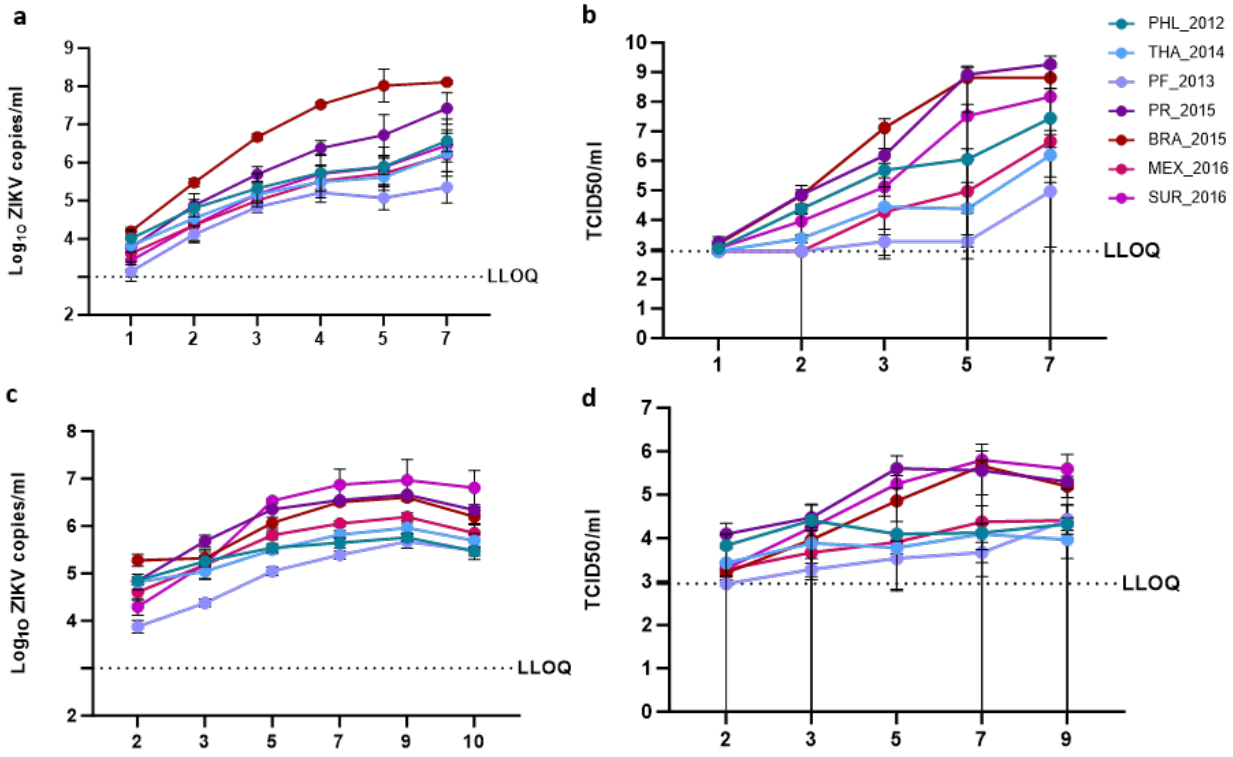

Figure 4.4: Replication kinetics of the pre-epidemic and epidemic ZIKV strains in human brain cells *in vitro*. **a,** Viral loads in neuroblastoma cells are shown in log_{10}-transformed viral genome copies at different days post-infection. **b,** Infectious virus in neuroblastoma cells depicted as log_{10}-transformed 50% tissue culture infectious dose (TCID50) per ml of supernatant at different days post-infection. **c,** Viral loads in human neural progenitor cells are shown in log_{10}-transformed viral genome copies at different days post-infection. **d,** Infectious virus in human neural progenitor cells depicted as log_{10}-transformed 50% tissue culture infectious dose (TCID50) per ml of supernatant at different days post-infection. Statistical significance of differences was determined by two-way Anova followed by Šídák's multiple comparisons test. Only statistically significant differences are displayed in Supplementary data 1-4.

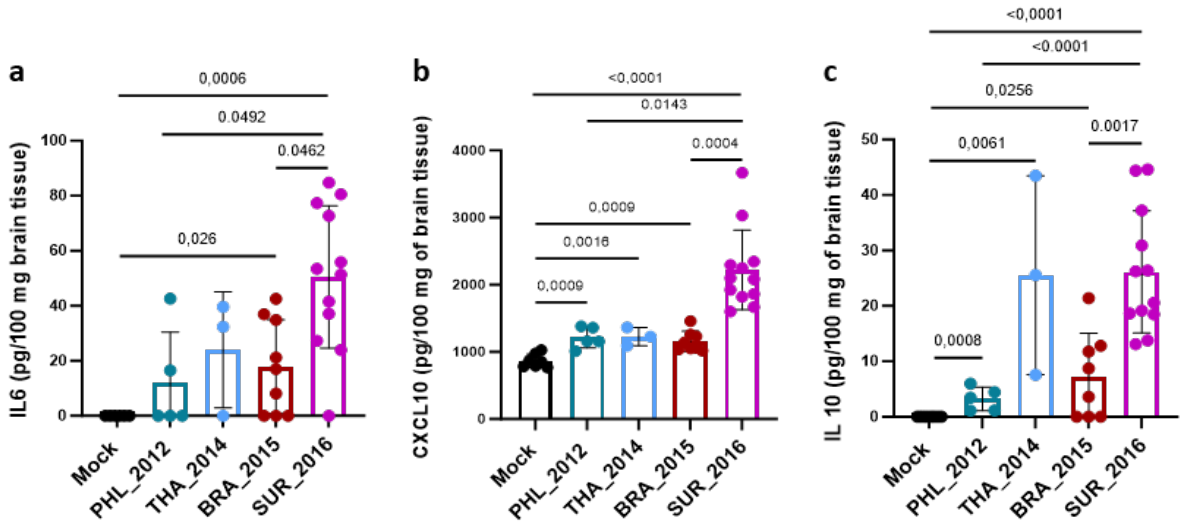

Figure 4.5: Immunological response in embryonic mouse brains after ZIKV infection. a-c, Measurements of IL-6 (**a**), CXCL10 (**b**) and IL-10 (**c**) levels in embryonic mouse brains after mock injection (n = 8) or after infection by either PHL_2012 (n = 5), THA_2014 (n = 3), BRA_2015 (n = 8) or SUR_2016 (n = 12). Statistical significance of differences between ZIKV-infected and Mock-infected brains were determined by Mann-Whitney test. Differences among ZIKV strains were determined by one-way Anova followed by Kruskal-Wallis multiple comparisons test for IL-6 and CXCL10 and by Brown-Forsythe and Welch Anova test for IL-10.

IV.4.6 Impact of S139N substitution on severity of brain defects

The individual preZIKV and epZIKV strains differ from each other by numerous amino acid changes in their viral genomes. Similarly, different substitutions are present in the genome of ZIKV strains belonging to the same group. However, the only amino acid separating preZIKV from epZIKV is the one at position 139 in the polyprotein (Supplementary Table 1), with a serine (S) shared by preZIKV and an asparagine (N) shared by epZIKV, as was reported previously[31]. Interestingly, this residue at position 139 was demonstrated to contribute to fetal microcephaly[40]. This prompted us to investigate whether and to what extent this amino acid contributes to the severity of brain abnormalities in embryonic mice using the IPL model. Since brain abnormalities were consistently more severe in (a larger proportion of) embryonic mice infected with preZIKV, the THA_2014 strain was selected for altering the amino acid at position 139. By employing the ISA method[56], the S was substituted to an N (S139N), resulting in a ZIKV strain referred to as THA_139N. The severity of the brain defects as well as the presence of microcephaly and ventriculomegaly at E18.5 was assessed as described earlier. Hypothetically, introducing the S139N substitution in the pre-epidemic THA_2014 strain should lead to a microcephalic phenotype similar to that induced by epZIKV. Compared with mock-infected embryos, those infected by THA_139N presented pronounced brain defects, as evidenced by a lower brain weight, a microcephalic phenotype, and ventriculomegaly (Fig.

4.6a-d). However, the severity of the brain abnormalities did not differ significantly between embryos infected with THA_139N and those infected with parental THA_2014.

We next investigated whether the S139N substitution affected the viral replication kinetics in neuroblastoma cells and hNPCs. In neuroblastoma cells, the THA_139N variant replicated to a significantly higher viral RNA load at 1 to 5 dpi than the THA_2014 strain (Fig. 4.6e). Levels of infectious virus were also higher, albeit only significantly at 3 dpi, in neuroblastoma cells infected with THA_139N than in those infected with the parental strain (Fig. 4.6f). By 7 dpi, the (significant) difference between the two ZIKV strains had disappeared. A similar difference in the replication profile between THA_139N and THA_2014 was noted in hNPCs, i.e., significant higher viral RNA levels (at 2-9 dpi) and virus titers (at 5 and 7dpi) for THA_139N than for THA_2014 (Fig. 4.6g, h). Interestingly, when determining the number of cells, the number of hNPCs infected by THA_139N increased from 1 to 4 dpi while those infected with THA_2014 decreased from 1 to 4 dpi (Fig. 4.6i). The difference in the number of hNPCs was significant at 4dpi. These results suggest that THA_139N may delay virus-induced cytopathic effect in hNPCs.

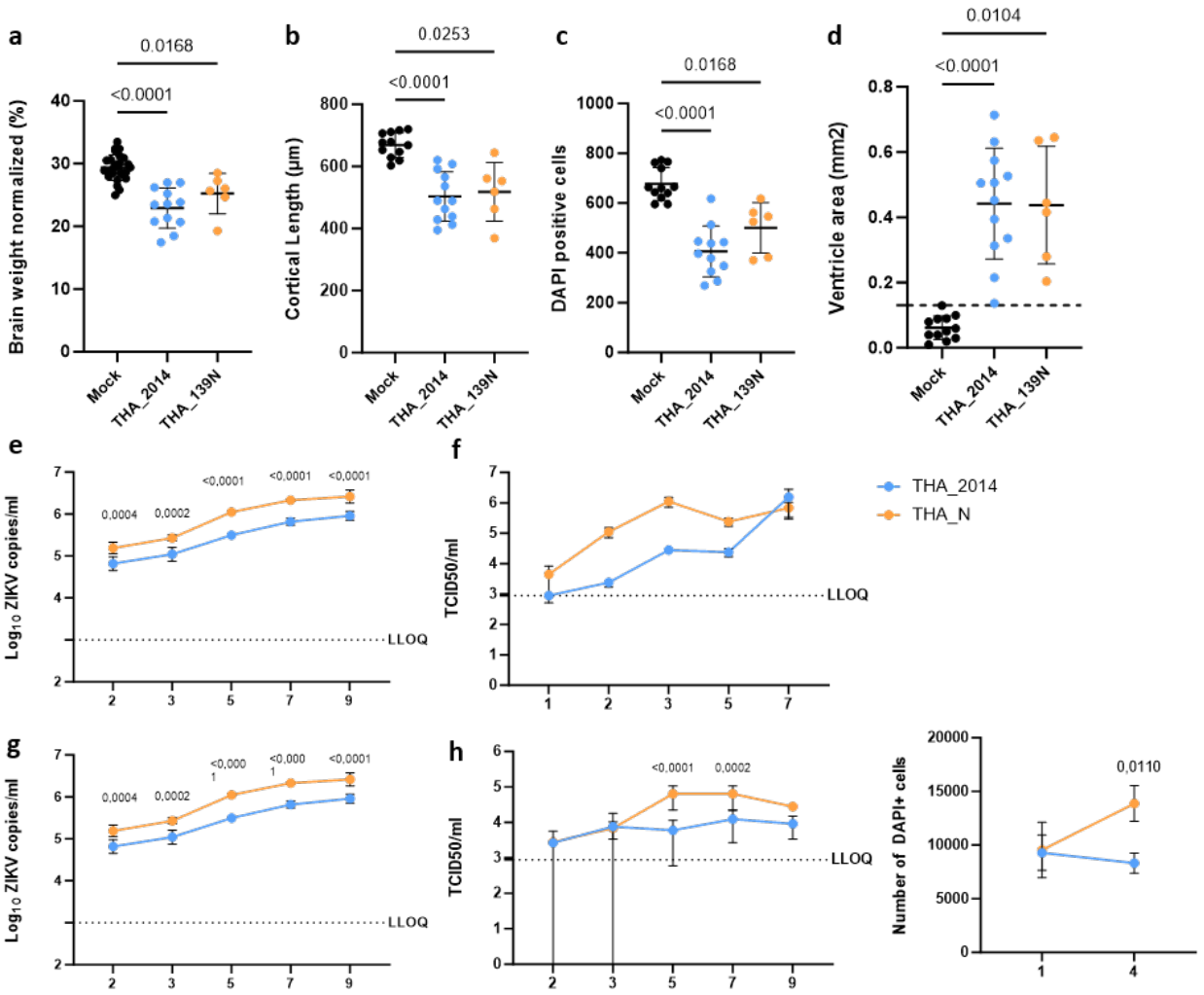

Figure 4.6: Brain pathogenicity and in vitro viral replication of ZIKV infectious clone THA_139N compared to WT THA_2014. **a-d**, Analyses of E18.5 embryonic mouse brain development after mock injection (n = 26 for brain weight and n = 12 otherwise) or after infection by either THA_2014 ZIKV strain (n = 12) or ZIKV THA_139N (n = 6). Embryonic brains were examined morphologically by measuring the brain weight normalized to head weight (**a**). Microcephalic phenotypes were assessed by measuring (**b**) cortical length and (**c**) number of DAPI-positive cells. Ventriculomegaly was estimated by measuring the ventricle area (**d**). **e**, Viral loads in neuroblastoma cells are shown in log_{10}-transformed viral genome copies at different days post-infection. **f**, Infectious virus in neuroblastoma cells depicted as log_{10}-transformed 50% tissue culture infectious dose (TCID50) per ml of supernatant at different days post-infection. **g**, Viral loads in human neural progenitor cells are shown in log_{10}-transformed viral genome copies at different days post-infection. **h**, Infectious virus in human neural progenitor cells depicted as log_{10}-transformed 50% tissue culture infectious dose (TCID50) per ml of supernatant at different days post-infection. **i**, Number of DAPI-positive cells at day 1 and day 4 post-infection of hNPCs. In (**a-d**), data for THA_2014 are the same as those presented in Supplementary figure 2. In (**a-i**) data are presented as mean ± standard deviation. Statistical significance of differences was determined by Brown-Forsythe and Welch Anova, followed by Dunnett's T3 multiple comparisons test. Only statistically significant differences are shown.

IV.5 Discussion

ZIKV strains of the Asian lineage are considered a major public health concern because of outbreaks in several regions around the world, such as Micronesia (2007), French Polynesia (2013) and South and Central America (2014-2016), which also increased in magnitude[54,55]. We provide a comprehensive comparison of the neurovirulent and pathogenic profile of Asian ZIKV strains belonging to the pre-epidemic group (ZIKV strains that emerged before PF_2013) or to the epidemic group (PF_2013 and all subsequent ZIKV strains). We employed the intraplacental mouse ZIKV challenge model to assess the impact on cortical development in embryonic brains infected with either preZIKV or epZIKV strains from the Asian lineage. In this model, ZIKV is injected at E10.5 directly in the placental labyrinth of immunocompetent mouse embryos to overcome the inability of ZIKV to cross the murine placental barrier. This allowed us to mimic the clinical course of fetal ZIKV infections in humans[26]. Moreover, at E10.5, the development of the cerebral cortex in mice is corresponding to that of humans during the first trimester of pregnancy[237]. Therefore, IPL injections at E10.5 correspond to congenital ZIKV infections early in the first trimester of human pregnancy.

We demonstrated that the propensity of ZIKV strains of the Asian lineage to cause brain abnormalities such as microcephaly and ventriculomegaly, is common to all ZIKV strains that were tested, regardless of their origin (pre-epidemic or epidemic). PreZIKV strains, however, were more pathogenic in that they invariably caused more severe brain abnormalities in the embryonic mice. Infections with EpZIKV strains, on the other hand, resulted in a greater variation in the severity of brain defects, with brains that did not present major abnormalities and those that were severely affected. This variability in brain defect severity is fully in line with what has been described in clinical reports, i.e., infants presenting varying degrees of adverse outcomes[47,48], from undetectable central nervous system malformations[49,50] to severe microcephalic phenotypes, and even perinatal mortality[48]. By contrast, the higher pathogenic profile of pre-epidemic ZIKV strains may have caused relatively more spontaneous abortions and stillbirths rather than birth defects, explaining the absence of previously reported CZS. Thus, our results support the hypothesis that ZIKV evolution along the Asian lineage led to an attenuation of pathogenicity.

The higher pathogenic profile of preZIKV strains as compared to epZIKV strains was also supported by the earlier appearance of subcutaneous edema in a larger proportion of the pre-

epidemic ZIKV-infected mouse embryos. Subcutaneous edema has also been described in a human fetus who had developed hydrops fetalis after congenital ZIKV infection[241]. Hydrops fetalis is characterized by severe swelling (edema) in unborn babies with mortality rates up to 50%[242]. Although it is extremely difficult to estimate the true incidence of hydrops fetalis caused by congenital ZIKV infections during the various ZIKV outbreaks around the world, the emergence of epidemic ZIKV strains with a reduced pathogenic profile may have contributed to the higher incidence of neurodevelopmental disorders and potentially less cases of fatal hydrops fetalis in infants born during the ZIKV epidemic.

To potentially link the pathogenic profile to the replication fitness, we examined the viral replication kinetics of the preZIKV and epZIKV strain, both *in vitro* and *in vivo*. Overall, the infectivity and replication competence of the pre-ZIKV and epZIKV strains were comparable in embryonic brains at all timepoints tested. Some differences were noted, however not consistently between (the same) preZIKV and epZIKV strains. In neuroblastoma cells and hNPCs, a significantly higher viral load (viral RNA and infectious virus) was found for some viruses, in particularly for epidemic BRA_2015 and PR_2015. In addition, the epZIKV strain SUR_2016 also exhibited superior replication kinetics in hNPCs. On the other hand, the strain with the most attenuated replication profile also belonged to the epZIKV strains: PF_2013. More interestingly, BRA_2015 and PF_2013 both caused comparable brain defect severity in embryonic mice, which seems to mirror the observed severity of brain defects in PF_2013- and BRA_2015-infected human fetuses[21,243]. Taken together, the results indicate that the more pathogenic profile of preZIKV strains was not associated with an increased viral replication fitness of these strains. Our results also point out that extrapolation of *in vitro* findings should be done with caution as critical determinants, such as the immune system, the interplay between the different cell types, and the developmental stage of the embryo, are absent in *in vitro* cell culture systems.

ZIKV infections have been associated with elevated concentrations of cytokines and chemokines, including IL-6, IL-10 and CXCL10[244]. Moreover, in another study CXCL10 and IL-10 expression levels differed significantly between ZIKV infections caused by the African MR766 strain and those caused by the Asian PF_2013 strains with higher CXCL10 and lower IL-10 levels after infection by MR766 compared to PF-2013 ZIKV infection[53]. We hence explored whether these biomarkers were differentially altered between the two ZIKV groups and could thus serve as a signature of pathogenicity.

Upon ZIKV infections by either preZIKV or epZIKV, an immunological response was measured in the embryo brains at 4 days post-infection. We observed heterogeneous results among all ZIKV strains tested, implying that one group (e.g., epZIKV) was not more immunogenic than the other (e.g., pre-epZIKV). Instead, the immunogenicity of ZIKV seems to be strain dependent. SUR_2016 was the most immunostimulatory ZIKV strain. The higher levels of mediators after SUR_2016 infection may indicate a better response to the infection that could be correlated to the lower neurovirulence observed in E18.5 brains. However, it cannot be excluded that excessive levels could also lead to worsening of disease because of inflammation. The interplay between ZIKV and the immune system may be the key to a better understanding of the pathogenicity.

To investigate whether the S139N substitution could have contributed to the reduced pathogenic profile of the epidemic ZIKV strains, the S139N substitution was introduced into the pre-epidemic THA_2014 strain, resulting in the THA_139N variant. The THA_139N replicated more efficiently *in vitro* than the parental strain. This result is in line with earlier obtained results using a modified (pre-epidemic) ZIKV Cambodia strain containing the same S139N substitution. This modified ZIKV strain also exhibited an increased replication profile in mouse neural progenitor cells[40]. We further showed that the S139N substitution did not alter the *in vivo* pathogenicity of THA_139N as compared to that of parental THA_2014, corroborating the undetectable differences in the pathogenic profile reported for a modified epZIKV strain (PR_2015 with the N139S substitution)[226]. Overall, our *in vitro* and *in vivo* findings are consistent with earlier reported findings that the S139N substitution seemed to contribute to ZIKV virulence *in vitro* (i.e., increased viral replication fitness) but did not correlate directly to differences in the *in vivo* pathogenicity between preZIKV and epZIKV strains. If the S139N substitution was involved at all, it was not the sole genetic determinant responsible for the differences in the clinical outcomes brought about by preZIKV and epZIKV strains. To identify genetic determinants underlying the development of ZIKV-associated brain abnormalities in fetuses and newborns in future studies, it is important to design holistic studies that comprehensively examine multiple ZIKV strains *in vitro* and *in vivo*.

In summary, we showed that different Asian ZIKV strains share neurotropic and neurovirulent properties. We further postulate that the Asian lineage progressively evolved towards an attenuated pathogenicity. The accelerating urbanization, particularly to the natural habitats of the *Aedes* mosquito vector[245], and its associated expanding geographical distribution[246] as well as the immune status of individuals represent additional factors contributing to the increased

incidence of ZIKV outbreaks around the world. Further investigations on ZIKV-mediated nervous system damage should include the collaborative development of predictive models that integrate the multivariate impacts due to climatic, ecological, social, and cultural factors to improve the public health response.

IV.6 Supplementary Data

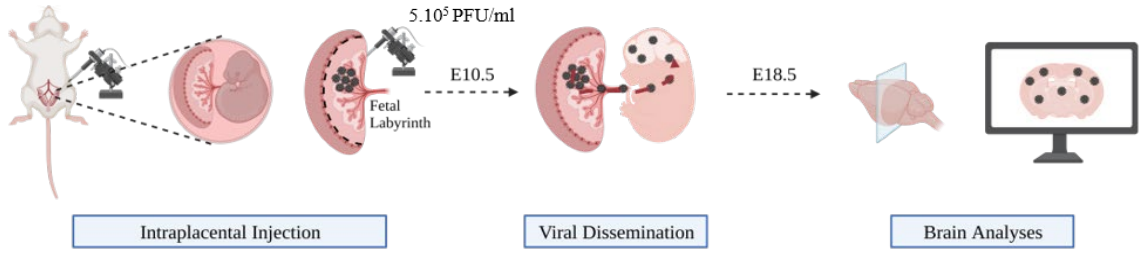

Supplementary Figure 4.1: Schematic representation of intraplacental infection technique. At the embryonic day 10.5 (E10.5), 1µl of ZIKV (5×10^5 PFU/ml) was injected in the fetal labyrinth of the placenta allowing the virus to reach the embryo through the umbilical cord and to disseminate within the embryo. At E18.5, embryonic brains were harvested and processed for different analyses.

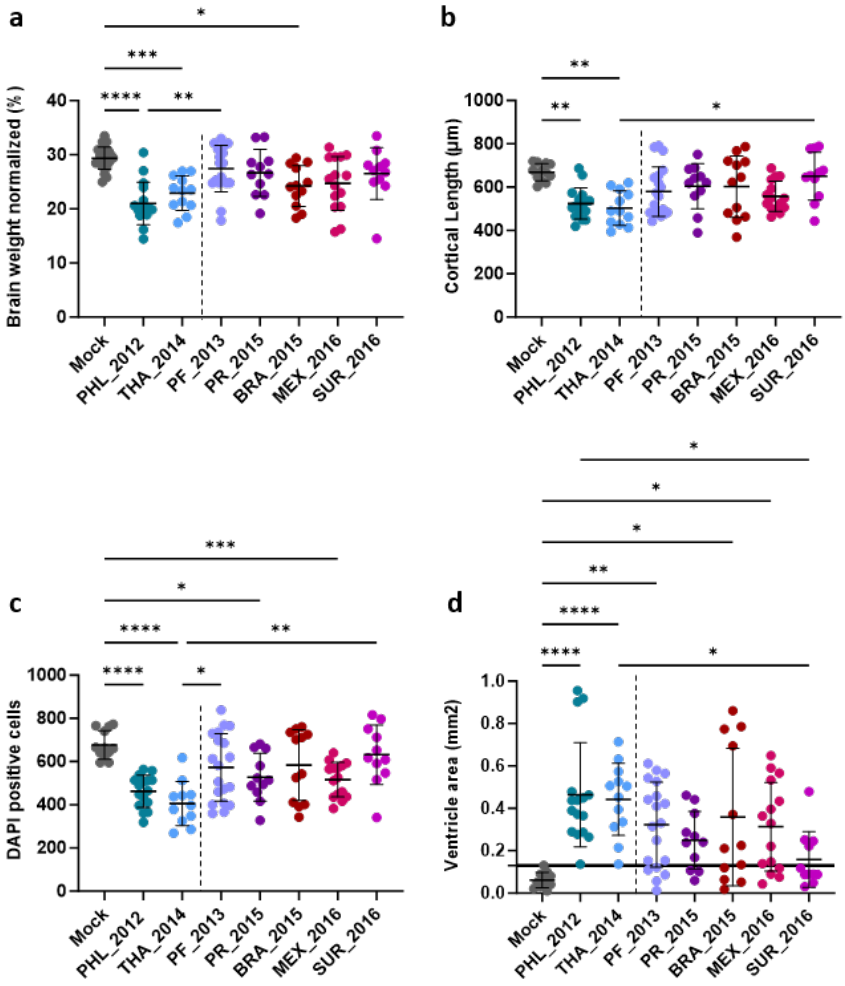

Supplementary Figure 4.2: Brain abnormalities in embryonic mice caused by several pre-epidemic and epidemic ZIKV strains a-d, Analyses of E18.5 embryonic mouse brain development after mock injection (n = 26 for brain weight and n = 12 otherwise) or infection by PHL_2012 (n = 16), by THA_2014 (n = 12), PF_2013 (n = 19), PRV_2015 (n = 11), BRA_2015 (n = 12), MEX_2016 (n = 15) and SUR_2016 (n = 11). **a**, Embryonic brains were examined morphologically by measuring the brain weight normalized to head weight. b,c, Microcephalic phenotypes were assessed by measuring (**b**) cortical length and (**c**) number of DAPI-positive cells. Ventriculomegaly was estimated by measuring the ventricle area (**d**). In (**a-d**) data are presented as mean ± standard deviation. Statistical significance of differences was determined by Brown-Forsythe and Welch Anova followed by Dunnett's T3 multiple comparisons test.

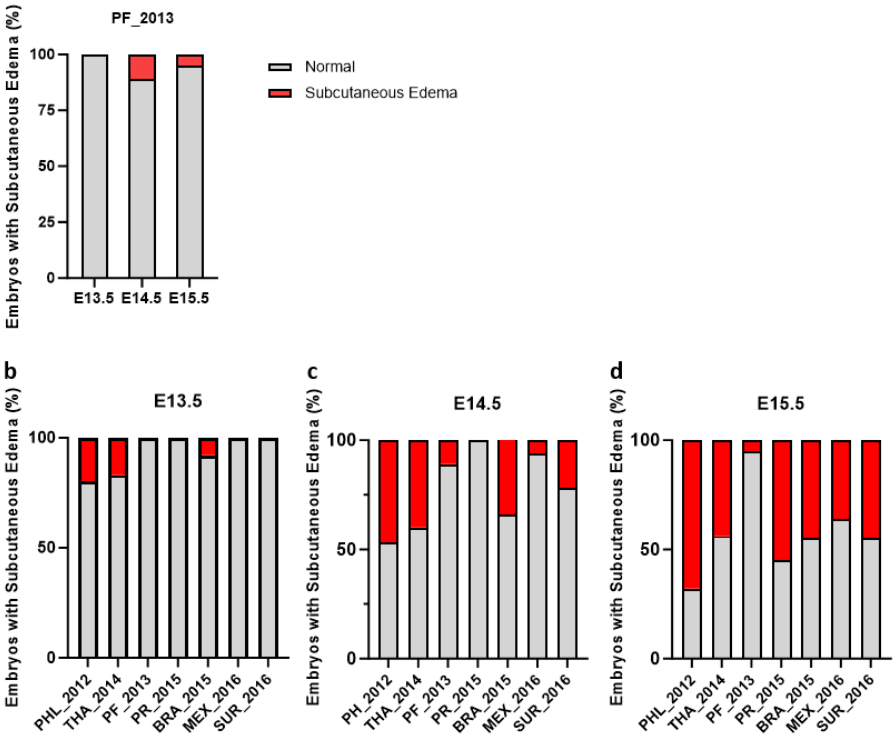

Supplementary Figure 4.3: Embryos infected by ZIKV develop subcutaneous edema.

a, Percentage of mouse embryos presenting subcutaneous edema at E13.5, E14.5 and E15.5 after infection by PF_2013 (n = 1, n = 14 and n = 18, respectively). **b,** Percentage of mouse embryos presenting subcutaneous edema at E13.5 after infection by PHL_2012 (n = 5), THA_2014 (n = 12), PF_2013 (n = 1), PR_2015 (n = 12), BRA_2015 (n = 12), MEX_2016 (n = 6) or SUR_2016 (n = 3). **c, d,** Percentage of mouse embryos presenting subcutaneous oedema at E14.5 (**c**) or E15.5 (**d**) after infection by PHL_2012 (n = 23 and n = 22, respectively), THA_2014 (n = 20 and n = 9, respectively), PF_2013 (n = 19 and n = 19, respectively), PRV_2015 (n = 7 and n = 11, respectively), BRA_2015 (n = 15 and n = 17, respectively), MEX_2016 (n = 13 and n = 14, respectively) or SUR_2016 (n = 23 and n = 11, respectively).

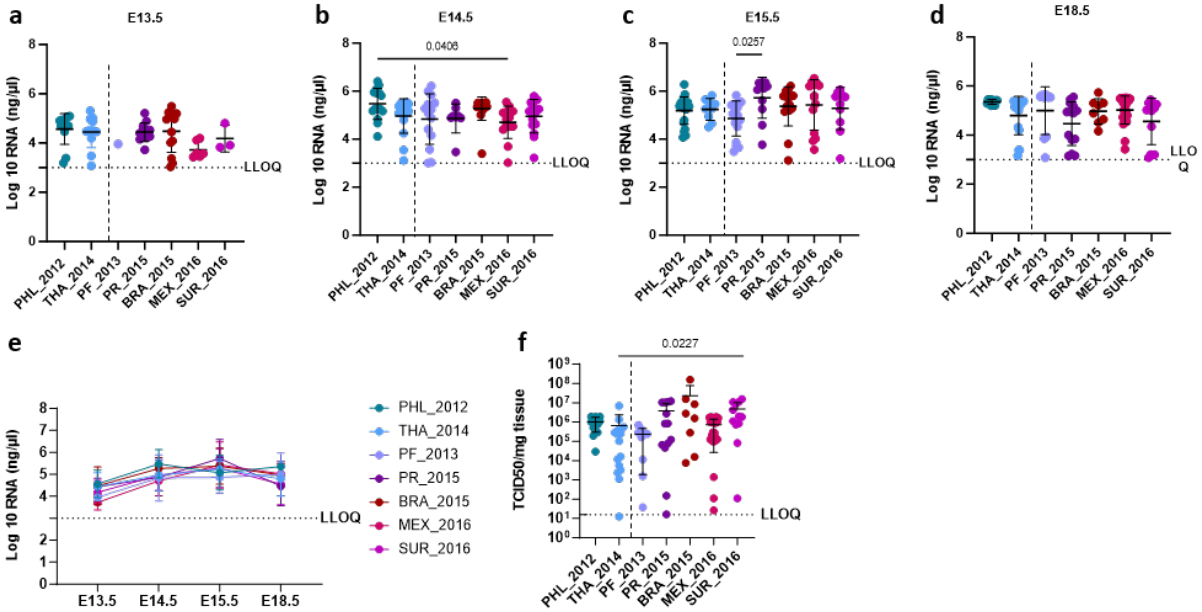

Supplementary Figure 4.4: Replication kinetics of the different pre-epidemic and epidemic ZIKV strains in embryonic mouse brain.

a-d, Brain viral loads for each ZIKV strains are shown in log_{10}-transformed viral genome copies for all timepoints. Viral loads in brains collected at E13.5 (**a**), E14.5 (**b**), E15.5 (**c**), E18.5 (**d**). **e**, Infectious virus in brain at E18.5 are shown in log_{10}-transformed 50% tissue-culture infectious dose (TCID50) per mg of tissue. N numbers are present in supplementary table 2. Data are presented as mean ± standard deviation. Statistical significance of differences was determined by one-way Anova followed by Kruskal-Wallis' multiple comparisons test. ns = not significant.

: Evolution of Asian Zika virus strains resulted in attenuated fetal brain pathogenicity

Supplementary Table 4.1. Details of the ZIKV strains used in this study

Name in study	Full name ZIKV strain	GenBank	AA at 139*
CAM_2010	ZIKV/H.sapiens-tc/KHM/2010/FSS13025	KU955593	S
PHL_2012	ZIKV/H.sapiens-tc/PHL/2012/CPC-0740	KU681082	S
THA_2014	ZIKV/H.sapiens-tc/THA/2014/SV0127-14	KU681081	S
PF_2013	ZIKV Pf13/251013-18	KY766069	N
PR_2015	ZIKV/Homo sapiens/PRI/PRVABC59/2015	KU501215	N
BRA_2015	ZIKV/H.sapiens/Brazil/PE243/2015	KX197192	N
MEX_2016	ZIKV/Aedes.sp/MEX/MEX_2-81/2016	KX446950	N
SUR_2016	ZIKV SL1602	KY348640	N

*The amino acid present at position 139 in the polyprotein of the ZIKV strains.

Supplementary Table 4.2. Number of embryos included in the in vivo studies per ZIKV strain and developmental stage

ZIKV strain	Viremia				TCID50
	E13.5	E14.5	E15.5	E18.5	E18.5
PHL_2012	12	15	22	11	11
THA_2014	12	16	9	17	16
PF_2013	1	14	18	10	9
PRV_2015	3	8	11	14	13
BRA_2015	13	18	16	8	8
MEX_2016	6	14	14	25	23
SUR_2016	3	15	11	14	12

Chapter V : General Discussion

V.1 ZIKV outbreaks of the African lineage

Since its discovery in 1947 in Uganda, ZIKV has evolved into two major lineages: the ancestral African lineage and the Asian lineage. The Brazilian ZIKV outbreak clearly demonstrated for the first time that ZIKV infections can lead to neurological complications in infants. More importantly, these complications seemed to be confined to ZIKV strains of the Asian lineage, as they have not been reported in the past for ZIKV strains of the African lineage. It raised questions in the scientific community as to why ZIKV outbreaks or ZIKV-associated neurological defects have not been previously reported in Africa, considering that the virus is endemic to the continent and has a long circulation history. In order to address this issue, several research groups have investigated whether African ZIKV strains are also capable of causing neurological defects and, if so, whether these are comparable to those induced by the Asian strains. While most studies point toward a higher virulence of African ZIKV as compared to Asian ZIKV, other studies reported conflicting results, making it difficult to draw firm conclusions about the potential of the African ZIKV lineage to induce neurological defects. Moreover, these studies had a major drawback. They were conducted using old African ZIKV strains (isolated in the 1960's and 1980's) or the original ZIKV MR766 strain which had been isolated in 1947 and since then passaged around 150 times, both *in vitro* and *in vivo* (in mouse brain)[204,205]. The pathogenicity of those ZIKV strains may not be representative of that of contemporary African ZIKV equivalents. Thus, in **chapter III**, we investigated the pathogenicity and epidemic potential of contemporary African ZIKV strains and whether like Asian ZIKV strains, they could cause brain defects in the developing embryo.

Our results using contemporary African ZIKV corroborated results from previous studies by showing that African ZIKV was more virulent than Asian ZIKV in both immunocompromised mice and in immunocompetent mouse embryos. We also showed that African ZIKV presented a neurotropism comparable to that caused by Asian ZIKV, suggesting that neurotropism is an intrinsic property of ZIKV and is thus not the result of a recent evolutionary event of the virus. Because of its extremely high virulent profile, *in utero* infections by African ZIKV during the first trimester of pregnancy may potentially cause more spontaneous abortions and stillbirths than neurological defects in fetuses. This hypothesis is supported by recent studies using non-human primates (NHP), which showed that infections by the African ZIKV during the first trimester of pregnancy led to 78% pregnancy loss versus only 26% pregnancy loss caused by Asian ZIKV[247]. Taken together, the higher virulence of African ZIKV might have played a role in the absence of reported cases of CZS that are associated with the African lineage.

The ability of the virus to cross the placental barrier is a crucial property to cause *in utero* infection leading to CZS. While the recent outbreaks highlighted this capacity for Asian ZIKV, it was unclear whether African ZIKV could also cross the placental barrier and consequently lead to the development of CZS. Unfortunately, the mode of infection in our mouse model (intraplacental injections) did not allow us to assess the vertical transmission properties of African ZIKV. However, studies using NHPs showed that, like their Asian counterparts, ZIKV strains from the African lineage can cross the placental barrier[225,248].

Given its highly virulent *in utero* profile, African lineage ZIKV requires close surveillance as it may pose a significant epidemic risk to humans. Furthermore, my collaborators at Institute Pasteur in Paris showed in **chapter III** as well as in another publication[163] that the natural mosquito vector *Aedes aegypti* from Asia and the Americas were more susceptible to African ZIKV strains because these strains showed higher infection rates and transmission efficiencies than did the Asian ZIKV strains. These results underscore the need for intensive surveillance of the African ZIKV lineage, as spread of the virus out of the African continent by a more competent vector, i.e., Asian/American *Aedes aegypti* mosquitoes, may lead to massive ZIKV outbreaks.

V.2 ZIKV outbreaks of the Asian lineage

As I wrote earlier, all ZIKV outbreaks that were associated with the development of CZS were caused by ZIKV of the Asian lineage. However, like African ZIKV, Asian ZIKV had also been circulating for decades prior to the emergence of ZIKV epidemics[249]. The first major ZIKV outbreak occurred on the Yap Island in 2007 with an estimated 73% of the population that got infected. However, unlike later ZIKV outbreaks causing epidemics in French Polynesia and Brazil, amongst others, it was not associated with the development of CZS or neurological diseases in infants[250]. This has led to the hypothesis that the ZIKV-associated neurological defects could have originated from a recent evolutionary event within the Asian ZIKV lineage. While some studies suggest that epidemic ZIKV strains (i.e., ZIKV French Polynesia and all those evolving from it) became more virulent than the pre-epidemic ZIKV strains (i.e., ZIKV strains circulating before ZIKV French Polynesia) due to the acquisition of certain genetic mutations[26,251], other studies reported the opposite[226,252]. These contradictions in the literature make it difficult to link the evolution of Asian ZIKV with the emergence of ZIKV-associated CZS cases. In **chapter IV**, I therefore conducted a comparative analysis of pre-epidemic and epidemic Asian ZIKV strains to ascertain whether a link exists between the evolution of the Asian lineage and the emergence of CZS.

Our study showed that neurotropism and neurovirulence were not the result of a recent evolutionary event of Asian ZIKV as these traits are shared by all Asian ZIKV strains, regardless of their status (pre-epidemic versus epidemic). However, although all ZIKV strains were detrimental to brain development, our data suggested that *in utero* infections by pre-epidemic ZIKV strains more consistently caused severe brain defects than infections by epidemic ZIKV. In addition, infections by pre-epidemic ZIKV led to an earlier and higher proportion of embryos developing subcutaneous oedema. These results indicate that all Asian ZIKV strains share similar properties, but that the pre-epidemic ZIKV strains displayed a more pathogenic profile than the epidemic ZIKV strains, suggesting that fetal pathogenicity brought about by Asian ZIKV evolved towards attenuation rather than exacerbation. The decreased neurovirulence of contemporary Asian ZIKV combined with the higher transmissibility of Asian ZIKV, the high rate of human infections, and the higher susceptibility of Asian/American *Aedes aegypti* mosquitoes may have increased the likelihood of developing congenital Zika syndrome (CZS).

V.3 IPL challenge: a mouse model to decipher mechanisms underlying CZS-associated brain abnormalities

To study ZIKV-associated brain abnormalities several mouse models were used. The most common model using WT mice involves intracerebral injection of ZIKV in newborn pups. While this model provided insights on ZIKV infection of brain cells, it may not be the most suitable model to study the development of brain abnormalities following ZIKV infection[26,41,226]. Indeed, at the post-natal stage, the cerebral cortex (which has been described as most susceptible to ZIKV infection) is already almost completely developed in mice and therefore may not represent the same stage in human brain developmental. Moreover, an injection of ZIKV directly into the brain parenchyma may affect the behavior of the virus, e.g., by modifying its cell tropism and distribution within the brain, amongst others, which may not reflect the natural physiopathology of ZIKV in the brain. In some studies the intracerebral injections were conducted at the embryonic stage, which more closely resembles the stage in human brain development, but as discussed above, the route of infection may conceivably impact brain pathology[26]. In our model, intraplacental injection allows ZIKV to more naturally reach the embryo and subsequently disseminate to the brain and other tissues. In addition, at E10.5, cortical development in mice corresponds to that of humans in the first trimester of pregnancy. Finally, these injections were not performed in immunodeficient mice, as was done in many other studies[138,253], but in immunocompetent dams. These characteristics of our IPL

mouse model allow us to mimic human fetal brain infections during the first trimester of pregnancy, hence making it a highly suitable model to study the pathology of ZIKV-associated fetal brain abnormalities.

In humans, fetuses exhibit a broad spectrum of brain abnormalities. Severe brain malformations in fetuses lead to fetal loss[79] or perinatal death[254] while some survive but develop severe neurological and neurodevelopmental complications[255]. Similarly to what was observed in human infants[243,254,256], a wide range of brain abnormalities was observed in our IPL ZIKV challenge mouse model, ranging from embryos without obvious brain defects to embryos presenting a moderate phenotype, and embryos having severe brain defects. Unravelling the underlying mechanism(s) responsible for the variability in the severity of brain abnormalities notwithstanding a similar infection is extremely complex. One option would be to study the mechanisms that are affected the same or differently following a ZIKV infection in poorly affected brains versus those with a severe phenotype. Markers that significantly altered in the severe cases compared to those in the less affected brains could be responsible for the increased virulence. Identifying these markers may subsequently allow the discovery of the mechanisms that are specifically dysregulated in the severe cases, which may aid in mitigating the development of severe brain abnormalities associated with ZIKV infection.

V.4 IPL challenge: a mouse model to study CZS-associated disorders

Despite the huge health threat posed by ZIKV to developing embryos, no routine ZIKV screening has been implemented to date for pregnant women except when the mother presents with symptoms suspected to be ZIKV related. The risk of transmitting ZIKV and developing neurological defects, however, is not directly correlated with the (a)symptomatic status of the mother[241,257,258]. Consequently, cases of prenatal ZIKV exposures are likely to go unnoticed as ZIKV infections mostly have an asymptomatic course. They are generally first discovered when detectable abnormalities in embryos are found during regular ultrasonic check-ups of pregnant women. In addition, several infants prenatally exposed to ZIKV do not present with microcephaly at birth but do experience neurodevelopmental delays (language, cognition, motor functions)[259]. Some of them even develop microcephaly postnatally[260].

Although the development of brain abnormalities is a main characteristic of CZS, it is only one facet of the syndrome which encompasses a much wider range of disorders with various affected organs and tissues. Affected organs associated with CZS are the eyes, the spinal cord, the lungs and the heart. Ocular abnormalities are a common finding in children with CZS.

Clinical studies showed that eyes abnormalities can be found in 20% to 30% of infants with CZS[93,261,262]. The main defects involve the retina and the optical nerve. The development of eye defects is more common in children with severe CZS but can also occur in children without neurological abnormalities[261,262]. Clinicians are therefore advocating eye screenings in all children with suspected prenatal ZIKV exposure, regardless of the CZS severity. The spinal cord is a preferential site of ZIKV infection. Spinal cord abnormalities observed in ZIKV-infected infants are arthrogryposis, spinal cord thickness reduction, architectural distortion, neuronal loss and microcalcifications[263–265]. Lung pathologies, on the other hand, have not been extensively described. A study by Alvino and co-workers showed that around 50% of the neonates with CZS and microcephaly suffered from early respiratory distress and 22% died from respiratory failure[266]. A post-mortem study reported pulmonary hypoplasia in all neonates, while intra-alveolar hemorrhages were found in a smaller number of neonates, and interstitial lymphocytic pulmonary infiltrations and an expansion of alveolar septa in only one neonate[267]. The heart was also shown to be targeted by ZIKV, as evidenced by the occurrence of heart abnormalities, albeit minor, in neonates with CZS[268,269]. Yet, another study that evaluated the morphology and the biventricular function of the heart in children with CZS, indicated that these children may experience early cardiac impairment due to a reduction in cardiac dimensions and biventricular dysfunctions[270], which can lead to severe heart failure. The lethality of these conditions was additionally demonstrated by a study conducted on deceased children with CZS, showing that they presented a higher percentage of deaths after the first year of life that was associated with circulatory system disorders, with cardiomyopathy, other cardiac arrhythmias and heart failures being the main cause[271]. While not all of these conditions are life-threatening, some will lead to permanent pain and disabilities, resulting in impairment of the quality of life and wellbeing of these children.

My studies in **chapter III** and **chapter IV** using the IPL ZIKV challenge mouse model, showed that ZIKV has a similar organ and tissue tropism as has been reported in human cases. We observed infection of the brain, the lungs and the heart, as detected either by RT-qPCR or immunofluorescence, and infection of the eyes and the spinal cord, as detected by immunofluorescence. We already demonstrated that our mouse model closely recapitulates the development of embryonic brain abnormalities after *in utero* infection during the first trimester of pregnancy in humans. Based on the similar infection pattern in the other organs, we anticipate that our embryonic mouse model may also recapitulate the other conditions associated with

CZS. Further characterization of our model could make this an extremely valuable tool to better understand the full pathogenicity of ZIKV in the developing fetus.

V.5 IPL challenge: a mouse model to study the immune system response

Inflammation is an essential process to protect the brain by inducing tissue repair[272]. In contrast, overactivation of the inflammatory pathways can cause chronic brain inflammation which can lead to tissue damages[273]. The major component of the immune system in the brain are the microglial cells. Microglial cells are the most abundant mononuclear phagocytes within the brain parenchyma[274]. They play an essential role in the pathogen's clearance from the brain through their phagocytic activity. Upon activation, the microglial cells can be differentiated in M1 pro-inflammatory microglia, which secrete proinflammatory cytokines and chemokines such as TNF-α and IL-6, or in M2 anti-inflammatory microglia, which release anti-inflammatory cytokines such as IL-10[274]. While a self-limited inflammation is neuroprotective, an excess of pro-inflammatory mediators or a chronic inflammation can lead to overactivation of microglial cells, causing a switch of the microglia to an M1 state[275]. In neurodegenerative diseases, activated microglia are suspected to be involved in the aggravation of the disease[272,273,275]. Studies have shown that ZIKV is able to infect microglial cells both *in vitro*[216,217] and *in vivo*[276]. Moreover, ZIKV infected microglial cells secrete more pro-inflammatory cytokines[217,276]. Hence, ZIKV infection of microglial cells could potentially induce a switch to a M1 state of the microglia, leading to an increased secretion of pro-inflammatory modulators. Taken together, the inflammation caused by a ZIKV infection, along with an increased release of pro-inflammatory cytokines and chemokines by activated microglial cells, could cause a deleterious effect on embryonic brain development.

As described in **chapter I**, ZIKV, through its non-structural proteins, can control and block the immune response. In our model, ZIKV infection of the fetal brain induced an immunological response, as observed on day 4 post-infection (**chapter IV**). The expression of the pro-inflammatory cytokine IL-6 and the chemokine CXCL10 (which is induced by IFN-γ), and the anti-inflammatory cytokine IL-10 was increased upon ZIKV infection. The presence of an immune response in the brain in our mouse model provides a great opportunity to better understand the potential role of the immune system in controlling or worsening of the brain defects during congenital ZIKV infections. To investigate this, infected brains could be harvested at different timepoints post-infection to determine the magnitude of the immune response, more specifically that of the inflammatory response, by quantifying the expression levels of various pro- and anti-inflammatory cytokines and chemokines. To examine the

potential detrimental effect of a prolonged and strong inflammatory response, diverse strategies can be considered. Amongst them is the administration of anti-inflammatory drugs at different timepoints post-infection to explore whether these could reduce the brain damages; some of these drugs have shown to be effective against ZIKV infections *in vitro*[277,278]. However, even if the efficacy of anti-inflammatory drugs against ZIKV is proven, their use should be closely monitored in areas where the closely related DENV also circulates since non-steroidal anti-inflammatory drugs are contraindicated in the case of DENV infection[8].

However, in our experiments in chapter IV, peripheral immune cells could also have contributed to the increased secretion as the embryos were not perfused. Related to this, a study using an *in vitro* human BBB model showed that ZIKV infection led to an increase in inflammatory cytokines and adhesion molecules levels which may lead to the recruitment of immune cells at the BBB. Therefore, the use of proper markers and mouse models that are specific to either the microglial cells or the peripheral blood cells is crucial to further investigate the role of these cells in causing elevated cytokine/chemokine levels upon ZIKV infection.

To study the protective or negative role of microglial cells on fetal brain development after ZIKV infection, specifically engineered transgenic mouse lines could be used. One is the TMEM119^{GFP} in which the green-fluorescent protein (GFP) is specifically expressed in microglial cells. Using this mouse line, the colonization of the brain by the microglial cells can be monitored and their number can be quantified. In combination with specific markers, such as Iba1 (Ionized calcium binding adaptor molecule 1) and CD68 (Cluster of Differentiation 68) that are expressed by activated microglial cells[279], the proportion of activated microglial cells following a ZIKV infection can be determined over a certain period of time. Another mouse line, TMEM119$^{CRE-ERT2}$, in which microglial cells can be depleted by injection of tamoxifen, could potentially be deployed to study the role of microglial cells in the development of brain defects. By depleting the microglial cells in the dams at different time points post-infection, the involvement of these in worsening the brain alterations could potentially be assessed. Moreover, these experiments may also aid in identifying the critical window at which the microglial cells switch from a protective to a damaging role in their attempt to cure the brain from the ZIKV infection.

These strategies combined with ELISA and FACS experiments using brain samples may elucidate the consequences of ZIKV-induced brain inflammation as well as the role of the different immune-modulating actors in the development of ZIKV-mediated brain abnormalities.

V.6 IPL challenge: a mouse model for vaccines and antivirals development

An important milestone that still needs to be achieved in our fight against ZIKV and its dramatic consequences is the development of potent and effective vaccines and antiviral compounds. So far, no vaccines or antiviral compounds are available, although several vaccines are currently undergoing clinical trials. One is a DNA vaccine that is now in a clinical phase II study[280], while two other vaccines are mRNA vaccines that both successfully completed a clinical phase I trial[281]. By contrast, no antiviral compound identified so far exhibited promising anti-ZIKV activity and pharmacokinetics to warrant their testing in clinical trials. An additional complicating factor in Zika drug development is a possible teratogenic effect of the drug, prohibiting their use in ZIKV-infected, pregnant women.

Our mouse model is also highly suitable for testing the *in vivo* efficacy and safety profile of potentially novel vaccine and antiviral drug candidates. Indeed, immunization of dams with a chimeric (yellow fever-Zika) vaccine prior to the IPL ZIKV challenge at E12.5 successfully protected the fetal brain against ZIKV infection as well as against ZIKV-induced brain malformations[235]. Similarly, the efficacy of promising antiviral compounds could be evaluated in our mouse model, provided that they are safe to both the mother and the fetuses and exhibit a favorable pharmacokinetic profile.

Limitations of the IPL ZIKV challenge mouse model

As described above, the IPL ZIKV challenge animal model represents a valuable animal model to study the alterations of the brain during embryonic development upon ZIKV infection. However, it also presents evident limitations. As evoked previously, the animal model relies on the microsurgery to bypass the mouse placental barrier and therefore does not allow to study differences in vertical transmission of the studied ZIKV strains. Indeed, one hypothesis explaining the sudden upsurge of CZS that occurred in the Pacific and Latin-America could be that the epidemic ZIKV strains are more capable of crossing the placental barrier (i.e., require lower viral titers) than the pre-epidemic ZIKV strains. This theory cannot be tested in our animal model. However, so far, all ZIKV strains that were tested to assess their vertical transmission capacity and the development of CZS, were shown to be able to cross the placental barrier in NHP[225,248].

Another important limitation of our IPL challenge mouse model is that it does not allow to study the susceptibility of the different placental cells to ZIKV infection. Indeed, the first trimester of pregnancy has been linked to higher vertical transmission rates with suspected increased susceptibility of the placenta's cells[126]. Unfortunately, the possible differences in

susceptibility of the different placental cells cannot be assessed in our mouse model, as the injection of the virus is performed directly into the labyrinth, which may induce a bias regarding the cells that are infected, the susceptibility and the timing of ZIKV infection, and the natural spread of ZIKV within the placenta.

Bibliography

1. Kuno, G., Chang, G.-J. J., Tsuchiya, K. R., Karabatsos, N. & Cropp, C. B. Phylogeny of the Genus Flavivirus . *J. Virol.* **72**, 73–83 (1998).
2. Valderrama, A., Díaz, Y. & López-Vergès, S. Interaction of Flavivirus with their mosquito vectors and their impact on the human health in the Americas. *Biochem. Biophys. Res. Commun.* **492**, 541–547 (2017).
3. Ciota, A. T. & Kramer, L. D. Vector-virus interactions and transmission dynamics of West Nile virus. *Viruses* **5**, 3021–3047 (2013).
4. European Centre for Disease Prevention and Control. Mosquito maps. https://www.ecdc.europa.eu/en/disease-vectors/surveillance-and-disease-data/mosquito-maps (2023).
5. Kraemer, M. U. G. *et al.* The global distribution of the arbovirus vectors Aedes aegypti and Ae. Albopictus. *Elife* **4**, 1–18 (2015).
6. Zahouli, J. B. Z. *et al.* Urbanization is a main driver for the larval ecology of Aedes mosquitoes in arbovirus-endemic settings in south-eastern Côte d'Ivoire. *PLoS Negl. Trop. Dis.* **11**, 1–23 (2017).
7. Lindsey, N. P. *et al.* Yellow fever resurgence: An avoidable crisis? *npj Vaccines* **7**, 2–4 (2022).
8. World Health Organization. Dengue and severe denguee. https://www.who.int/news-room/fact-sheets/detail/dengue-and-severe-dengue (2023).
9. Centers for Disease Control and Prevention. Dengue Around the World | Dengue | CDC. https://www.cdc.gov/dengue/areaswithrisk/around-the-world.html (2023).
10. Centers for Disease Control and Prevention. Dengue in Africa and the Middle East. https://wwwnc.cdc.gov/travel/notices/level1/dengue-africa-middle-east (2023).
11. World Health Organization. Zika virus. https://www.who.int/news-room/fact-sheets/detail/zika-virus (2022).
12. Heukelbach, J., Alencar, C. H., Kelvin, A. A., de Oliveira, W. K. & de Góes Cavalcanti, L. P. Zika virus outbreak in Brazil. *J. Infect. Dev. Ctries.* **10**, 116–120 (2016).
13. Baud, D., Gubler, D. J., Schaub, B., Lanteri, M. C. & Musso, D. An update on Zika virus infection. *Lancet* **390**, 2099–2109 (2017).
14. Cuevas-Juárez, E., Pando-Robles, V. & Palomares, L. A. Flavivirus vaccines: Virus-like particles and single-round infectious particles as promising alternatives. *Vaccine* **39**, 6990–7000 (2021).
15. Aguiar, M. & Stollenwerk, N. Dengvaxia: age as surrogate for serostatus. *Lancet Infect. Dis.* **18**, 245 (2018).
16. Achee, N. L. *et al.* Alternative strategies for mosquito-borne arbovirus control. *PLoS Negl. Trop. Dis.* **13**, 1–22 (2019).
17. Mead, P. S., Hills, S. L. & Brooks, J. T. Zika virus as a sexually transmitted pathogen.

Curr. Opin. Infect. Dis. **31**, 39–44 (2018).

18. Pomar, L. *et al.* Zika virus during pregnancy: From maternal exposure to congenital Zika virus syndrome. *Prenat. Diagn.* **39**, 420–430 (2019).

19. World Health Organization. Zika Virus Microcephaly and Guillain-Barré Syndrome. 1–15 (2016).

20. Cao-Lormeau, V. M. *et al.* Guillain-Barré Syndrome outbreak associated with Zika virus infection in French Polynesia: A case-control study. *Lancet* **387**, 1531–1539 (2016).

21. Cauchemez, S. *et al.* Association between Zika virus and microcephaly in French Polynesia, 2013-15: A retrospective study. *Lancet* **387**, 2125–2132 (2016).

22. Hu, T., Li, J., Carr, M. J., Duchêne, S. & Shi, W. The Asian Lineage of Zika Virus: Transmission and Evolution in Asia and the Americas. *Virol. Sin.* **34**, 1–8 (2019).

23. Pettersson, J. H. O. *et al.* How did zika virus emerge in the Pacific Islands and Latin America? *MBio* **7**, (2016).

24. Liu, Z. *et al.* A single nonsynonymous mutation on ZIKV E protein-coding sequences leads to markedly increased neurovirulence in vivo. *Virol. Sin.* **37**, 115–126 (2022).

25. Shan, C. *et al.* A Zika virus envelope mutation preceding the 2015 epidemic enhances virulence and fitness for transmission. *Proc. Natl. Acad. Sci. U. S. A.* **117**, 20190–20197 (2020).

26. Yuan, L. *et al.* A single mutation in the prM protein of Zika virus contributes to fetal microcephaly. *Science (80-.).* **358**, 933–936 (2017).

27. Regla-Nava, J. A. *et al.* A Zika virus mutation enhances transmission potential and confers escape from protective dengue virus immunity. *Cell Rep.* **39**, 110655 (2022).

28. Haddow, A. D. *et al.* Genetic characterization of zika virus strains: Geographic expansion of the asian lineage. *PLoS Negl. Trop. Dis.* **6**, (2012).

29. Leung, J. Y. *et al.* Role of Nonstructural Protein NS2A in Flavivirus Assembly. *J. Virol.* **82**, 4731–4741 (2008).

30. Sirohi, D. & Kuhn, R. J. Zika Virus Structure, Maturation, and Receptors. *J. Infect. Dis.* **216**, S935–S944 (2017).

31. Klase, Z. A. *et al.* Zika Fetal Neuropathogenesis: Etiology of a Viral Syndrome. *PLoS Negl. Trop. Dis.* **10**, 1–32 (2016).

32. Pierson, T. C. & Diamond, M. S. The emergence of Zika virus and its new clinical syndromes. *Nature* **560**, 573–581 (2018).

33. Mukhopadhyay, S., Kuhn, R. J. & Rossmann, M. G. A structural perspective of the Flavivirus life cycle. *Nat. Rev. Microbiol.* **3**, 13–22 (2005).

34. Pierson, T. C. & Diamond, M. S. The continued threat of emerging flaviviruses. *Nat. Microbiol.* **5**, 796–812 (2020).

35. Yoshii, K. *et al.* A conserved region in the prM protein is a critical determinant in the assembly of flavivirus particles. *J. Gen. Virol.* **93**, 27–38 (2012).

36. Xie, X. *et al.* Dengue NS2A Protein Orchestrates Virus Assembly. *Cell Host Microbe*

26, 606-622.e8 (2019).

37. Barrows, N. J. *et al.* Biochemistry and Molecular Biology of Flaviviruses. *Chem. Rev.* **118**, 4448–4482 (2018).

38. Zhang, X. *et al.* Genetic and biochemical characterizations of Zika virus NS2A protein. *Emerg. Microbes Infect.* **8**, 585–602 (2019).

39. Dabrowska, A., Milewska, A., Ner-Kluza, J., Suder, P. & Pyrc, K. Mass spectrometry versus conventional techniques of protein detection: Zika virus NS3 protease activity towards cellular proteins. *Molecules* **26**, (2021).

40. Peter M. Howley, David M. Knipe , Sean Whelan, , Eric O. Freed, J. L. C. *Fields Virology: RNA Viruses*. (2022).

41. Lin, C. S. *et al.* A Reverse Mutation E143K within the PrM Protein of Zika Virus Asian Lineage Natal RGN Strain Increases Infectivity and Cytopathicity. *Viruses* **14**, (2022).

42. Zeng, J. *et al.* The Zika Virus Capsid Disrupts Corticogenesis by Suppressing Dicer Activity and miRNA Biogenesis. *Cell Stem Cell* **27**, 618-632.e9 (2020).

43. Li, H. *et al.* Zika Virus Protease Cleavage of Host Protein Septin-2 Mediates Mitotic Defects in Neural Progenitors. *Neuron* **101**, 1089-1098.e4 (2019).

44. Liang, Q. *et al.* Zika Virus NS4A and NS4B Proteins Deregulate Akt-mTOR Signaling in Human Fetal Neural Stem Cells to Inhibit Neurogenesis and Induce Autophagy. *Cell Stem Cell* **19**, 663–671 (2016).

45. Li, P. *et al.* Non-Structural Protein 5 of Zika Virus Interacts with p53 in Human Neural Progenitor Cells and Induces p53-Mediated Apoptosis. *Virol. Sin.* **36**, 1411–1420 (2021).

46. Chan, Y. T. *et al.* Immune Recognition versus Immune Evasion Systems in Zika Virus Infection. *Biomedicines* **11**, 1–19 (2023).

47. Guo, Z., Li, Y. & Ding, S. W. Small RNA-based antimicrobial immunity. *Nat. Rev. Immunol.* **19**, 31–44 (2019).

48. Sui, L. *et al.* Flavivirus prM interacts with MDA5 and MAVS to inhibit RLR antiviral signaling. *Cell Biosci.* **13**, 1–14 (2023).

49. Xia, H. *et al.* An evolutionary NS1 mutation enhances Zika virus evasion of host interferon induction. *Nat. Commun.* **9**, 414 (2018).

50. Wu, Y. *et al.* Erratum: Zika virus evades interferon-mediated antiviral response through the co-operation of multiple nonstructural proteins in vitro. *Cell Discov.* **3**, 17014 (2017).

51. Grant, A. *et al.* Zika Virus Targets Human STAT2 to Inhibit Type I Interferon Signaling. *Cell Host Microbe* **19**, 882–890 (2016).

52. Azevedo, R. S. S. *et al.* In situ immune response and mechanisms of cell damage in central nervous system of fatal cases microcephaly by Zika virus. *Sci. Rep.* **8**, 1–11 (2018).

53. Foo, S. S. *et al.* Asian Zika virus strains target CD14+ blood monocytes and induce M2-skewed immunosuppression during pregnancy. *Nat. Microbiol.* **2**, 1558–1570 (2017).

54. Colavita, F. *et al.* ZIKV infection induces an inflammatory response but fails to activate types I, II, and III IFN response in human PBMC. *Mediators Inflamm.* **2018**, (2018).

55. Clé, M. *et al.* Zika Virus Infection Promotes Local Inflammation, Cell Adhesion Molecule Upregulation, and Leukocyte Recruitment at the Blood-Brain Barrier. *MBio* **11**, 1–25 (2020).

56. Stefanik, M. *et al.* Characterisation of Zika virus infection in primary human astrocytes. *BMC Neurosci.* **19**, 1–8 (2018).

57. Jeong, G. U. *et al.* Zika Virus Infection Induces Interleukin-1β-Mediated Inflammatory Responses by Macrophages in the Brain of an Adult Mouse Model. *J. Virol.* **97**, 1–15 (2023).

58. Ellenbroek, B. & Youn, J. Rodent models in neuroscience research: is it a rat race? *Dis. Model. Mech.* **9**, 1079–1087 (2016).

59. Bayer, S. A., Altman, J., Russo, R. J. & Zhang, X. Timetables of neurogenesis in the human brain based on experimentally determined patterns in the rat. *Neurotoxicology* **14**, 83–144 (1993).

60. Silk, J., Short, J., Roberts, J. & Kusnitz, J. Gestation length in rhesus macaques (Macaca mulatta). *Int. J. Primatol.* **14**, 95–104 (1993).

61. Chen, V. S. *et al.* Histology Atlas of the Developing Prenatal and Postnatal Mouse Central Nervous System, with Emphasis on Prenatal Days E7.5 to E18.5. *Toxicol. Pathol.* **45**, 705–744 (2017).

62. Gao, P., Sultan, K. T., Zhang, X.-J. & Shi, S.-H. Lineage-dependent circuit assembly in the neocortex. *Development* **140**, 2645–2655 (2013).

63. Greig, L. C., Woodworth, M. B., Galazo, M. J., Padmanabhan, H. & Macklis, J. D. Molecular logic of neocortical projection neuron specification, development and diversity. *Nat. Rev. Neurosci.* **14**, 755–769 (2013).

64. Mukhtar, T. & Taylor, V. Untangling Cortical Complexity During Development. *J. Exp. Neurosci.* **12**, (2018).

65. Taverna, E., Götz, M. & Huttner, W. B. *The Cell Biology of Neurogenesis: Toward an Understanding of the Development and Evolution of the Neocortex*. *Annual Review of Cell and Developmental Biology* vol. 30 (2014).

66. Tan, X. & Shi, S. H. Neocortical neurogenesis and neuronal migration. *Wiley Interdiscip. Rev. Dev. Biol.* **2**, 443–459 (2013).

67. Noctor, S. C., Martínez-Cerdeño, V. & Kriegstein, A. R. Distinct behaviors of neural stem and progenitor cells underlie cortical neurogenesis. *J. Comp. Neurol.* **508**, 28–44 (2008).

68. Vasilakis, N. & Weaver, S. C. Flavivirus transmission focusing on Zika. *Curr. Opin. Virol.* **22**, 30–35 (2017).

69. Valentine, M. J., Murdock, C. C. & Kelly, P. J. Sylvatic cycles of arboviruses in non-human primates. *Parasites and Vectors* **12**, 1–18 (2019).

70. Wolfe, N. D. *et al.* Sylvatic transmission of arboviruses among Bornean orangutans. *Am. J. Trop. Med. Hyg.* (2001) doi:https://doi.org/10.4269/ajtmh.2001.64.310.

71. Tongthainan, D. *et al.* Seroprevalence of Dengue, Zika, and Chikungunya Viruses in Wild Monkeys in Thailand. *Am. J. Trop. Med. Hyg.* **103**, 1228–1233 (2020).

72. Mongkol, N. *et al.* Seroprevalence of Chikungunya and Zika virus in nonhuman primates: A systematic review and meta-analysis. *One Heal.* **15**, 100455 (2022).

73. Grard, G. *et al.* Zika Virus in Gabon (Central Africa) - 2007: A New Threat from Aedes albopictus? *PLoS Negl. Trop. Dis.* **8**, 1–6 (2014).

74. Wong, P. S. J., Li, M. zhi I., Chong, C. S., Ng, L. C. & Tan, C. H. Aedes (Stegomyia) albopictus (Skuse): A Potential Vector of Zika Virus in Singapore. *PLoS Negl. Trop. Dis.* **7**, 1–5 (2013).

75. Petersen, L. R., Jamieson, D. J., Powers, A. M. & Honein, M. A. Zika Virus. *N. Engl. J. Med.* **374**, 1552–1563 (2016).

76. Hills, S. L. *et al.* Transmission of Zika Virus Through Sexual Contact with Travelers to Areas of Ongoing Transmission — Continental United States, 2016. *MMWR. Morb. Mortal. Wkly. Rep.* **65**, 215–216 (2016).

77. Atkinson, B. *et al.* Presence and persistence of zika virus RNA in semen, United Kingdom, 2016. *Emerg. Infect. Dis.* **23**, 611–615 (2017).

78. Centers for Disease Control and Prevention. Men and Zika. *https://www.cdc.gov/zika/men/index.html* (2019).

79. Pomar, L. *et al.* Maternal-fetal transmission and adverse perinatal outcomes in pregnant women infected with Zika virus: prospective cohort study in French Guiana. *BMJ* **363**, 4431 (2018).

80. Adebanjo, T. *et al.* Update: Interim Guidance for the Diagnosis, Evaluation, and Management of Infants with Possible Congenital Zika Virus Infection — United States, October 2017. **66**, (2006).

81. Hoen, B. *et al.* Pregnancy Outcomes after ZIKV Infection in French Territories in the Americas. *N. Engl. J. Med.* **378**, 985–994 (2018).

82. Sanz Cortes, M. *et al.* Clinical assessment and brain findings in a cohort of mothers, fetuses and infants infected with ZIKA virus. *Am. J. Obstet. Gynecol.* **218**, 440.e1-440.e36 (2018).

83. Severino, M. *et al.* Definitions and classification of malformations of cortical development: Practical guidelines. *Brain* **143**, 2874–2894 (2020).

84. Gladwyn-Ng, I. *et al.* Stress-induced unfolded protein response contributes to Zika virus-associated microcephaly. *Nat. Neurosci.* **21**, 63–73 (2018).

85. Li, C. *et al.* Zika Virus Disrupts Neural Progenitor Development and Leads to Microcephaly in Mice. *Cell Stem Cell* **19**, 120–126 (2016).

86. Gabriel, E. *et al.* Recent Zika Virus Isolates Induce Premature Differentiation of Neural Progenitors in Human Brain Organoids. *Cell Stem Cell* **20**, 397-406.e5 (2017).

87. Boston Children's Hospital. Ventriculomegaly. *https://www.childrenshospital.org/conditions/ventriculomegaly* https://www.childrenshospital.org/conditions/ventriculomegaly.

88. Mccartney, E. & Squier, W. Patterns and pathways of calcification in the developing brain. *Dev. Med. Child Neurol.* **56**, 1009–1015 (2014).

89. Chen, W. *et al.* Zika virus NS3 protease induces bone morphogenetic protein-dependent brain calcification in human fetuses. *Nat. Microbiol.* **6**, 455–466 (2021).

90. Tavares, J. de S. *et al.* Classification of Congenital Zika Syndrome: Muscle Tone, Motor Type, Body Segments Affected, and Gross Motor Function. *Dev. Neurorehabil.* **24**, 296–302 (2021).

91. Maia, C. Q., Lima, W. G., Nizer, W. S. da C. & Ferreira, J. M. S. Epilepsy in children with Congenital Zika Syndrome: A systematic review and meta-analysis. *Epilepsia* **62**, 1193–1207 (2021).

92. Satterfield-Nash, A. *et al.* Health and Development at Age 19–24 Months of 19 Children Who Were Born with Microcephaly and Laboratory Evidence of Congenital Zika Virus Infection During the 2015 Zika Virus Outbreak — Brazil, 2017. *MMWR. Morb. Mortal. Wkly. Rep.* **66**, 1347–1351 (2017).

93. De Paula Freitas, B. *et al.* Ocular findings in infants with microcephaly associated with presumed zika virus congenital infection in Salvador, Brazil. *JAMA Ophthalmol.* **134**, 529–535 (2016).

94. Oliveira, C. S. de *et al.* Seguimento de crianças expostas intraútero ao vírus Zika na Região Metropolitana de Belém, Pará, Brasil. *Rev. Pan-Amazônica Saúde* **11**, 1–7 (2020).

95. National Health Service. Guillain-Barré syndrome. *https://www.nhs.uk/conditions/guillain-barre-syndrome/symptoms/* https://www.nhs.uk/conditions/guillain-barre-syndrome/symptoms/ (2020).

96. Berg, B. Van Den, Bunschoten, C. & Doorn, P. A. Van. Mortality in Guillain-Barré syndrome. (2013).

97. Barbi, L., Coelho, A. V. C., Alencar, L. C. A. de & Crovella, S. Prevalence of Guillain-Barré syndrome among Zika virus infected cases: a systematic review and meta-analysis. *Brazilian J. Infect. Dis.* **22**, 137–141 (2018).

98. National Institutes of Health. Guillain-Barré Syndrome. *https://www.ninds.nih.gov/health-information/disorders/guillain-barre-syndrome* https://www.ninds.nih.gov/health-information/disorders/guillain-barre-syndrome (2023).

99. Peixoto, H. M., Romero, G. A. S., De Araújo, W. N. & Fernandes de Oliveira, M. R. Guillain–Barré syndrome associated with Zika virus infection in Brazil: A cost-of-illness study. *Trans. R. Soc. Trop. Med. Hyg.* **113**, 252–258 (2019).

100. Boyer, S., Calvez, E., Chouin-Carneiro, T., Diallo, D. & Failloux, A.-B. An overview of mosquito vectors of Zika virus. *Microbes Infect.* **20**, 646–660 (2018).

101. Gutiérrez-Bugallo, G. *et al.* Vector-borne transmission and evolution of Zika virus. *Nat. Ecol. Evol.* **3**, 561–569 (2019).

102. Dick, G. W. A., Kitchen, S. F. & Haddow, A. J. Zika Virus (I). Isolations and serological specificity. *Trans. R. Soc. Trop. Med. Hyg.* **46**, 509–520 (1952).

103. Musso, D. & Gubler, D. J. Zika Virus. *Clin. Microbiol. Rev.* **29**, 487–524 (2016).

104. Kindhauser, M. K., Allen, T., Frank, V., Santhana, R. S. & Dye, C. Zika: the origin and spread of a mosquito-borne virus. *Bull. World Health Organ.* **94**, 675-686C (2016).

105. Duffy, M. R. *et al. Zika Virus Outbreak on Yap Island, Federated States of Micronesia*.

106. Cao-Lormeau, V.-M. Zika Virus, French Polynesia, South Pacific, 2013. *Emerg. Infect. Dis.* **20**, 1960 (2014).

107. Cao-Lormeau, V.-M. & Musso, D. Emerging arboviruses in the Pacific. *Lancet* **384**, 1571–1572 (2014).

108. Musso, D., Ko, A. I. & Baud, D. Zika Virus Infection — After the Pandemic. *N. Engl. J. Med.* **381**, 1444–1457 (2019).

109. Oehler, E. *et al.* Zika virus infection complicated by Guillain-Barré syndrome – case report, French Polynesia, December 2013. *Eurosurveillance* **19**, (2014).

110. Liu, Z.-Y., Shi, W.-F. & Qin, C.-F. The evolution of Zika virus from Asia to the Americas. *Nat. Rev. Microbiol.* **17**, 131–139 (2019).

111. Duong, V. *et al.* Low Circulation of Zika Virus, Cambodia, 2007-2016. *Emerg. Infect. Dis.* **23**, 296–299 (2017).

112. Ruchusatsawat, K. *et al.* Long-term circulation of Zika virus in Thailand: an observational study. *Lancet. Infect. Dis.* **19**, 439–446 (2019).

113. Maurer-Stroh, S. *et al.* South-east Asian Zika virus strain linked to cluster of cases in Singapore, August 2016. *Euro Surveill.* **21**, 30347 (2016).

114. Chu, D.-T., Ngoc, V. T. N. & Tao, Y. Zika virus infection in Vietnam: current epidemic, strain origin, spreading risk, and perspective. *Eur. J. Clin. Microbiol. & Infect. Dis.* **36**, 2041–2042 (2017).

115. Grubaugh, N. D., Ishtiaq, F., Setoh, Y. X. & Ko, A. I. Misperceived Risks of Zika-related Microcephaly in India. *Trends Microbiol.* **27**, 381–383 (2019).

116. Lan, P. T. *et al.* Fetal Zika Virus Infection in Vietnam. *PLoS Curr.* **9**, ecurrents.outbreaks.1c8f631e0ef8cd7777d639eba48647 (2017).

117. Moi, M. L. *et al.* Zika virus infection and microcephaly in Vietnam. *Lancet Infect. Dis.* **17**, 805–806 (2017).

118. Kuadkitkan, A., Wikan, N., Sornjai, W. & Smith, D. R. Zika virus and microcephaly in Southeast Asia: A cause for concern? *J. Infect. Public Health* **13**, 11–15 (2020).

119. Wongsurawat, T. *et al.* Case of Microcephaly after Congenital Infection with Asian Lineage Zika Virus, Thailand. *Emerg. Infect. Dis.* **24**, 1758–1761 (2018).

120. Lourenço, J. *et al.* Epidemiology of the Zika Virus Outbreak in the Cabo Verde Islands, West Africa. *PLoS Curr.* **10**, ecurrents.outbreaks.19433b1e4d007451c691f138e1e67e (2018).

121. Faye, O. *et al.* Genomic epidemiology of 2015-2016 zika virus outbreak in Cape Verde. *Emerg. Infect. Dis.* **26**, 1084–1090 (2020).

122. Hill, S. C. *et al.* Emergence of the Asian lineage of Zika virus in Angola: an outbreak investigation. *Lancet. Infect. Dis.* **19**, 1138–1147 (2019).

123. Anfasa, F. *et al.* Phenotypic Differences between Asian and African Lineage Zika Viruses in. *mSphere* **2**, 1–10 (2017).

124. Bowen, J. R. *et al.* Zika Virus Antagonizes Type I Interferon Responses during Infection of Human Dendritic Cells. *PLOS Pathog.* **13**, e1006164 (2017).

125. Hamel, R. *et al.* African and Asian Zika virus strains differentially induce early antiviral responses in primary human astrocytes. *Infect. Genet. Evol.* **49**, 134–137 (2017).

126. Sheridan, M. A. *et al.* Vulnerability of primitive human placental trophoblast to Zika virus. *Proc. Natl. Acad. Sci. U. S. A.* **114**, E1587–E1596 (2017).

127. Simonin, Y. *et al.* Zika Virus Strains Potentially Display Different Infectious Profiles in Human Neural Cells. *EBioMedicine* **12**, 161–169 (2016).

128. Smith, D. R. *et al.* African and asian zika virus isolates display phenotypic differences both in vitro and in vivo. *Am. J. Trop. Med. Hyg.* **98**, 432–444 (2018).

129. Pompon, J. *et al.* A Zika virus from America is more efficiently transmitted than an Asian virus by Aedes aegypti mosquitoes from Asia. *Sci. Rep.* **7**, 1215 (2017).

130. Weger-Lucarelli, J. *et al.* Vector Competence of American Mosquitoes for Three Strains of Zika Virus. (2016) doi:10.1371/journal.pntd.0005101.

131. Roundy, C. M. *et al.* Variation in Aedes aegypti Mosquito Competence for Zika Virus Transmission. *Emerg. Infect. Dis.* **23**, 625–632 (2017).

132. Calvez, E. *et al.* Differential transmission of Asian and African Zika virus lineages by Aedes aegypti from New Caledonia. *Emerg. Microbes Infect.* **7**, 159 (2018).

133. Lazear, H. M. *et al.* A Mouse Model of Zika Virus Pathogenesis. *Cell Host Microbe* **19**, 720–730 (2016).

134. Tripathi, S. *et al.* A novel Zika virus mouse model reveals strain specific differences in virus pathogenesis and host inflammatory immune responses. *PLoS Pathog.* **13**, 1–19 (2017).

135. Widman, D. G. *et al.* A Reverse Genetics Platform That Spans the Zika Virus Family Tree. *MBio* **8**, e02014-16 (2017).

136. Dowall, S. D. *et al.* A Susceptible Mouse Model for Zika Virus Infection. *PLoS Negl. Trop. Dis.* **10**, e0004658–e0004658 (2016).

137. Shao, Q. *et al.* The african zika virus mr-766 is more virulent and causes more severe brain damage than current asian lineage and dengue virus. *Dev.* **144**, 4114–4124 (2017).

138. Jaeger, A. S. *et al.* Zika viruses of African and Asian lineages cause fetal harm in a mouse model of vertical transmission. *PLoS Negl. Trop. Dis.* **13**, 1–18 (2019).

139. Goodfellow, F. T. *et al.* Strain-dependent consequences of zika virus infection and differential impact on neural development. *Viruses* **10**, (2018).

140. Willard, K. A. *et al.* Zika Virus Exhibits Lineage-Specific Phenotypes in Cell Culture, in Aedes aegypti Mosquitoes, and in an Embryo Model. *Viruses* **9**, 383 (2017).

141. Duggal, N. K. *et al.* Differential neurovirulence of African and Asian genotype Zika virus isolates in outbred immunocompetent mice. *Am. J. Trop. Med. Hyg.* **97**, 1410–1417 (2017).

142. Aliota, M. T. *et al.* Heterologous Protection against Asian Zika Virus Challenge in Rhesus Macaques. *PLoS Negl. Trop. Dis.* **10**, e0005168–e0005168 (2016).

143. Rayner, J. O. *et al.* Comparative pathogenesis of Asian and African-lineage Zika virus in Indian rhesus macaque's and development of a non-human primate model suitable for the evaluation of new drugs and vaccines. *Viruses* **10**, (2018).

144. Koide, F. *et al.* Development of a zika virus infection model in cynomolgus macaques. *Front. Microbiol.* **7**, 1–8 (2016).

145. Cugola, F. R. *et al.* The Brazilian Zika virus strain causes birth defects in experimental models. *Nature* **534**, 267–271 (2016).

146. Liu, S., Delalio, L. J., Isakson, B. E. & Wang, T. T. AXL-Mediated Productive Infection of Human Endothelial Cells by Zika Virus. *Circ. Res.* **119**, 1183–1189 (2016).

147. Simonin, Y., van Riel, D., Van de Perre, P., Rockx, B. & Salinas, S. Differential virulence between Asian and African lineages of Zika virus. *PLoS Negl. Trop. Dis.* **11**, e0005821–e0005821 (2017).

148. Lequime, S., Bastide, P., Dellicour, S., Lemey, P. & Baele, G. nosoi: A stochastic agent-based transmission chain simulation framework in r. *Methods Ecol. Evol.* **11**, 1002–1007 (2020).

149. Baidaliuk, A. *et al.* Cell-Fusing Agent Virus Reduces Arbovirus Dissemination in Aedes aegypti Mosquitoes In Vivo. *J. Virol.* **93**, e00705-19 (2019).

150. Fontaine, A., Jiolle, D., Moltini-Conclois, I., Lequime, S. & Lambrechts, L. Excretion of dengue virus RNA by Aedes aegypti allows non-destructive monitoring of viral dissemination in individual mosquitoes. *Sci. Rep.* **6**, 24885 (2016).

151. Zmurko, J. *et al.* The Viral Polymerase Inhibitor 7-Deaza-2'-C-Methyladenosine Is a Potent Inhibitor of In Vitro Zika Virus Replication and Delays Disease Progression in a Robust Mouse Infection Model. *PLoS Negl. Trop. Dis.* **10**, e0004695–e0004695 (2016).

152. Lequime, S., Richard, V., Cao-Lormeau, V.-M. & Lambrechts, L. Full-genome dengue virus sequencing in mosquito saliva shows lack of convergent positive selection during transmission by Aedes aegypti. *Virus Evol.* **3**, vex031–vex031 (2017).

153. Bolger, A. M., Lohse, M. & Usadel, B. Trimmomatic: a flexible trimmer for Illumina sequence data. *Bioinformatics* **30**, 2114–2120 (2014).

154. Langmead, B. & Salzberg, S. L. Fast gapped-read alignment with Bowtie 2. *Nat. Methods* **9**, 357–359 (2012).

155. Boisvert, S., Laviolette, F. & Corbeil, J. Ray: simultaneous assembly of reads from a mix of high-throughput sequencing technologies. *J. Comput. Biol.* **17**, 1519–1533 (2010).

156. Nurk, S., Meleshko, D., Korobeynikov, A. & Pevzner, P. A. metaSPAdes: a new versatile metagenomic assembler. *Genome Res.* **27**, 824–834 (2017).

157. Altschul, S. F., Gish, W., Miller, W., Myers, E. W. & Lipman, D. J. Basic local alignment search tool. *J. Mol. Biol.* **215**, 403–410 (1990).

158. Katoh, K. & Standley, D. M. MAFFT multiple sequence alignment software version 7: improvements in performance and usability. *Mol. Biol. Evol.* **30**, 772–780 (2013).

159. Kalyaanamoorthy, S., Minh, B. Q., Wong, T. K. F., von Haeseler, A. & Jermiin, L. S. ModelFinder: fast model selection for accurate phylogenetic estimates. *Nat. Methods* **14**, 587–589 (2017).

160. Hoang, D. T., Chernomor, O., von Haeseler, A., Minh, B. Q. & Vinh, L. S. UFBoot2: Improving the Ultrafast Bootstrap Approximation. *Mol. Biol. Evol.* **35**, 518–522 (2018).

161. Nguyen, L.-T., Schmidt, H. A., von Haeseler, A. & Minh, B. Q. IQ-TREE: a fast and effective stochastic algorithm for estimating maximum-likelihood phylogenies. *Mol. Biol. Evol.* **32**, 268–274 (2015).

162. Gong, Z., Xu, X. & Han, G.-Z. The Diversification of Zika Virus: Are There Two Distinct Lineages? *Genome Biol. Evol.* **9**, 2940–2945 (2017).

163. Aubry, F. *et al.* Enhanced Zika virus susceptibility of globally invasive *Aedes aegypti* populations. *Science (80-.).* **370**, 991–996 (2020).

164. L.J. REED and H.MUENCH. A simple method of estimating fifty per cent endpoints. *Am. J. Hyg.* **27**, 45–59 (2015).

165. Fontaine, A. *et al.* Epidemiological significance of dengue virus genetic variation in mosquito infection dynamics. *PLoS Pathog.* **14**, e1007187–e1007187 (2018).

166. Yakob, L., Kucharski, A., Hue, S. & Edmunds, W. J. Low risk of a sexually-transmitted Zika virus outbreak. *Lancet Infect. Dis.* **16**, 1100–1102 (2016).

167. Lequime, S. & Lambrechts, L. Vertical transmission of arboviruses in mosquitoes: A historical perspective. *Infect. Genet. Evol.* **28**, 681–690 (2014).

168. Favier, C. *et al.* Influence of spatial heterogeneity on an emerging infectious disease: the case of dengue epidemics. *Proceedings. Biol. Sci.* **272**, 1171–1177 (2005).

169. Andraud, M., Hens, N., Marais, C. & Beutels, P. Dynamic epidemiological models for dengue transmission: a systematic review of structural approaches. *PLoS One* **7**, e49085–e49085 (2012).

170. Ritz, C., Baty, F., Streibig, J. C. & Gerhard, D. Dose-Response Analysis Using R. *PLoS One* **10**, e0146021–e0146021 (2015).

171. Tesla, B. *et al.* Estimating the effects of variation in viremia on mosquito susceptibility, infectiousness, and R0 of Zika in Aedes aegypti. *PLoS Negl. Trop. Dis.* **12**, e0006733–e0006733 (2018).

172. Ogunrinade, A. The measurement of blood meal size in Aedes aegypti (L.). *Afr. J. Med. Med. Sci.* **9**, 69–71 (1980).

173. Zhang, W. *et al.* In utero infection of Zika virus leads to abnormal central nervous system development in mice. *Sci. Rep.* **9**, 1–12 (2019).

174. Osuna, C. E. & Whitney, J. B. Nonhuman Primate Models of Zika Virus Infection, Immunity, and Therapeutic Development. *J. Infect. Dis.* **216**, S928–S934 (2017).

175. Aliota, M. T. *et al.* Characterization of Lethal Zika Virus Infection in AG129 Mice. *PLoS Negl. Trop. Dis.* **10**, e0004682–e0004682 (2016).

176. Rossi, S. L. & Vasilakis, N. Modeling Zika Virus Infection in Mice. *Cell Stem Cell* **19**, 4–6 (2016).

177. Kumar, A. *et al.* Zika virus inhibits type-I interferon production and downstream signaling. *EMBO Rep.* **17**, 1766–1775 (2016).

178. Seong, R.-K., Lee, J. K. & Shin, O. S. Zika Virus-Induction of the Suppressor of

Cytokine Signaling 1/3 Contributes to the Modulation of Viral Replication. *Pathog. (Basel, Switzerland)* **9**, 163 (2020).

179. Österlund, P. *et al.* Asian and African lineage Zika viruses show differential replication and innate immune responses in human dendritic cells and macrophages. *Sci. Rep.* **9**, 15710 (2019).

180. Weaver, S. C. Emergence of Epidemic Zika Virus Transmission and Congenital Zika Syndrome: Are Recently Evolved Traits to Blame? *MBio* **8**, e02063-16 (2017).

181. Haby, M. M., Pinart, M., Elias, V. & Reveiz, L. Prevalence of asymptomatic Zika virus infection: a systematic review. *Bull. World Health Organ.* **96**, 402-413D (2018).

182. Herrera, B. B. *et al.* Continued Transmission of Zika Virus in Humans in West Africa, 1992-2016. *J. Infect. Dis.* **215**, 1546–1550 (2017).

183. Kayiwa, J. T. *et al.* Confirmation of Zika virus infection through hospital-based sentinel surveillance of acute febrile illness in Uganda, 2014-2017. *J. Gen. Virol.* **99**, 1248–1252 (2018).

184. Kisuya, B., Masika, M. M., Bahizire, E. & Oyugi, J. O. Seroprevalence of Zika virus in selected regions in Kenya. *Trans. R. Soc. Trop. Med. Hyg.* **113**, 735–739 (2019).

185. Mathé, P. *et al.* Low Zika virus seroprevalence among pregnant women in North Central Nigeria, 2016. *J. Clin. Virol.* **105**, 35–40 (2018).

186. Nurtop, E. *et al.* A Report of Zika Virus Seroprevalence in Republic of the Congo. *Vector-Borne Zoonotic Dis.* **20**, 40–42 (2020).

187. L'Azou, M. *et al.* Dengue seroprevalence: data from the clinical development of a tetravalent dengue vaccine in 14 countries (2005-2014). *Trans. R. Soc. Trop. Med. Hyg.* **112**, 158–168 (2018).

188. Gake, B. *et al.* Low seroprevalence of Zika virus in Cameroonian blood donors. *Braz. J. Infect. Dis.* **21**, 481–483 (2017).

189. Buchwald, A. G., Hayden, M. H., Dadzie, S. K., Paull, S. H. & Carlton, E. J. Aedes-borne disease outbreaks in West Africa: A call for enhanced surveillance. *Acta Trop.* **209**, 105468 (2020).

190. Garske, T. *et al.* Yellow Fever in Africa: estimating the burden of disease and impact of mass vaccination from outbreak and serological data. *PLoS Med.* **11**, e1001638–e1001638 (2014).

191. Gloria-Soria, A. *et al.* Global genetic diversity of Aedes aegypti. *Mol. Ecol.* **25**, 5377–5395 (2016).

192. Kotsakiozi, P. *et al.* Population structure of a vector of human diseases: Aedes aegypti in its ancestral range, Africa. *Ecol. Evol.* **8**, 7835–7848 (2018).

193. Sassetti, M. *et al.* First case of confirmed congenital Zika syndrome in continental Africa. *Trans. R. Soc. Trop. Med. Hyg.* **112**, 458–462 (2018).

194. Rosenstierne, M. W. *et al.* Zika Virus IgG in Infants with Microcephaly, Guinea-Bissau, 2016. *Emerg. Infect. Dis.* **24**, 948–950 (2018).

195. Tsetsarkin, K. A. *et al.* Chikungunya virus emergence is constrained in Asia by lineage-

specific adaptive landscapes. *Proc. Natl. Acad. Sci. U. S. A.* **108**, 7872–7877 (2011).

196. Syenina, A. *et al.* Positive epistasis between viral polymerase and the 3' untranslated region of its genome reveals the epidemiologic fitness of dengue virus. *Proc. Natl. Acad. Sci. U. S. A.* **117**, 11038–11047 (2020).

197. Vermillion, M. S. *et al.* Intrauterine Zika virus infection of pregnant immunocompetent mice models transplacental transmission and adverse perinatal outcomes. *Nat. Commun.* **8**, 14575 (2017).

198. Sheridan, M. A. *et al.* African and Asian strains of Zika virus differ in their ability to infect and lyse primitive human placental trophoblast. *PLoS One* **13**, e0200086–e0200086 (2018).

199. Tabata, T. *et al.* Zika Virus Replicates in Proliferating Cells in Explants From First-Trimester Human Placentas, Potential Sites for Dissemination of Infection. *J. Infect. Dis.* **217**, 1202–1213 (2018).

200. Tabata, T. *et al.* Zika Virus Targets Different Primary Human Placental Cells, Suggesting Two Routes for Vertical Transmission. *Cell Host Microbe* **20**, 155–166 (2016).

201. Morris, J. *et al.* Prevalence of microcephaly: The Latin American Network of Congenital Malformations 2010-2017. *BMJ Paediatr. Open* **5**, 1–8 (2021).

202. Freitas, D. A. *et al.* Congenital Zika syndrome: A systematic review. *PLoS One* **15**, 1–27 (2020).

203. Filgueirasid, I. S. *et al.* The clinical spectrum and immunopathological mechanisms underlying zikv-induced neurological manifestations. *PLoS Negl. Trop. Dis.* **15**, 1–15 (2021).

204. Goodfellow, F. T. *et al.* Strain-Dependent Consequences of Zika Virus Infection and Differential Impact on Neural Development. *Viruses* **10**, 550 (2018).

205. Anfasa, F. *et al.* Phenotypic Differences between Asian and African Lineage Zika Viruses in Human Neural Progenitor Cells. *mSphere* **2**, (2017).

206. Garcez, P. P. *et al.* Zika virus: Zika virus impairs growth in human neurospheres and brain organoids. *Science (80-.).* **352**, 816–818 (2016).

207. Manet, C. *et al.* Zika virus infection of mature neurons from immunocompetent mice generates a disease-associated microglia and a tauopathy-like phenotype in link with a delayed interferon beta response. *J. Neuroinflammation* **19**, 1–21 (2022).

208. Sher, A. A., Glover, K. K. M. & Coombs, K. M. Zika virus infection disrupts astrocytic proteins involved in synapse control and axon guidance. *Front. Microbiol.* **10**, 1–20 (2019).

209. Rubio-Hernández, E. I. *et al.* Astrocytes derived from neural progenitor cells are susceptible to Zika virus infection. *PLoS One* **18**, 1–25 (2023).

210. Chen, J. *et al.* AXL promotes Zika virus infection in astrocytes by antagonizing type i interferon signalling. *Nat. Microbiol.* **3**, 302–309 (2018).

211. Limonta, D. *et al.* Human fetal astrocytes infected with zika virus exhibit delayed apoptosis and resistance to interferon: Implications for persistence. *Viruses* **10**, 1–19 (2018).

212. Schultz, V. *et al.* Oligodendrocytes are susceptible to Zika virus infection in a mouse model of perinatal exposure: Implications for CNS complications. *Glia* **69**, 2023–2036 (2021).

213. Li, C. *et al.* Disruption of glial cell development by Zika virus contributes to severe microcephalic newborn mice. *Cell Discov.* **4**, 1–12 (2018).

214. Schultz, V. *et al.* Zika virus infection leads to demyelination and axonal injury in mature cns cultures. *Viruses* **13**, (2021).

215. Lum, F. M. *et al.* Zika virus infects human fetal brain microglia and induces inflammation. *Clin. Infect. Dis.* **64**, 914–920 (2017).

216. Xu, P. *et al.* Role of microglia in the dissemination of zika virus from mother to fetal brain. *PLoS Negl. Trop. Dis.* **14**, 1–21 (2020).

217. Diop, F. *et al.* Zika virus infection modulates the metabolomic profile of microglial cells. *PLoS One* **13**, 1–16 (2018).

218. Viedma, M. D. P. M. & Pickett, B. E. Characterizing the different effects of Zika virus infection in placenta and microglia cells. *Viruses* **10**, 1–16 (2018).

219. Dang, J. *et al.* Zika Virus Depletes Neural Progenitors in Human Cerebral Organoids through Activation of the Innate Immune Receptor TLR3. *Cell Stem Cell* **19**, 258–265 (2016).

220. Li, H. *et al.* Zika Virus Infects Neural Progenitors in the Adult Mouse Brain and Alters Proliferation. *Cell Stem Cell* **19**, 593–598 (2016).

221. Gabriel, E. *et al.* Recent Zika Virus Isolates Induce Premature Differentiation of Neural Progenitors in Human Brain Organoids. *Cell Stem Cell* **20**, 397-406.e5 (2017).

222. Gladwyn-Ng, I. *et al.* Stress-induced unfolded protein response contributes to Zika virus–associated microcephaly. *Nat. Neurosci.* **21**, 63–71 (2017).

223. Saade, M. *et al.* Multimerization of Zika Virus-NS5 Causes Ciliopathy and Forces Premature Neurogenesis. *Cell Stem Cell* **27**, 920-936.e8 (2020).

224. Plociennikowska *et al.* TLR3 Activation by Zika Virus Stimulates In fl ammatory Cytokine. *J. Virol.* **95**, 1–24 (2021).

225. Rosinski, J. R. *et al.* Frequent first-trimester pregnancy loss in rhesus macaques infected with African-lineage Zika virus. *PLoS Pathog.* 2022.12.09.519791 (2022) doi:10.1371/journal.ppat.1011282.

226. Jaeger, A. S. *et al.* Zika viruses of African and Asian lineages cause fetal harm in a mouse model of vertical transmission. *PLoS Negl. Trop. Dis.* **13**, e0007343–e0007343 (2019).

227. Shao, Q. *et al.* The African Zika virus MR-766 is more virulent and causes more severe brain damage than current Asian lineage and dengue virus. *Development* **144**, 4114–4124 (2017).

228. Duggal, N. K. *et al.* Differential Neurovirulence of African and Asian Genotype Zika Virus Isolates in Outbred Immunocompetent Mice. *Am. J. Trop. Med. Hyg.* **97**, 1410–1417 (2017).

229. Aubry, F. *et al.* Recent African strains of Zika virus display higher transmissibility and

fetal pathogenicity than Asian strains. *Nat. Commun.* **12**, 1–14 (2021).

230. Inagaki, T. *et al.* Leu-to-Phe substitution at prM146 decreases the growth ability of Zika virus and partially reduces its pathogenicity in mice. *Sci. Rep.* **11**, 1–12 (2021).

231. Carbaugh, D. L. *et al.* Two Genetic Differences between Closely Related Zika Virus Strains Determine Pathogenic Outcome in Mice. *J. Virol.* **94**, (2020).

232. Shi, Y., Kirwan, P. & Livesey, F. J. Directed differentiation of human pluripotent stem cells to cerebral cortex neurons and neural networks. *Nat. Protoc.* **7**, 1836–1846 (2012).

233. Van Boheemen, S. *et al.* Quasispecies composition and evolution of a typical Zika virus clinical isolate from Suriname. *Sci. Rep.* **7**, 1–7 (2017).

234. Donald, C. L. *et al.* Full Genome Sequence and sfRNA Interferon Antagonist Activity of Zika Virus from Recife, Brazil. *PLoS Negl. Trop. Dis.* **10**, 1–20 (2016).

235. Kum, D. B. *et al.* A yellow fever–Zika chimeric virus vaccine candidate protects against Zika infection and congenital malformations in mice. *npj Vaccines* **3**, (2018).

236. Aubry, F. *et al.* Single-stranded positive-sense RNA viruses generated in days using infectious subgenomic amplicons. *J. Gen. Virol.* **95**, 2462–2467 (2014).

237. Stagni, F., Giacomini, A., Guidi, S., Ciani, E. & Bartesaghi, R. Timing of therapies for downsyndrome: The sooner, the better. *Front. Behav. Neurosci.* **9**, (2015).

238. Tanaka, T., Narazaki, M. & Kishimoto, T. IL-6 in Inflammation, Immunity, and Disease. *Cold Spring Harb. Perspect. Biol.* **6**, (2023).

239. Liu, M. *et al.* CXCL10/IP-10 in infectious diseases pathogenesis and potential therapeutic implications. *Cytokine Growth Factor Rev.* **22**, 121–130 (2011).

240. Mosser, D. M. & Zhang, X. Interleukin-10: New perspectives on an old cytokine. *Immunol. Rev.* **226**, 205–218 (2008).

241. Sarno, M. *et al.* Zika Virus Infection and Stillbirths: A Case of Hydrops Fetalis, Hydranencephaly and Fetal Demise. *PLoS Negl. Trop. Dis.* **10**, 5–9 (2016).

242. Stanford Medicine & Children's, H. Hydrops Fetalis. https://www.stanfordchildrens.org/en/topic/default?id=hydrops-fetalis-90-P02374 (2023).

243. Brasil, P. *et al.* Zika Virus Infection in Pregnant Women in Rio de Janeiro. *N. Engl. J. Med.* **375**, 2321–2334 (2016).

244. Petphong, V. *et al.* Detection of Anti-ZIKV NS1 IgA, IgM, and Combined IgA/IgM and Identification of IL-4 and IL-10 as Potential Biomarkers for Early ZIKV and DENV Infections in Hyperendemic Regions, Thailand. *Trop. Med. Infect. Dis.* **8**, 1–22 (2023).

245. Kolimenakis, A. *et al.* The role of urbanisation in the spread of aedes mosquitoes and the diseases they transmit—a systematic review. *PLoS Negl. Trop. Dis.* **15**, 1–21 (2021).

246. Kraemer, M. U. G. *et al.* Past and future spread of the arbovirus vectors Aedes aegypti and Aedes albopictus. *Nat. Microbiol.* **4**, 854–863 (2019).

247. Dudley, D. M. *et al.* Miscarriage and stillbirth following maternal Zika virus infection in nonhuman primates. *Nat. Med.* **24**, 1104–1107 (2018).

248. Koenig, M. R. *et al.* Vertical transmission of African-lineage Zika virus through the fetal membranes in a rhesus Macaque (Macaca mulatta) model. *PLoS Pathog.* 2023.03.13.532348 (2023) doi:10.1371/journal.ppat.1011274.

249. Duong, V., Dussart, P. & Buchy, P. Zika virus in Asia. *Int. J. Infect. Dis.* **54**, 121–128 (2017).

250. Duffy, M. R. *et al.* Zika Virus Outbreak on Yap Island, Federated States of Micronesia.

251. Shan, C. *et al.* A Zika virus envelope mutation preceding the 2015 epidemic enhances virulence and fitness for transmission. *Proc. Natl. Acad. Sci. U. S. A.* **117**, 20190–20197 (2020).

252. Tripathi, S. *et al.* A novel Zika virus mouse model reveals strain specific differences in virus pathogenesis and host inflammatory immune responses. *PLoS Pathog.* **13**, e1006258–e1006258 (2017).

253. Bohm, E. K. *et al.* Zika Virus Infection of Pregnant Ifnar1 −/− Mice Triggers Strain-Specific Differences in Fetal Outcomes . *J. Virol.* **95**, (2021).

254. De Oliveira Melo, A. S. *et al.* Congenital Zika virus infection: Beyond neonatal microcephaly. *JAMA Neurol.* **73**, 1407–1416 (2016).

255. Wheeler, A. C. *et al.* Developmental Outcomes Among Young Children With Congenital Zika Syndrome in Brazil. *JAMA Netw. open* **3**, e204096 (2020).

256. Grant, R. *et al.* In utero Zika virus exposure and neurodevelopment at 24 months in toddlers normocephalic at birth: a cohort study. *BMC Med.* **19**, 1–11 (2021).

257. Paixao, E. S., Leong, W. Y., Rodrigues, L. C. & Wilder-Smith, A. Asymptomatic prenatal Zika virus infection and congenital Zika syndrome. *Open Forum Infect. Dis.* **5**, 1–5 (2018).

258. Zorrilla, C. D., García, I. G., García Fragoso, L., De, A. & Vega, L. The Journal of Infectious Diseases Zika Virus Infection in Pregnancy: Maternal, Fetal, and Neonatal Considerations. doi:10.1093/infdis/jix448.

259. Peçanha, P. M. *et al.* Neurodevelopment of children exposed intra-uterus by Zika virus: A case series. *PLoS One* **15**, e0229434 (2020).

260. van der Linden, V. *et al.* Description of 13 Infants Born During October 2015–January 2016 With Congenital Zika Virus Infection Without Microcephaly at Birth — Brazil. *MMWR. Morb. Mortal. Wkly. Rep.* **65**, 1343–1348 (2016).

261. Zin, A. A. *et al.* Screening Criteria for Ophthalmic Manifestations of Congenital Zika Virus Infection Supplemental content. *JAMA Pediatr* **171**, 847–854 (2017).

262. Tsui, I. *et al.* Eye findings in infants with suspected or confirmed antenatal Zika virus exposure. *Pediatrics* **142**, (2018).

263. Ramalho, F. S. *et al.* Congenital Zika Virus Infection Induces Severe Spinal Cord Injury. *Clin. Infect. Dis.* **65**, 687–690 (2017).

264. Hageman, G. & Nihom, J. Fetuses and infants with Amyoplasia congenita in congenital Zika syndrome: The evidence of a viral cause. A narrative review of 144 cases. *Eur. J. Paediatr. Neurol.* **42**, 1–14 (2023).

265. Aragao, M. F. V. V. *et al.* Spectrum of spinal cord, spinal root, and brain mri abnormalities in congenital Zika syndrome with and without Arthrogryposis. *Am. J. Neuroradiol.* **38**, 1045–1053 (2017).

266. Alvino, A. C. M. I., de Mello, L. R. M. & de Oliveira, J. do A. M. M. Association of arthrogryposis in neonates with microcephaly due to Zika virus - a case serie. *Rev. Bras. Saude Matern. Infant.* **16**, S83–S88 (2016).

267. Sousa, A. Q. *et al.* Postmortem findings for 7 neonates with congenital Zika virus infection. *Emerg. Infect. Dis.* **23**, 1164–1167 (2017).

268. Orofino, D. H. G. *et al.* Cardiac findings in infants with in utero exposure to Zika virus-a cross sectional study. *PLoS Negl. Trop. Dis.* **12**, 1–9 (2018).

269. Rosado, L. E. P. *et al.* Risk of adverse pregnancy and infant outcomes associated with prenatal Zika virus infection: a post-epidemic cohort in Central-West Brazil. *Sci. Rep.* **13**, 1–12 (2023).

270. Barbosa, I. C. Q. *et al.* Evaluation of morphology and biventricular cardiac function in children with congenital zika syndrome. *Eur. Heart J.* **43**, 2530 (2022).

271. Paixao, E. S. *et al.* Mortality from Congenital Zika Syndrome — Nationwide Cohort Study in Brazil. *N. Engl. J. Med.* **386**, 757–767 (2022).

272. Sochocka, M., Diniz, B. S. & Leszek, J. Inflammatory Response in the CNS: Friend or Foe? *Mol. Neurobiol.* **54**, 8071–8089 (2017).

273. Kim, Y. S. & Joh, T. H. Microglia, major player in the brain inflammation: their roles in the pathogenesis of Parkinson's disease. *Exp. Mol. Med.* **38**, 333–347 (2006).

274. Colonna, M. & Butovsky, O. Microglia function in the central nervous system during health and neurodegeneration. *Annu. Rev. Immunol.* **35**, 441–468 (2017).

275. Perry, V. H. & Teeling, J. Microglia and macrophages of the central nervous system: The contribution of microglia priming and systemic inflammation to chronic neurodegeneration. *Semin. Immunopathol.* **35**, 601–612 (2013).

276. Oliveira, F. B. C. de *et al.* ZIKV Strains Elicit Different Inflammatory and Anti-Viral Responses in Microglia Cells. *Viruses* **15**, (2023).

277. Pan, T. *et al.* Nonsteroidal Anti-inflammatory Drugs Potently Inhibit the Replication of Zika Viruses by Inducing the Degradation of AXL. *J. Virol.* **92**, 1–18 (2018).

278. Chuang, F. K. *et al.* Anti-inflammatory Compound Shows Therapeutic Safety and Efficacy against Flavivirus Infection. *Antimicrob. Agents Chemother.* **64**, 1–11 (2020).

279. Jurga, A. M., Paleczna, M. & Kuter, K. Z. Overview of General and Discriminating Markers of Differential Microglia Phenotypes. *Front. Cell. Neurosci.* **14**, 1–18 (2020).

280. National Institute of Allergy and Infectious Diseases (NIAID). VRC 705: A Zika Virus DNA Vaccine in Healthy Adults and Adolescents (DNA). https://clinicaltrials.gov/study/NCT03110770 (2023).

281. Essink, B. *et al.* The safety and immunogenicity of two Zika virus mRNA vaccine candidates in healthy flavivirus baseline seropositive and seronegative adults: the results of two randomised, placebo-controlled, dose-ranging, phase 1 clinical trials. *Lancet Infect. Dis.* **23**, 621–633 (2023).

282. Lee, J. K. & Shin, O. S. Advances in zika virus–host cell interaction: Current knowledge and future perspectives. *Int. J. Mol. Sci.* **20**, (2019).

283. Van Den Elsen, K., Quek, J. P. & Luo, D. Molecular insights into the flavivirus replication complex. *Viruses* **13**, 1–28 (2021).

Scientific Acknowledgments:

Chapter III: We thank the laboratory of Prof. Louis Lambrechts for performing the mosquito experiments. We thank the laboratory of Prof. Johan Neyts for performing the AG129 mice experiments. We thank Dr. Maxime Gilsoul for his technical assistance for RNA isolation of mouse embryo organs and embryonic brain cryosectioning.

Chapter IV: We thank Stijn Hendrickx for its incredible help and technical assistance in *in vitro* infection, RNA isolation, RT-qPCR experiments. We thank Dr. Franck Touret for his assistance in setting up the ISA method with supervision of Prof. Xavier de Lamballerie. We thank Prof. Pedro E. Marques and Emily Slowikowski for performing the ELISA experiments as well as the analysis. We thank Prof. Catherine Verfaillie and Karan Ahuja for generating and providing the hNPCs. We thank Dr. Lorena Sanchez-Felipe for her help in the setting up the ISA method at KU Leuven. We thank Ivan Gladwyn-Ng for his massive contribution in the writing of the manuscript.

Author contributions

All the data presented in the thesis are a result of a personal and collaborative efforts.

Chapter III:

S.J.F.K. and L.L. contributed equally to the design and coordination of the study.

V.-M.C.-L., R.G.J., C.T.D., Oum. F., Ous.F., and A.A.S. obtained the virus isolates and organized their transfer.

F.A., C.M., X.M., and L.L. designed and implemented the mouse-to-mosquito transmission assay. F.A., N.J., E.F.M., S.D., C.M., and A.B. carried out the mosquito experiments. S.L. and A.F. conducted the epidemiological modeling. S.D., S.L., F.G., and E.S.-L. performed the virus sequencing. F.A. and A.B. performed the phylogenetic analyses. C.M.R.-V. conducted the field collections to initiate the mosquito colony from Colombia.

S.J., L.D., and S.J.F.K. designed and performed the AG129 mouse experiments. J.N. supervised the AG129 mouse experiments.

M.G. provided technical assistance in sample processing in vertical transmission experiments. L.N. supervised the vertical transmission experiments.

F.A., S.J., **M.D.**, S.J.F.K., and L.L. prepared the figures. F.A. and L.L. analyzed the data and wrote the paper with input from all other authors.

Chapter IV:

S.J.F.K.: Supervision of the project.

S.J.F.K. and J.N.: Securing of funding.

M.D. and S.J.F.K. wrote the manuscript with contributions from I.G.-N., P.E.M., and J.N., and comments from all authors.

F.T., X.L and L.S.F: ISA method set up assistance.

S.H.: Technical assistance.

K.A. and C.V.: Provided hNPCs.

Personal contributions:

Chapter III: Conceptualization and design of IPL ZIKV challenge experiments. Surgical mouse experiments. Mice follow-up. Embryonic samples processing. Data acquisition and analyses of IPL experiments. Writing results IPL experiments.

Chapter IV: Conceptualization and design of the project. Surgical mouse experiments. Mice follow-up. Embryonic samples processing (brain and embryonic dissections, cryosectioning, RNA isolation, RT-qPCR, immunostainings, image acquisitions). *In vitro* infections assay (infections, RNA isolation, RT-qPCR, titration assays, immunostainings). ISA method implementation and single mutant THA_139N generation. Data acquisitions and analyses. Writing of the manuscript.

Conflict of interest:

No conflict of interest to declare.